المجلد ١ العدد ٣ رمضان ١٤٢٩هـ

المجلة العربية للكيميـاء

الراعي الرسمي لهذه المجلة:
مدينة الملك عبدالعزيز للعلوم والتقنية

تصدر هذه المجلة بدعم من الجمعية الكيميائية السعودية

المجلة الرسمية لاتحاد الكيميائيين العرب

Arabian Journal of Chemistry ,Volume 1-Number 3 September 2008

Volume 1-Number 3- September 2008

ARABIAN JOURNAL OF CHEMISTRY

Published By Saudi Chemical Society

The Official Journal For the Arab Union of Chemists

ARABIAN JOURNAL OF CHEMISTRY

The international Journal of Pure and Applied Chemistry

Peer Review Policy for Arabian Journal of Chemistry
The practice of peer review is to ensure that good science is published. It is an objective process at the heart of good scholarly publishing and is carried out on all reputable scientific journals. Our referees therefore play a vital role in maintaining the high standards of Arabian Journal of Chemistry and all manuscripts are peer reviewed following the procedure outlined below.

Special issues are also subject to peer review and may involve the assistance of Guest Editors. Authors contributing to these projects will receive full details of the peer review process from the Editor in Charge . Arabian Journal of Chemistry applies the same criteria of acceptance of manuscripts to all types of submissions, irrespective of whether these are submitted for regular issue or special issues.

Initial manuscript evaluation
One of the Editors first evaluate the manuscript. Some manuscripts may be rejected at this stage if they are deemed insufficiently original, have serious scientific flaws, or are outside the aims and scope of the journal. Those manuscripts that meet these minimum criteria are passed on to experts for review.

Type of Peer Review
This journal employs double blind review, where the referees remain anonymous throughout the process.

How the reviewer is selected
Reviewers are matched to the paper by the Editor according to their expertise. Arabian Journal of Chemistry's reviewer database is constantly being updated. The Editors welcome suggestions for reviewers from the author though these recommendations may not be used, and these should not be close colleagues or collaborators, i.e., should be independent experts.

Reviewers reports
Reviewers are asked to evaluated whether the manuscripts:

- Is original and novel
- Is conceptually and scientifically sound
- Is methodologically sound
- Contributes significantly to advancement of the research area
- Follows appropriate ethical guidelines
- Has results which are clearly presented and support the conclusions
- Correctly references previous relevant work

Reviewers are not expected to correct or copyedit manuscripts.
Language correction is not part of the peer review process.

How long does the review process take?
Typically the manuscript will be reviewed within 2 months. Should the reviewers` reports contradict one another or a report is unnecessarily delayed a further expert opinion may be sought. Revised manuscripts may be returned to the initial referees. The Editors may request more than one revision of a manuscript.

Final Report
A final decision to accept or reject the manuscript will be sent to the author along with any recommendations made by the reviewers, and may include verbatim comments by the reviewers and Editor.

Editor's decision is final
Reviewers advise the Editor, who is responsible for the final decision to accept or reject the article.

The International Conference For Nanotechnology Industries

The Leading Technology of 21st Century

King Abdullah Institute for Nanotechnology

April 5-7 - 2009
King Saud University
Riyadh – Saudi Arabia

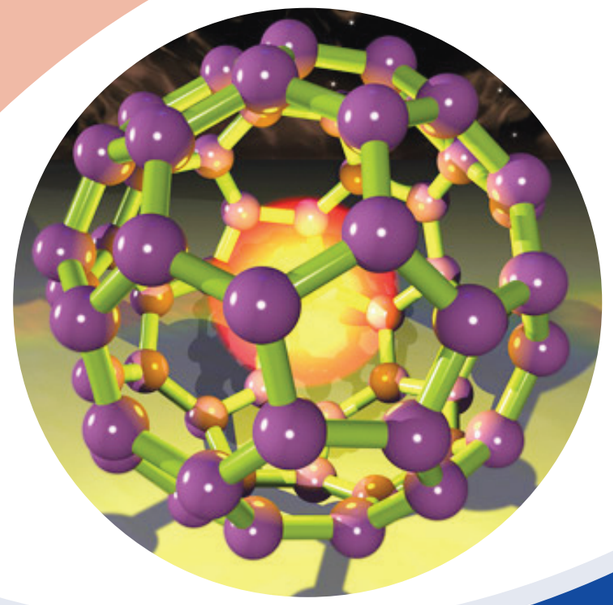

Important Dates:

- Abstract Submission deadline Jan.7,2009
- Full Paper Submission deadline Mar.7, 2009
- Registration deadline Mar. 15,2009

Conference Website:http://nano.ksu.edu.sa/conferences/ICNI

Arabian Journal of Chemistry

Editor -in- Chief

Prof. Abdulrahman A . Alwarthan
Chemistry Department
King Saud University,
Riyadh, Saudi Arabia
E-mail: awarthan@ksu.edu.sa

Vice-editors -in- Chief

Prof. Sultan T. Abu-Orabi
Tafila Technical University/President
Tafila, P.O. Box 179, Jordan,
Jordanian Chemical Society
Arab Union of Chemists/Secretary General
E-mail: abuorabi@excite.com

Prof. Yousry M. Issa
Chemistry Department
Cairo University, Cairo
Egypt
E-mail: yousrymi@yahoo.com

EDITORIAL BOARD

Prof. Belkheir Hammouti
Director, Laboratory of Applied Chemsitry and Environment
Faculty of Science
University of Mohammed Premier
Morocco
E-mail: hammoutib@yahoo.com

Prof. Mamia El Rhazi
Chemistry Department
Faculty of Science and Technology
Hassan II Univeristy-Mohammedia
Morocco
E-mail: elrhazim@hotmail.com

Prof. Hassan M. Al-Hazimi
Chemistry Department
Science College, King Saud University
Saudi Arabia
E-mail: hhazimi@ksu.edu.sa

Prof. Hamad Z. Al-Khathlan
Chemistry Department
Science College, King Saud University
Saudi Arabia
E-mail: Khathlan@ksu.edu.sa

Prof. Ibrahim A. Jibril
Chemistry Department
Yarmouk University
Irbid, Jordan
E-mail: iajibril@yahoo.com

Prof. El Sayed H. El Ashry
Chemistry Department
Faculty of Science
University of Alexandria
Alexandria, Egypt
E-mail: eelashry60@hotmail.com

Dr. Lassaad Baklouti
Laboratoire de Chimie des Interactions Moleculaires
Faculte de Sciences de Bizerte
7021 Zarzouna, Tunisie
E-mail: bakloutilassaad@yahoo.fr

Prof. Saad M. H. Ayoub
Chemistry Department
Elneleen University
Khartoum, Sudan
E-mail:

Prof. Abdalsalam A. Daffaalla
Chemistry Department
Science College,Sudan University of Science and Technology
P.O.Box: 407
Khartoum, Sudan
E-mail:aadafa@hotmail.com

Prof. Ahmed-Yacine Badjah-Hadj-Ahmed
University of Science and Technology
Houari Boumadiene
Faculty of Chemistry
BP 32 El Alia.
16111 Bab Ezzouar
Algiers, Algeria
E-mail: Ybadjah@hotmail.com

Abdelkader Bengueddach
laboratoire de Chimie des Materiaux
Deparment of Chemistry
Faculty of Science
University of Oran
P.O.Box 1524 el Mnouar
31000-Oran, Algerie
E-mail: aek-bengueddach@univ.oran.dz

Mohammad Hourani
Deartment of Chemistry, Al Balqa Applied University, Al-Salt, Jordan.
E-mail:mhouran@bau.edu.jo

Prof. Mahmoud F. Farhat
Professor of Organic Chemistry
Chemistry Department
Faculty of Science
Al-Fateh University
P.O.Box: 13494
Tripole, Libya
E-mail: mf_farhat@yahoo.com

Prof. Nouria A. Al-Awadi
Professor of Organic Chemsitry
Department of Chemistry
Faculty of Science
P.O.Box: 5969 Safat-13060
Kuwait University
E-mail: eam_hc5@kuc01.kuniv.edu.kw

Dr. Abdulaziz A. AlNajjar

Applied Science, College of Technological Studies,
Public Authority of Applied Education and Training
P.O. Box 34484 Adeilia, 73255, Kuwait
e-mail: anajjar_55@yahoo.com

Dr. Ameera Saeed Al-Haddad

University of Bahrain, Kingdom of Bahrain ,
Department of Chemistry, P.O. Box 32028, Isa Town,
Kingdom of Bahrain
E=mail: ameera@sci.uoh.bh

INTERNATIONAL ADVISORY BOARD

Prof. Issa Yavari
Chemistry Department
Tarbiat Modarres University
Tehran, Iran
E-mail: yavarisa@modares.ac.ir

Dr. Paul S. Francis
School of Life and Environmental Sciences
Deakin University, Geelong
Victoria 3217, Australia
E-mail: psf@deakin.edu.au

Prof. Jose Martinez Calatayud
Chemistry Department
University of Valencia
Valencia, Spain
E-mail: jose.martinez@uv.es

Prof. Robert G. Michel
Department of Chemistry
University of Connecticut
55 North Eagleville Road
Storrs, CT 06269-3060
E-mail: robert.g.michel@uconn.edu

Prof. Motaza M. Khater
Chemistry Department
Cairo University
Cairo, Egypt
E-mail: motazakhater117@yahoo.com

Prof. Jacques Vicens
Directeur de recherche at CNRS
UMR 7178-CNRS
Institut Pluridisciplinaire Hubert Curien
Universite Louis Pasteur de Strasbourg
Laboratoire de Conception Moleculaire`
ECPM
25, rue Becquerel
F-67087
France
E-mail: vicens@chimie.u-strasbg.fr

Prof. Jean-Michel KAUFFMANN
Free University of Brussels
Lab, Instrumental Analysis and Bioelectrochemistry
Pharmaceutical Institute, ULB 205/6
Campus Plaine
B-1050 Brussels, Belgium
E-mail: jmkauf@ulb.ac.be

Prof. Essam Khamis Al-Hanash
Vice-Dean for Graduate Studies & Research.
Faculty of Science, Mohram Bey, Alexandria University.
Alexandria, Egypt
E-mail: ekaijac@yahoo.com

Prof. Bryan R. Henry
University of Guelph
Department of Chemistry
Guelph, Ontario NIG 2W1
Canada
E-mail: Chmhenry@uoguelph.ca

Prof. Samy El-Shall
Department of Chemistry,
Virginia Commonwealth University
Richmond,Virginia 23284-2006
USA
E-mail: mselshal@vcu.edu.

Prof. JIN, JUNG-IL(M)
35-41Ku-Ui 2-Dong
Kwang-Jin Ku, Seoul 133-202, Korea
Chemistry Department and Center for Electro-and Photo-Responsive Molecules, College of Sciences,
Korea University
5-1 Anam-Dong, Seoul 136-701, Korea
E-mail: jijin@korea.ac.kr, jijin@kcsnet.or.kr

Prof. Alan Townshend
The University of Hull
Department of Chemistry
Hull, HU6 7RX
United Kingdom
E-mail: a.townshend@hull.ac.uk

Dr. Danielle M. Cleveland
18347 woodland Ridge Drive # 14
Spring Lake, MI 49456
E-mail: danielle.cleveland@uconn.edu

Prof. Yuhan Sun
Institute of Coal Chemistry
Chinese Academy of Sciences
P.O.Box: 165,Taiyuan, Shanxi, 030001, PR. China
E-mail: yhsun@sxicc.ac.cn

Prof. Ishaque Khan
Director, Materials and Chemical Synthesis Program
Department of Biological Chemical and Physical Sciences
College of Science and Letters
Room 125, E1
10W, 32nd Street
Chicago, IL 60616-3793
E-mail: khan@117.edu

INTERNATIONAL ADVISORY BOARD

Prof. Mikhail M. Krayushkin
Head of Laboratory of Heterocyclic Compounds
N.D.Zelinsky Institute of Organic Chemistry,
Russian Academy of Sciences
119991, Moscow, Leninsky Propspect 47, Russia
E-mail: mkray@ioc.ac.ru

Prof. Volker Schurig,
Institute of Organic chemsitry,
University of Tubingen, Auf der Morgenstelle 18,72076
Tubingen, Germany
E-mail:Volker.schurig@uni-tuebingen.de

Prof. Angel Rios Castro
Department of Analytical Chemistry and food Tech.,
Faculty of Chemistry
University of Castilla- La Mancha
AV. Camilo Jose Cela. 10, E--13004 Ciudad Real, Spain.
Phone: +34 926 295232 /Fax: +34 926 295318
E-mail: angel.rios@uclm.es

Prof. Faiza M. Al-Kharafi
Department of Chemsitry
Faculty of Science
Kuait University
Kuwait
E-mail: chesc@kuc01.kuniv.edu.kw

Author Guidelines

Scope and Description

Arabian Journal of Chemistry (AJC) is an international quarterly peer-reviewed research journal issued by the Arab Union of Chemists, and published by the Saudi Chemical Society, Riyadh, Saudi Arabia. The Journal publishes new and original Research Articles, Short Communications, Technical Notes, Feature Articles and Review Articles encompassing all fields of chemistry, experimental and theoretical, written either in English or Arabic.

Introduction to Authors

Instructions to authors concerning manuscript organization and format apply to hardcopy submission by mail, and also to electronic online submission via the Journal homepage website (under construction).

Manuscript Submission

1- Hardcopy: The Original and three copies of the manuscript, together with a covering letter from the corresponding author, should submitted to the:

Editor-in-chief:
Prof. Abdulrahman. A. Alwarthan
Editor-in-Chief
Arabian Journal of Chemistry
Chemistry Department, Faculty of Science
King Saud University
P.O.Box: 2455, Riyadh-11451
Saudi Arabia
Tel: 00966 1 4676005
Fax: 00966 1 4675888
E-mail:awarthan@ksu.edu.sa

2- Online: follow the instructions at the journal homepage website.

Original Research Articles, Communications and Technical Notes are subject to critical review by at least two referees. Authors are encouraged to suggest names of competent reviewers. Feature Articles in active chemistry research fields, in which the author's own contribution and its relationship to other work in the field constitutes the main body of the article, appear as a result of an invitation from the Editorial Board, and will be so designated. The author of a Feature Article will be asked to provide a clear, concise and critical status report of the field as an introduction to the article. Review Articles on active and rapidly changing chemistry research fields will also be published. Authors of Review Articles are encouraged to submit two-page proposals to the Editor-in-Chief for approval. Manuscripts submitted in Arabic should also include an Abstract and Keywords in English.

Organization of the Manuscript

Manuscripts not exceeding 30 pages should be typed double-spaced on one side of high quality white A4 sheets (21.6×27.9 cm) with 3.71 cm margins, using Microsoft Word 2000 or a later version thereof. The sections should be arranged in the following order: Title Page, Abstract, Keywords, Introduction, Materials and Methods, Results, Discussion, Conclusion, Acknowledgments, Abbreviations (if any), References, Tables, a list of Figure Captions, and Figures. Only the first letters of words in the Title, Headings and Subheadings are capitalized. Headings should be in bold while Subheadings in italic fonts.

Title Page: Includes the title of the article, authors' names with full first names and middle initials, and affiliations. The affiliation should comprise the department, institution (university or company), city and state and should be typed as a footnote to the author's name. The name and complete mailing address, telephone and fax numbers, and e-mail address of the author responsible for correspondence (who is designated with an asterisk) should also be included for office purposes. The title should be carefully, concisely and clearly constructed to highlight the emphasis and content of the manuscript, which is very important for information retrieval.

Abstract: A one paragraph abstract not exceeding 200 words is required, which should be arranged to highlight the purpose, methods used, results and major findings, with the results comprising no less than 50% of the abstract.

Keywords: A list of 4-6 keywords, which express the precise content of the manuscript for indexing purposes, should follow the abstract.

Introduction: Should present the purpose of the studies to be reported and their relationship to earlier work in the field, but it should not be an extensive review of the literature (e.g., should not exceed 1 ½ typed pages).

Materials and Methods: Should be sufficiently informative to allow competent reproduction of the experimental procedures presented, yet concise enough not to be repetitive of earlier published procedures. Note that all unusual hazards in the chemicals, equipment or procedures used in the study must be clearly identified.

Results: Should present results in Tables and Figures plus some complimentary data in the Text without extensive discussion of results.

Discussion: Should be concise and focusing on the interpretation of the results without repetition of same results.

Conclusion: Should be a brief account of the major findings of the study not exceeding one typed page at the most.

Nomenclature: Registered trade names should be capitalized whenever they are used, while trade or trivial names should not be capitalized. The chemical name or composition should be given in parentheses at the first occurrence of that name. Nomenclature should be systematic conforming to those used by the Chemical Abstracts Service and recommended by IUPAC and IUBMB.

Abbreviations: Abbreviations are to be used sparingly, otherwise

provide a notation section indicating all nonstandard abbreviations on a separate page prior to the references section. The metric system should be used for all measurements, which must be indicated in lower case letters (e.g., g, kg, m, ml, s), while Standard International (SI) units are to be used conforming to IUPAC. Define all symbols used in equations and formulas. Include a list of all symbols in the notation section when extensively used.

Acknowledgments: Acknowledgments, including those for grant and financial support, should be typed in one paragraph directly preceding the References section.

References: References should be typed double-spaced and numbered sequentially in the order in which they are cited in the text. References should be cited in the text by the appropriate Arabic numerals, which are superscripted while enclosed in square brackets. Titles of journals are abbreviated according to the Chemical Abstracts Service Source Index (American Chemical Society). Authors are responsible for the accuracy of the references. The style and punctuation should conform to the following examples:

1. Journal Article:

For journals that are not paginated continuously throughout the year (e.g., page numbering does not continue from issue to the next), the volume number should be followed by the issue number in regular parentheses. In contrast, only the volume number is required for journals that are paginated continuously throughout the year. Examples:

a) Metallo, S. J.; Kane, R. S.; Holmlin, R. E.; Whitesides, G. M., J. Am. Chem. Soc. 2003, 125, 4534-4540.

b) Stevens, M. J., Langmuir 1999, 15, 2773-2778.

c) Walmsley, I.; Rabitz, H., Phys. Today 2003, 56(8), 43-49.

d) Freemantle, M., Chem. Eng. News 1988, 76(28), 15-16.

2. Books with authors, No Editors:

a) Calvert, J. G.; Pitts, J. N., Photochemistry; Wiley: New York, 1966, pp 156-186.

b) Zewail, A. H., Femtochemistry-Ultrafast Dynamics of the Chemical Bond; World Scientific: Singapore, 1994; Vol. I, pp 52-58.

3. Books with Authors and Editors:

a) The carbohydrates: Chemistry and Biochemistry; Pigman, W. W., Ed.; Academic Press: New York, 1970; pp 45-50.

b) Hilman, L. W., In Dye Laser Principles with Applications; Durate, F. J.; Hilman, L. W.; Eds.; Academic press: New York, 1990; Chapter 1.

c) Lochbrunner, S.; Stock, K.; De waele, V.; Riedle, E., Ultrafast Excited-State Proton Transfer: Reactive Dynamics by Multidimensional Wavepacket Motion. In Femtochemistry and Femtobiology: Ultrafast dynamics in Molecular Science; Douhal, A.; Santamaria, J., Eds.; World Scientific: Singapore, 2002; pp 202-212.

d) Femtochemistry and Femtobiology: Ultrafast Reaction Dynamics at Atomic Scale Resolution; Sundstrom, V., Ed.; World Scientific: Singapore, 1997; Chapter 2.

4.TechnicalReport: Schneider, A. B. Technical Report No. 1234-56, 1985; ABC Company, New York.

5.Patent: Kealy, T. J. US Patent 3 062 820, 1962; Chem. Abstr. 1963, 58, 9101.

6. Thesis:

Flink, S. Sensing Monolayers on Gold and Glass. Ph.D. Thesis, University of Twente, Enschede, the Netherlands, 2000.

7. Conference or Symposium Proceedings:

Huber, O.; Szejtli, J. Proceedings of the IV International Symposium on Cyclodextrins; Munchen; Kluwer Academic Publishers: Dordrecht, 1988.

8. Software Acquired from a Company:

Alchemy: A Molecular Modeling System for the IBMPC; Tripos Associates, Inc.: St. Louis, MO, 1988.

9. Software Accessed through the Internet:

CLOGP Program. Daylight Chemical Information systems, Inc. http://www.daylight.com/daycgi/clogp.

10. Internet Source:

Should include Author names (if any), Title, Internet website, URL, and (date of access).

11. Prepublication Online Articles (Already accepted for publication) :

Should include Author names (if any), Title of Digital Database, Database Website, URL, and (date of access).

Tables: Tables should be numbered with Arabic numerals and referred to by number in the Text (e.g., Table 1). Each Table should be typed on a separate page with the legend above the Table, while explanatory footnotes, which are indicated by superscript lowercase letters, should be typed below the Table.

Illustrations: Figures, drawings, diagrams, charts and photographs are to be numbered in a consecutive series of Arabic numerals in the order in which they are cited in the text. Computer-generated illustrations and good-quality digital photographic prints are accepted. They should be black and white originals (not photocopies) provided on separate pages and identified with their corresponding numbers. Actual size graphics should be provided, which need no further manipulation, with lettering (Arial or Helvetica) not smaller than 4.5 points, lines no thinner than 0.5 points, and each of uniform density. All color should be removed from graphics except for those graphics to be considered for publication in color. If graphics are to be submitted digitally, they should conform to the following minimum resolution requirements: 1200 dpi for black and white line art, 600 dpi for grayscale art, and 300 dpi for color art. All graphic files must be saved as TIFF images, and all illustrations must be submitted in the actual size at which they should appear in the journal. Note that good quality hardcopy original illustrations are required for both online and mail submissions of manuscripts.

Text Footnotes: The use of text footnotes is to be avoided. When their use is absolutely necessary, they should be typed at the bottom of the page to which they refer, and should be cited in the text by a superscript asterisk or multiples thereof. Place a line above the footnote, so that it is set off from the text.

Supplementary Material: Authors are encouraged to provide all supplementary materials that may facilitate the review process, including any detailed mathematical derivations that may not appear in whole in the manuscript, crystallographic information files (CIFs) and cited preprints. As to CIF files, the author must deposit the corresponding CIFs with the Cambridge Crystallograghic Data Centre (CCDC). The E-mail address of CCDC is: (deposit@ccdc.cam.ac.uk).

The deposited material is indicated in the manuscript by a footnote as follows:

Supplementary data: Crystallographic data for the structural

analysis reported in this paper have been deposited with the Cambridge Crystallographic Data Centre, CCDC, Number (...). Copies of the information may be obtained free of charge from Director, CCDC, 12 Union Road, Cambridge, CB2 1EZ, UK (Fax: +44-1223-336033; e-mail; deposit@ccdc.cam.ac.uk, home page: http//www.ccdc.cam.ac.uk).

Theoretical Calculations: Reporting the results of electronic structure calculations should follow the guidelines in J. E. Boggs (Pure and Appl. Chem. 1998, 70(4), 1015-1018). Reporting force field parameters and other energy surface data should follow the guidelines in D. J. Raber and W. C. Guida (Pure and Appl. Chem. 1998, 70(10), 2047-2049). Both sets of guidelines are available online at the IUPAC Website (http://www.iupac.org/reports/1998/index.html).

X-Ray Data: X-ray data presented in the text and/or tables should provide information on the empirical formula, unit cell dimensions (a, b, c in pm or Å; α, β, χ in degrees) with corresponding standard error estimates, number of formula units in the unit cell, density (measured or calculated), crystal system, space group symbol, diffractometer type, radiation, and monochromator used, temperature, data collection mode, the θ-range and reciprocal lattice segments, number of reflections measured, number of symmetry-independent reflections, cut-off criterion, linear absorption coefficient, absorption correction method, method of solution and refinement, positional and atomic displacement parameters, final R and Rw. A table of selected bond distances and bond angles may also be included.

Revised Manuscript and Computer Disks: Following the acceptance of a manuscript for publication and the incorporation of all required revisions, authors should submit an original and one more copy of the final manuscript typed double-spaced plus a 3½" disk containing the complete manuscript in Microsoft Word for Windows 2000 or a later version thereof. Original Figures should be submitted with the final, revised manuscript even if art is submitted electronically. All graphic files must be saved as TIFF images, and all illustrations must be submitted in the actual size at which they should appear in the journal. A list of the software programs used for text, art and file names on the disk should also be provided. Label the Disk with the author's last name, title of the manuscript, and date. Package the disk in a disk mailer or protective cardboard.

Reprints: Twenty (20) reprints are provided to the author responsible for correspondence free of charge. For orders of more reprints, a reprint order form and prices will be sent with article proofs, which should be returned directly to the Editor for processing.

Copyright

Submission is an admission by the authors that the manuscript has neither been previously published nor is being considered for publication elsewhere. A statement transferring copyright from the authors to Saudi Chemical Society is required before the manuscript can be accepted for publication. The necessary form for such transfer is supplied by the Editor-in-Chief with the article proofs. Reproduction of any part of the contents of a published work is forbidden without a written permission by the Editor-in-Chief.

Disclaimer

Articles, communication or editorials published by AJC represent the sole opinions of the authors. The publisher shoulders no responsibility or liability whatsoever for the use or misuse of the information published by AJC.

Indexing

AJC is currently applying for indexing and abstracting to all related International Services, including the Chemical Abstract Service and the Science Citation Index Service

Arabian Journal of Chemistry

Table of Contents

Arabian J. Chem. Vol. 1, No. 3, 219-226 (2008)

Disappearance of Chlorpyrifos Ethyl Pesticide Residues on Tomatoes, Citrus Fruits and Sugar Beet Grown in the Open Field

R. Salghi[1], H. Zerouali [2], M. Zougagh[3], A. Hormatallah[4], L. Bazzi[5], A. Chakir[6], A. Rios[3♣]

[1]Laboratoire d'Ingénieries des Procédés de l'Energie et de l'Environnement, Ecole Nationale des Sciences Appliquées, B.P 1136 Agadir, Maroc
[2]Laboratoire Régionale de l'Etablissement Autonome de Contrôle et de Coordination des Exportations de Berkane, Maroc
[3]Department of Analytical Chemistry and Food Technology, Faculty of Chemistry, University of Castilla-La Mancha, Av. Camilo José Cela s/n, E-13004 Ciudad Real, Spain
[4]Laboratoire des pesticides, Institut Agronomique et Vétérinaire Hassan II, Complexe Horticole d'Agadir, Maroc
[5]Laboratoire Environnement & Matériaux, Faculté des Sciences, B.P 8106 Agadir, Maroc
[6] GSMA,UMR CNRS 6089, Département de Chimie, laboratoire de Chimie-Physique, Faculté des Sciences, université de Reims, UMR 6089,Moulin de la housse, BP :1039, FR-51687 Reims Cedex 2, France

Abstract

In this study, the prevalence of chlorpyrifos ethyl in tomatoes, citrus fruit and sugar beet produced in an area of Northern Morocco (Berkane) was investigated. Samples were taken from the major production areas during 2005–2006. Another objective of this work was to evaluate the degradation behaviour and residue levels of chlorpyrifos ethyl in tomatoes, citrus fruits, and sugar beet grown in open fields under the typical climatic and growing conditions of Berkane. Analysis was carried out using gas chromatography with a nitrogen/phosphorus detector (GC-NPD) after extraction of samples with dichloromethane and clean-up using a florisil column. It was found that residue levels of chlorpyrifos ethyl ranged from 0.011 to 0.403 mg/kg for oranges, 0.004 to 0.405 mg/kg for tomatoes and 0.003 to 0.097 mg/kg for sugar beet. Most of the residue values obtained were far below the values imposed by European Union (EU) legislation. Only three samples contained chlorpyrifos ethyl levels that exceeded the recommended maximum limit in oranges for most of the EU markets. The decline behaviour of chlorpyrifos residues in oranges can be described as a pseudo-first order reaction. Residue levels and decline rates of chlorpyrifos ethyl in tomatoes, oranges and sugar beet sprayed with Dursban after the treatment were higher than the maximum residue limit established by the EU, the only exception was after pre-harvest intervals (PHI) of 21 days (tomatoes), 52 days (oranges) and 14 days (sugar beet). Half-life periods ($t_{1/2}$) were calculated for sugar beet (2 days), oranges (21 days) and tomatoes (8 days).

Keywords: Chlorpyrifos ethyl; oranges; tomatoes; sugar beet

♣ Corresponding author e-mail: angel.rios@uclm.es (A.Rios). telephone +34 926 29 53 00; fax +34 926295318,

1. Introduction

Knowledge of the dissipation rate of a pesticide after application is important to assess the behaviour of its residue. The time required to decrease the residues to half of their initial concentration, or less frequently to 1/5 or 1/10 of the initial concentration, is used to compare the persistence of the residues under different climatic or growing conditions. The decline curve can also be used to estimate the time required to decrease the average residue content below a specified level. On the basis of this information the pre-harvest interval can be adjusted to ensure that the residue content of the harvested crop will comply with a maximum residue limit (MRL)[1].

Numerous studies have previously been carried out on pesticides persistence and the dissipation of their residues in fruits [2-9], and since that time many pesticides (organochlorin and organophosphorus compounds, pyrethroides, etc.) have been monitored for MRLs in fruit and vegetables according to EU regulations [10].

Long-cycle tomatoes grown in a greenhouse develop throughout winter and part of spring. Fruits ripen gradually and are usually harvested weekly. Therefore, to protect tomatoes from pathogens, such as grey mold (Botrytis cinerea) and grey mildew (Phytophtora infestans), pesticides with a short pre-harvest interval (PHI) of one week or less are required. Conventional fungicides [11-12] have shown resistance phenomena due to their extensive use. As a result, these compounds do not give sufficient protection and the PHI of most of these pesticides is too long and this makes them unsuitable for greenhouse harvesting periods.

In Morocco, tomatoes and citrus crops are considered to be high value cash crops for farmers and they are also a source of hard currency. The annual production of these crops is over 1200,000 tons, of which about 60% is exported – particularly to EU countries. Souss Massa valley (Agadir) and the North of Morocco (Berkane) are the major regions for tomato and citrus production in Morocco, exporting about 80% of the crops to the EU [13]. In an effort to improve the yield and the fruit quality, advanced technologies, such as the use of greenhouse systems and new irrigation and fertilization techniques, are considered and implemented by farmers.

Chlorpyrifos ethyl (O,O-diethyl-O-3,5,6-trichloro-2-pyridylphosphorothioate) is the common name of an organophosphorus insecticide discovered and introduced by Dow Agro Sciences, and this compound is effective for the control of a range of agronomic pests – particularly California red scale *Aonidiella auranti* in citrus crops, prodenia in sugar beet and noctueda in tomatoes [14]. The structure of chlorpyrifos ethyl is shown in **F**ig.1.

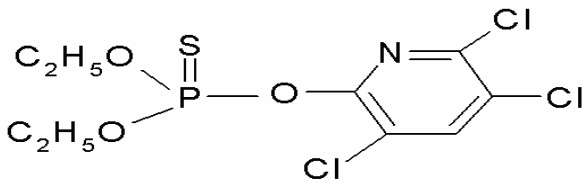

Figure 1. Chemical structure of chlorpyrifos ethyl.

The objective of the work described here was to investigate the prevalence of chlorpyrifos ethyl in citrus fruit, tomatoes and sugar beet produced in an area in Northern Morocco (Berkane). An additional objective of this work was to evaluate the degradation behaviour and residue levels of chlorpyrifos ethyl in citrus fruit, tomatoes and sugar beet grown in open fields under the typical climatic and growing conditions of Berkane.

2. Experimental

Materials and reagents

All organic solvents were obtained from Panreac (Barcelona, Spain). Chlorpyrifos ethyl certified standards of purity 99.6% were supplied by Dr. Ehrenstorfer (Augsburg, Germany) and provided by Labservice Analytica, Bologna (Italy). Standard stock solutions (500 mg/kg) were prepared in acetone. Standard solutions for gas chromatographic (GC) analysis were prepared by suitable dilution of the standard stock solutions with blank crop extracts. Florisil columns (Panreac, Barcelona, Spain) were used as received for the on-column clean-up. Anhydrous sodium sulphate pesticide (residue grade) (Panreac, Barcelona, Spain) was used.

Samples

The presence of chlorpyrifos ethyl found in citrus fruit, tomatoes and sugar beet in an area of Northern Morocco (Berkane) was investigated. A sample of 20 growers for each crop grown in open fields was randomly selected for this study. Each sample corresponds to a single grower. The collection dates for samples were between 15/10/05 and 15/07/06. Each sample consisted of 120 fruits. All samples were transported to the laboratory and stored in a cold room at 4 °C until further use. From the 120 fruit samples per grower, only a sub-sample of 10 fruits was chosen for analysis of pesticide residues according to the method described by [15].

The study was carried out at a farm located in the Triffa area of Northern Morocco (Berkane, Morocco). The plantation size was 1 hectar of citrus fruit, 500 m^2 of tomatoes and 900 m^2 of sugar beet. A plot planted with "Valencia" oranges in 1972 and grafted on sour orange rootstock at a spacing of 6 x 4 meters led to a density of about 250 trees/ha. The tomato planting density (variety Daniella) was 20000 plants/ha and sugar beet. The treatment was carried out with Dursban (chlorpyrifos ethyl 480 g/l) as a commercial formulation applied at the dose recommended by the manufacturer (150 cc/hL) with a portable motor sprayer. The pesticide was applied as a single application only. Three pre-treated samples were collected at random at 0, 3, 7, 14, 21, 28, 35, 42, 49, 56 and 66 days after spraying with pesticide; each sample consisted of 10 pieces of citrus fruit, however tomatoes and sugar beet. The maximum and minimum average temperatures were 30 and 25 °C, respectively.The samples were placed into polyethylene bags and transported to the laboratory, where they were chopped and thoroughly mixed. The samples were deep-frozen until analysis was carried out. In all cases, < 90 min passed between harvest and storage in the freezer and analyses were always carried out between 24 and 48 hours after samples were removed from the freezer.

Extraction and clean-up

The method used for the extraction of chlorpyrifos ethyl on citrus fruit, tomatoes and sugar beet was adapted from Charles and Raymond [16]. For each 50 g of the sample ground using a food processor (Type, model blender), 100 ml of acetone was added and the mixture was stirred for 2 hours. The extraction was carried out, with 100 ml and 50 ml of acetone, respectively. After filtration, the residues in acetone were partitioned with saturated aqueous sodium chloride (30 ml) and dichloromethane (70 ml) in a separating funnel. The dichloromethane fraction was collected and the separation process with (70 ml)

dichloromethane were combined and dried over anhydrous sodium sulphate. The solvent was removed under reduced pressure at 40 °C and the residues were dissolved in an acetone-hexane (1:9) mixture (10 ml) for clean up. For clean-up, 1 ml of the extract was passed through a florisil column that was conditioned with 5 ml of acetone/hexane (6:4) and also, with conditioned 5 ml of hexane. The pesticide residues were eluted with acetone/hexane (6:4) (4 ml).Then, samples were analysed by gas chromatography.

GC analysis

Analysis of the chlorpyrifos ethyl pesticide was carried out with a Hewlett–Packard 6890 gas chromatograph equipped with an NPD Detector, split/splitless injection port, and HP-5 column (5% diphenyl copolymer/95% dimethylpolysiloxane) (25 m × 0.32 mm ID, 0.52 μm film thickness). The temperature programme applied in GC/NPD was as follows: 80–160 °C at 25 °C/min, 160–220 °C at 10 °C/min, 220–240 °C at 1 °C/min, 80 °C (3.00 min), 160 °C (2.00 min), 220 °C (10.00 min) and 240 °C (8.80 min). The injection volume was 1 μl. The temperature of the detector was 300 ºC.

3. Results and discussion

Analytical procedure

Calibration graphs were obtained using standard solutions of chlorpyrifos ethyl over the range 0.002–1 mg/kg. Each solution was injected in triplicate. The linear range, intercept and slope of the curve are given in **T**able 1 along with the regression coefficient for chlorpyrifos ethyl.

Table 1. **Analytical characteristics of the method.**

Parameter	Chlorpyrifos ethyl	
Working concentration range (mg/kg)	0.002–0.05	0.05–1
Intercept (a±S_a)	0.2088±0.2957	–36.078±15.306
Slope (b±S_b)	1659.4±10.6	1717.4±31.8
Standard deviation of residuals ($S_{y/x}$)	0.4690	25.059
Regression Coefficient (R^2)	0.9998	0.9986
Precision, R.S.D. (%) (n = 10)	2	3
Detection limit (mg/kg)	0.001	0.044

The precision of the method for aqueous standards (evaluated as the relative standard deviation obtained after analysing 10 series of 10 replicates) was 2% at the 0.030 mg/kg level of chlorpyrifos ethyl and 3% at the 0.500 mg/kg level. The theoretical limit of detection, defined as the concentration of the analyte that gives a signal equivalent to the blank signal plus three times its standard deviation, was 0.001 mg/kg in the range 0.002–0.05 mg/kg and 0.044 mg/kg in the range 0.05–1 mg/kg.

Untreated samples were fortified by adding intermediate chlorpyrifos ethyl solution in dichloromethane. Samples were allowed to equilibrate for 2 hours prior to extraction and were processed according to the earlier procedure. The recovery, repeatability at the LOQ level and MRLs established by the EU or Spanish legislation are given in **T**able 2.

Table 2. **Average recoveries and coefficient of variation percentages for chlorpyrifos ethyl subjected to analysis**

Food sample	LOQs[a] (mg/kg)	N of Samples	Average recovery (%)	R.S.D (%)	MRLs (mg/kg)
Tomatoes	0.003	50	93	5.5	0.5
Citrus fruit	0.007	20	92	6.3	0.3
Sugar beet	0.002	60	98	4.5	0.05

[a]LOQ was defined as the minimum level at which chlorpyrifos ethyl can be quantified with acceptable accuracy (>80%) and precision (<10%).

The LOQs range from 0.002 to 0.007 mg/kg, which are well below the permitted MRLs. The results obtained showed that this method is efficient for the analysis of chlorpyrifos ethyl in orange, tomato and sugar beet samples.

Monitoring data

The chlorpyrifos ethyl concentrations found in tomato, citrus fruit and sugar beet samples analysed are given in **T**able 3.

Of the 20 tomato samples analysed, chlorpyrifos ethyl was detected in 18 (90%) at concentrations ranging from 0.004 to 0.405 mg/kg, but the levels of this pesticide were below the MRLs established by the European communities, 2004. Chlorpyrifos ethyl was detected in all orange samples analysed (100%), at concentrations ranging from 0.011 to 0.403 mg/kg and three of these samples (15%) showed levels higher than those established by MRLs. In the case of sugar beet, chlorpyrifos ethyl was detected in 16 samples (80%) at concentrations ranging from 0.003 to 0.097 mg/kg, with four samples (20%) exceeding the EU MRLs.

Disappearance of chlorpyrifos ethyl from tomatoes, oranges and sugar beet

The residue data, including mean values and standard deviations, obtained in the decline study after treatment of chlorpyrifos ethyl are summarized in **T**able 4.

Table 3. Occurrence of chlorpyrifos ethyl residue in tomatoes, oranges and sugar beet

	Residues (mg/kg) mean ± S.D		
Sample	Tomatoes	Oranges	Sugar beet
1	0.303 ± 0.010	0.130 ± 0.006	0.008 ± 0.002
2	0.105 ± 0.007	0.015 ± 0.004	0.009 ± 0.007
3	0.024 ± 0.003	0.105 ± 0.007	0.045 ± 0.008
4	n.d	0.152 ± 0.001	0.017 ± 0.002
5	0.025 ± 0.003	0.171 ± 0.004	0.023 ± 0.003
6	0.120 ± 0.002	0.012 ± 0.003	0.004 ± 0.001
7	0.015 ± 0.001	0.091 ± 0.004	n.d
8	0.132 ± 0.004	0.354 ± 0.005	0.065 ± 0.005
9	0.011 ± 0.002	0.021 ± 0.006	0.004 ± 0.001
10	0.009 ± 0.001	0.403 ± 0.008	n.d
11	0.008 ± 0.001	0.325 ± 0.008	0.097 ± 0.001
12	0.405 ± 0.009	0.011 ± 0.001	n.d
13	0.152 ± 0.009	0.253 ± 0.009	0.041 ± 0.004
14	0.120 ± 0.001	0.032 ± 0.005	0.040 ±0.001
15	0.004 ± 0.001	0.015 ± 0.006	0.003 ± 0.001
16	n.d	0.014 ± 0.004	0.072 ± 0.005
17	0.053 ± 0.003	0.043 ± 0.009	0.065 ± 0.004
18	0.032 ± 0.009	0.012 ± 0.003	0.021 ± 0.006
19	0.015 ± 0.001	0.205 ± 0.006	n.d
20	0.053 ± 0.008	0.114 ± 0.009	0.003 ± 0.001

Table 4. **Disappearance of chlorpyrifos ethyl from tomatoes, oranges and sugar beet after treatment**.

No. days	Residue (mg/kg), Mean ± S.D, Days after treatment		
	Tomatoes	Orange	Sugar beet
0	1.93 ± 0.08	1.50 ± 0.02	6.20 ± 0.06
3	1.52 ± 0.04	1.30 ± 0.03	0.47 ± 0.05
7	1.10 ± 0.20	1.11 ± 0.05	0.15 ± 0.05
14	0.70 ± 0.01	0.90 ± 0.08	0.05 ± 0.01
21	0.50 ± 0.04	0.80 ± 0.03	0.02 ± 0.00
28	0.07 ± 0.01	0.61 ± 0.02	-
35	0.01± 0.00	0.59 ± 0.01	-
42	-	0.50 ± 0.02	-
49	-	0.46 ± 0.05	-
56	-	0.28 ± 0.07	-
66	-	0.20 ± 0.05	-
$t_{1/2}$ (days)	8	25	2
PHI (days)	21	52	14

Chlorpyrifos ethyl residue levels in tomatoes, oranges and sugar beet after treatment were higher than the maximum residue limit established by the European communities, 2004 as shown in (**T**able 4). The only exception was after pre-harvest intervals (PHI) of 21 days (tomatoes) and 52 days (oranges). These results indicate that the pre-harvest interval (PHI) was about 14 days for sugar beet. Similar results were reported by Oturan & al [17] for procymidone, iprodion and imazalil in grapes. The $t_{1/2}$ value calculated for sugar beet (2 days) is very similar to those obtained by Aguilera & al, 2003 for green beans grown in the greenhouse and by Navarro & al [18] for grapes. The $t_{1/2}$ value obtained in this work for oranges (21 days) is comparable to the $t_{1/2}$ value reported by Montemurro & al [19]. The $t_{1/2}$ value reported for tomatoes (8 days) is the same as that obtained by Gonzalez & al [20] for methamidophos and by Castillo & al [21] for procymidone.

The logarithms of the residue concentrations are plotted versus time in **F**ig. 2.

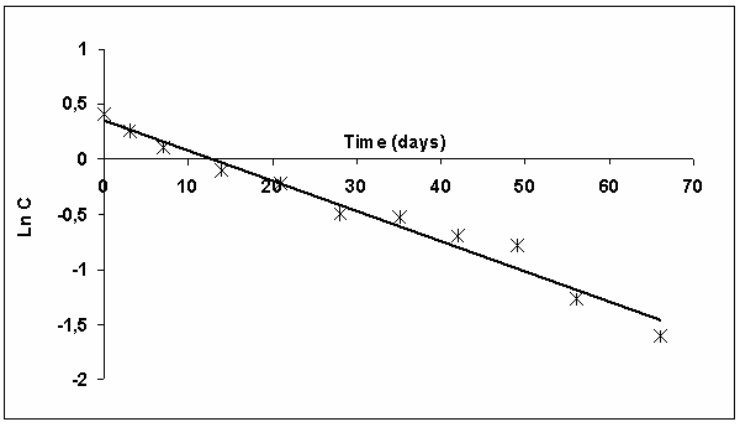

Figure 2. **A graph shows the residue decline curve for chlorpyrifos in oranges [C : Residues (mg/kg)].**

The graph indicates that the decline behaviour of chlorpyrifos residues in oranges can be described as a pseudo-first order reaction. This is the approach usually assumed for the interpretation of residue decline experiments [22-25].

4. Conclusions

The results obtained in the work described here enable to draw a number of conclusions. The residue level for chlorpyrifos ethyl found in oranges ranges from 0.01 to 0.40 ppm, tomatoes (0.004 to 0.30) and sugar beet 0.003 to 0.09 ppm . Most of the residue levels determined are well below the limits imposed by EU legislation.

Only three samples were found to have a value above 0.40 ppm of chlorpyrifos ethyl, which is higher than the recommended maximum limit of 0.30 ppm in oranges for most EU markets.

Residue levels and decline rates of chlorpyrifos ethyl in tomatoes, oranges and sugar beet sprayed with Dursban after treatment were higher than the maximum residue limit established by the EU, the only exception was after pre-harvest intervals (PHI) of 21 days (tomatoes), 52 days (orange) and 14 days (sugar beet). The half-life periods ($t_{1/2}$) were calculated for sugar beet (2 days), oranges (21 days) and tomatoes (8 days). The decline behaviour of chlorpyrifos residues in oranges can be described as a pseudo-first order reaction.

References

[1] Ambrus, A., Lantos, J., *J. Agric. Food. Chem*, 50, 4846 (2002).

[2] Zerouali, E., Salghi, R., Hormatallah, A., Hammouti, B., Benkaddour, M., Zine, E., & Bazzi, L., *Phys. Chem. News*, 32, 102 (2006).

[3] Zine, E., Salghi, R., Bazzi, L., Hormatallah, A., Ait Addi, E., Ait Oubahou, A., & Chaabene, H., *Fresen. Environ. Bull*, 15 (4), 255 (2006).

[4] Zerouali, E., Salghi, R., Hormatallah, A., Hammouti, B., & Bazzi, L., *Fresen.Environ. Bull*, **15 (4),** 267 (2006).

[5] Salghi, R., Hormatallah, A., Boulaid, M., & Bazzi, L., *Phys. Chem. News*, **32**, 70 (2006).

[6] Hormatallah, A., Zine, E., Salghi, R., & Benabdi, R ., Proceedings du Symposium sur la protection intégrée des cultures dans la Région Méditerranéenne, Rabat, 29-31.Dépôt légal 681/2001. 321 (2001).

[7] Munoz, J. A., Fernandez, E.F., Aguso, L.E.G., Casado, A.G., & Rodiguez, L. C., TALANTA, **60**, 433 (2003) 447.

[8] Ito, Y., Ikai, Y., Oka, H., Hayakawa, J., & Kagami,T.(1998)., *Journal of Chromatography A*, **810**, 81 (1998).

[9] Lbeda,C., Pico,Y., Font, G., & Manes, J. (1994)., *Journal of AOAC*, **77**, 74 (1994).

[10] Anastassiades,M,. Lehotay,S.J., Štajnbaher, D., & Schenck, F.J.(2003)., *Journal of AOAC*, **86 (2),** 412 (2003).

[11] Cabras, P.; Cabitza, F.; Meloni, M.;& Pirisi, F. M., *J. Agric. Food Chem*, **33**, 935 (1985).

[12] Cabras, P.; Meloni, M.; Pirisi, F. M.; & Cabitza, F., *J. Agric. Food Chem*, **33**, 86 (1985)

[13] Etablissement Autonome de Contrôle et de Coordination des Exportations (EACCE). Ministre de l'Agriculture et de la Pêche Maritime. (2006). Statistiques Export Maroc, www.eacce.org.ma

[14] Direction de la Protection des Végétaux des Contrôles Techniques et de la Répression des Fraudes (DPVCTRF), Ministère de l'Agriculture et des Pêches Maritines, Index Phytosanitaire 2007

[15] Direction Générale de la Concurrence et de la Consommation des Répressions de la France (DGCCRF) (1998), Méthode d'échantillonnage des fruits et légumes.

[16] Charles, R. W., & Raymond, T.H.T.(1991). The Pesticide Manual, 9th edition, 212

[17] Oturan, M.A., Aaron, J.J., Oturan, N.,& Pinson, J. (1999)., *Pesticide Science*, 55, 558 (1999).

[18] Navarro, S., Oliva, J., Navarro, G., & Barba, A., Ann. *J.Vitic*, 52, 35 (2001).

[19] Montemurro,N., Grieco, F., Lacertosa, G., & Visconti, A., (2002)., *J. Agric. Food Chem*, 50 (21); 5975 (2002).

[20] Gonzalez, F. J. E., Martinez Vidal, J.L.; Castro C.M.L., & Martinez Galera.M., *J. Chromatography*, 829 (1998) 251

[21] Castillo Sanchez, J., Aguilera del Real,A., Roodriguez Sanchez, M., & Valverde Garcia, A., J. Agri. Food Chem, 48, 2991 (2000).

[22] Aguilera del Real, A., Rodriguez Sanchez,M., & Valverde Garcia, A. (2003)., *Ital. J. Food Sci*, 15, 141 (2003).

[23] Murray,R.T., Von Stein,C., Kennedy,I.R., & Anchez Bayo,F.(2001). *J. Agric. Food Chem*, 49, 2844 (2001)

[24] Bouaid, A., Martin Esteban,A.,Fernandez, A., & Camara,C., *Amn. Chim*, 91, 93 (2001)

[25] Mukherjee, I., & Gopal, M., *Pestic.Sci*, 36(3), 175 (1992).

Acknowledgements

The Agencia Española de Cooperación Internacional (AECI) is gratefully acknowledged for funding this work with Grant A6326/06. The support given through a "Juan de la Cierva" research contract for M.Z. is also acknowledged. The authors wish to thank the NATO program (CBP.MD.CLG 983108) for supporting this Work.

Arabian J. Chem. Vol. 1, No. 3, 227-238 (2008)

Simultaneous Dissolution Profile of Two Drugs in Solid Oral Dosage Forms by the Standard Official Assembly

Joana D. de Rocha Pereira, Cláudia I. T. Gouvinhas, J. R.

Albert-Garcia and J. Martinez Calatayud*

Department of Analytical Chemistry. University of Valencia. Valencia(Spain)

***Corresponding author (jose.martinez@uv.es)**

Abstract

The article is dealing with the simultaneous determination of three dissolution profiles of pharmaceutical formulations containing two drugs with overlapped UV-vis spectra. The officially proposed procedure from the pharmacopeias is adapted to the derivative spectrophotometery methodology. The simultaneous determination of the three profiles is based on the first derivative spectra and the zero crossing mathematical procedure. The empirical profile was adjusted by regression analysis using different approaches. The three simultaneously obtained profiles were the " global profile" and the corresponding to each one of the two present active principles. Tested couples of pharmaceuticals were Paracetamol – Methocarbamol and Hesperidin- Diosmin.

Keywords: Pharmaceutical; Dissolution profiles; In-vitro availability tests; Paracetamol, Methocarbamol; Hesperidin; Diosmin.

1. Introduction

Test the dissolution rates of the active principles present in a pharmaceutical formulation, also, known as " in vitro-availability, is a test established as a compulsory in relevant international pharmacopeias [1-3] not only as a test of the availability [4] of the formulation; but it is an interesting way to check the reproducibility of the manufacture and even to check the generic formulations.

The results of this test not only are due to the chemical contents but also to physical properties of the dosage as the particle size or the binder composition [5]. Dissolution testing is relevant due to different reasons as it facilitates drug quality control and in addition, it derives comprehensive information about the dynamics of the dissolution processes which is a first step to facilitate the development of new dosage forms.

The officially recommended method resulted in a "global" (overall) dissolution profile; the spectro-photometeric measurements are the result of all soluble compounds present in a formulation; only insoluble products are separated on-line. However, efforts are made to obtain "individual" profiles and more strategies have been developed [6-10]. The importance of an individual profile is also interesting on the basis of the reasons for obtaining the global profile; as the availability or the manufacture control.

Paracetamol also known as acetaminophen is the *N*-(4-hydroxiphenil)acetamide and its molecular structure is illustrated in Figure 1. It is a crystalline white powder , odourless and soluble in water (1/70)[11]. It is widely used as analgesic and antipyretic for headache and other moderated pains. It is also considered as a light anti-

inflammatory and is also formulated jointly with other non-steroid anti-inflammatories for more serious pain.

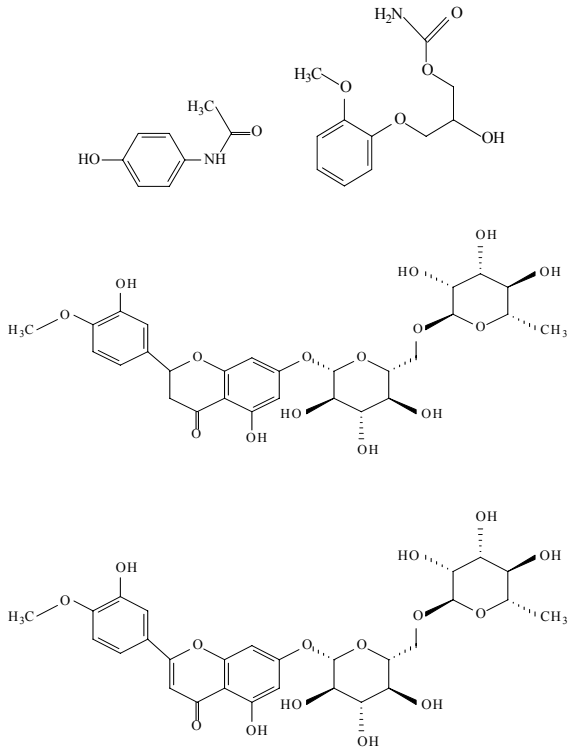

Figure 1. Structural formula of the studied pharmaceuticals on top, Paracetamol (left) and Methocarbamol (right). Hespiridin (middle) and Diosmin (bottom)

Methocarbamol is the [2-hydroxi-3-(methoxiphenoxi)-propil] aminoformate [12,13] and its structural formula is depicted also in Figure 1. It is odourless white powder soluble in water (1/40). Methocarbamol, a muscle relaxant, is used with rest, physical therapy, and other measures to relax muscles and relieve pain and discomfort caused by strains, sprains, and other muscles injuries.

Hesperidin is a flavonoid (a flavonone glycoside) and the molecular structure is illustrated in Figure 1; it is the 4H-1-Benzopyran-4-one,7-[[6-O-(6-deoxy-alpha-L-mannopyranosyl)-beta-D-glucopyranosyl]-oxy]-2,3-dihydr-5-hydroxy-2-(3-hydroxy-4-methoxy-phenyl) and it is prescribed as antioxidant according to in vitro studies. In human nutrition it contributes to the integrity of the blood vessels . Various recent preliminary studies reveal novel pharmaceutical properties [14,15].

The Diosmin is the 7-((6-O-(6-Deoxy-ga-L-mannopyranosyl)-beta-D-glucopyranosyl) oxy)-5-hydroxy-2-(3-hydroxy-4-methoxyphenyl)-4H-1-benzopyran-4-one. It is also a member of the flavonoid family and is considered as a semi-synthetic phlebotropic drug. It is also used in the treatment of venous disease, ie, chronic venous insufficiency and hemorrhoidal disease (with the Hesperidin), in acute or chronic hemorrhoids, in place of rubber-band ligation , in combination with fiber supplement, or as an adjuvant therapy to hemorrhoidectomy, in order to reduce secondary bleeding. The molecular structure is shown in Figure 1.[16].

This article deals with the simultaneous recording of the " global" profile according to the pharmacopeias and simultaneously the two "individual" dissolution profiles from the two active principles present in the same pharmaceutical formulation . All this was performed with the aid of a diode array UV-vis spectrophotometer allowing a simultaneous recording the absorbance of the solution at several wavelength values. The procedure is based on the derivative spectrophotometery for deconvolution of overlapped spectra. The use, applications and advantages of derivative spectrophotometry to drug analysis have been reported elsewhere [17-24]. For the present work two binary mixtures of pharmaceuticals, Paracetamol-Methocarbamol and Hesperidin-Diosmin were selected. The proposed mathematical method is the zero crossing on the spectrum from the first derivative.

2. Experimental

Reagents and apparatus :

All reagents used were analytically pure unless stated otherwise. Solutions were prepared in a purified water by reverse osmosis and then deionised (18 MΩ-cm) with a Sybron /Barnstead Nanopure II water purification system provided with a fiber filter of 0.2 μm pore-size.

The assayed pharmaceuticals were Paracetamol (Guinama), Methocarbamol (Guinama), Diosmin (Sigma) and Hesperidin (Fluka). Other used reagents were acids and alkalis to adjust the pH of the solutions, mainly hydrochloric acid and sodium hydroxide (both from Scharlau Chemie S.A) and, organic solvents to check other media, like acetonitrile (Scharlau Chemie S.A), and methanol (Merck KGaA). Pharmaceutical formulations were ROBAXISAL COMPUESTO, (from FAES FARMA, S.A.) with the following contents: Paracetamol 300 mg and Methocarbamol 380 mg; and, DAFLON 500 mg with label claim, Diosmin 450 mg and Hesperidin 50 mg (from Laboratőrios Servier, S.L. Madrid).

Assembly

pH of the solutions was potentiometrically measured using a pH-meter Crisom GLP (from Crisom Instruments, S.A) provided with a double electrode glass/calomel. UV-vis spectra and solution profiles were recorded with the aid of a diode array spectrophotometer model HP5453 (from Hewlett Packard) with a flow-cell Helma 6Q (Helma GmbH & co Mùlheim) of 1 cm light-path using the software UV-Visible Chemstation (Agilent Technologies) while data were treated with the aid of the Microsoft Office Excel, 2003 (Microsoft Corporation).

The flow assembly to obtain dissolution profiles was provided with a mechanical stirrer Heidolph RZR 2021(Heidolph) at 50 rpm (120 rpm for the mixture Diosmin-Hesperidin) and a home-made glass dissolution vessel with a size and shape according to the instructions from pharmacopeias. This vessel was immersed into a water bath at 37 ^{o}C, model Tectron 2000(J.P Selecta, S.A). The continuous-flow was generated by a peristaltic pump Minipuls 2 (from Gilson) and all tubings were of PTFE with 0.8 mm internal diameter (from Omnifit). The pump tubing was of Tygon R3607 (Ismatec) with an i.d. 2.06 mm; and an on-line nylon filter (pore-size 0.4 mm) placed at the tip of the tubing to retain insoluble matter from solution vessel. The experimental assembly is shown in Fig. 2.

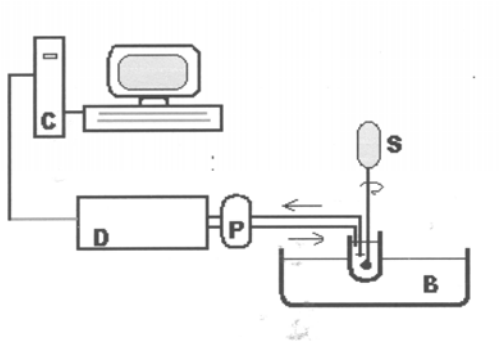

Figure 2. Experimental assembly to obtain the solution profiles C, computer, D, Spectrophotometeric detector; B, water-bath; P, peristaltic pump; and S, mechanical stirrer arm.

Procedure

Sample preparation and treatment:

For UV-vis spectra recording (in batch) several tablets were taken and powdered and the required amount was separated and weighed, dissolved and filtered to avoid any insoluble excipients to mark with the required medium.

To obtain solution profiles a tablet was placed in a platinum basket nesting in the tip of the metallic rod of the mechanical stirrer as described in the Pharmacopoeia, then introduced in a 0.1 mol l^{-1} HCl solution (mixture Paracetamol-Methocarbamol) or 0.01 mol l^{-1} NaOH

solution (mixture Diosmin-Hesperidin) both of them at 37 ^{o}C.

Dissolution profiles:

Preliminary experiments in batch aimed to establish the procedure for the simultaneous profiles of both pharmaceuticals; optimum pH or solvents. Solutions were tested at different pH values to select the best pH for simultaneous determination after obtaining the first and second spectral derivatives.

Finally the dissolution profiles were experimentally performed and the obtained results were adjusted by regression with the aid of the software program KaleidaGraph 4.0, from Synergy software. Absorbance at 254 nm was used to obtained the " global" dissolution profile of the whole formulation.

Regression analysis of the obtained plots

To check the reproducibility of the resulting profiles two different kind of equations were tested : first. Several degree polynomial equations were tested and their comparative study based on the calculation of the average of the RSD (in %) for each coefficient. The 3-parameters regression [25] and the equation which has been proposed for the mathematical fitting of the hyperbolic type plots like the obtained enzymatic reactions (body-antibody kinetic processes).

$$V_2 = a/(1 + b/V_1)^c$$

The depicted parameter meanings are:

a: signal figure (first absorbance derivative) when the total solution is finished; b: half-maximum signal or the signal at half-time of the required interval for total dissolution ; and c: the exponent corresponding to the slope of the increasing interval of the profile.

Computerised calculations were performed with the aid of the program "Statistica" working in windows, (Copyright Statsoft. Inc 1993) and the results can be seen in Table 1.

Table 1. Calibration graph for Paracetamol, Methacarbamol Diosmin and Hesperidin .. (Tested linear 2.5-25 mg l^{-1})

Parameter	Paracetamol (213 nm)	Methocarbamol(216 nm)	Hesperidin (248 nm)	Diosmin (286 nm)
Slope*	0.00230	0.00034	0.00227	0.00962
R.S.D(%)	4.8	4.3	3.5	4.9
Correl. Coeffic.*	0.9978	0.9995	0.9998	0.9998
R.S.D(%)	0.86	0.35	0.62	0.64

3. Results and Discussion

1. Mixture Paracetamol-Methocarbamol

Tests were carried out to assay the simultaneous determination of Paracetamol and Methocarbamol in a binary mixture. The first step was to record spectra of individual solutions containing 25 mg l^{-1} of the dissolved pharmaceutical; spectra were recorded from 190.0 to 400.0 nm and then the corresponding first and second derivative spectra were obtained to find the zero crossings. The studied pH range was from 1 to 12; it was potentiometrically controlled by adding drops of HCl or NaOH, as needed.

After recording first and second derivatives of each studied pH value, the corresponding spectra for Paracetamol and Methocarbamol (at same pH and derivative order) were compared. The first conclusion was that the second derivative at zero crossings did not present clear advantages over the first ones. In addition to that (as expected) the signals were found to be lower than the corresponding first derivative. Consequently, only the first derivative spectra were selected for further work.

The second conclusion from the comparative study that could be drawn was found that either the acidic media or a media with pH over 8.5 presented higher $dA/d\lambda$ values, especially in the range 0.5-2.5. Thus the pH range over 0.5-2.5 and from 8.5 to 10.5 were refined as they presented the best possibility to differentiate both pharmaceuticals. Then, the first order outputs were found higher in the acidic pH range and small pH variations do not resulted in significant spectral changes which mean also better reproducibility.

Different solvent mixtures (water-methanol and water-acetonitrile at 1%, 5% and 10% organic solvent) were also tested to find better differences in zero crossings, with pharmaceutical content was 10 mg l^{-1}. The results obtained were not better than the results obtained by using pure aqueous medium. Same conclusion obtained even when using different ratios of the mixture of water-methanol; i.e 9:1 , 8:2 , 7:3 , 6:4 and 5:5, in addition to using pure methanol.

According to these experimental results and the Pharmacopeias recommendation to use 0.1 mol l^{-1} HCl solution to obtain the solution profiles for this kind of pharmaceuticals, the 0.1 mol l^{-1} HCl was selected. This means that neither pH changes were required from vessel solution to spectrophotometric measured, nor an FIA or Multicommutation manifolds were requirement for the simultaneous determination of dissolution profiles as it was established in previous papers[6-10]. Due to that, the standard recommended assembly[1] was reproduced.

Several zero crossings were found in the first derivative of both pharmaceuticals, namely : a) from the Methocarbamol first derivative spectra were selected 213, 222 and 246 nm; then, b) 216 and 243 nm from Paracetamol results.

To implement the obtained results, calibration graphs were plotted either in batch and in continuous-flow as a way to check the reproducibility. Calibrations were performed on the results of $dA/d\lambda$ at the pre-selected zero crossings and reported above. Solutions of each separated active principle were prepared (2.5 , 5 , 10, 15 and 25 mg l^{-1}) at pH 1 with HCl. Flow measurements were performed by using a simple assembly comprising a peristaltic pump and a solenoid valve to control the sample volume. Five independent assays were performed to obtain the R.S.D. (%). According to the obtained results (slope and correlation coefficient) the selected wavelengths were 213 and 216 nm for Paracetamol and Methocarbamol, respectively. To check the reproducibility, five independent calibrations were performed in different days and with freshly prepared solutions and the calculated R.S.D (%)

were 4.8 and 4.3 for Paracetamol and Methocarbamol, respectively. Results obtained could be seen in Fig. 3 and Table 1.

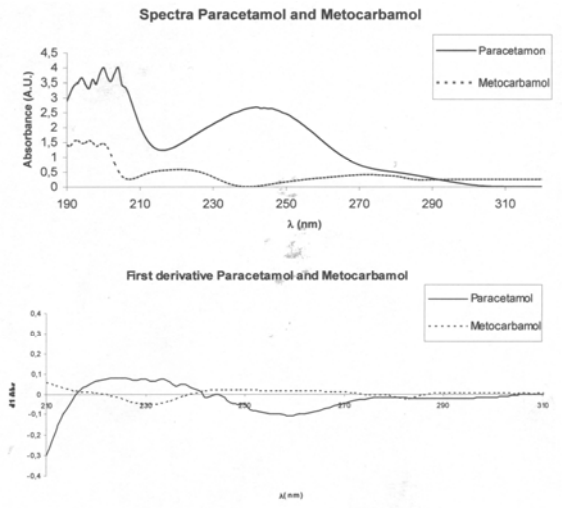

Figure 3. Spectra of Paracetamol (pH 1.2) and Methacarbamol (pH 1.6) at acidic media .

2. Mixture Hesperidine-Diosmin

The performed tests to assay the simultaneous determination of Hesperidin and Diosmin in a binary mixture tried to follow a similar experimental procedure as described for the mixture Paracetamol-Methocarbamol ; the difference was the small aqueous solubility of these pharmaceuticals or almost null depending on the pH. The first step was to record spectra of individual solution which was performed on saturated solutions (under 25 mg l^{-1}) of the dissolved pharmaceutical; spectra were also recorded on the pH range from 1 to 12 and the wavelengths used from 190.0 to 400.0 nm. Then, the first and second derivative spectra were obtained to find the zero crossings by comparing the corresponding spectra of Hesperidin and Diosmin. Results clearly demonstrate that the solubility of both pharmaceuticals increased with the pH resulting in having suitable spectra at pH 12 (NaOH 0.01 mol l^{-1}) and over.

Aqueous solutions were prepared containing different pharmaceutical concentrations, from 2.5 to 25 mg l^{-1}, and spectra were recorded from 190 to 400 nm. Zero, first and second order drrivatives were recorded. Both drugs presented similar spectra as it was expected from their structural formulae; only small differences were observed at higher tested concentrations where the peak at 240 (see Figure 4) showed a bathochromic shift for Diosmin. Peaks at 240, 270 and 290 (for both pharmaceuticals) are due to the presence of multi-chromophoric groups with electronic transitions π-π^* as both have aromatic rings with increased activity by the auxochromic OH^- group. The obtained useful " zero crossings" in the first derivative spectra were as follows: two crossings at λ 248 nm and 268 nm from Diosmin spectra; and three zero points at 241, 264 and 286 nm for Hesperidin. Second derivative spectra resulted in lower outputs, thus only the first derivatives spectra were selected for further work. Dissolution profiles were obtained at 120 rpm as a lower speed (while the recommended speed is 50 rpm) the kinetics of the solubility resulted in filter occlusions. pH 12 was selected for further work.

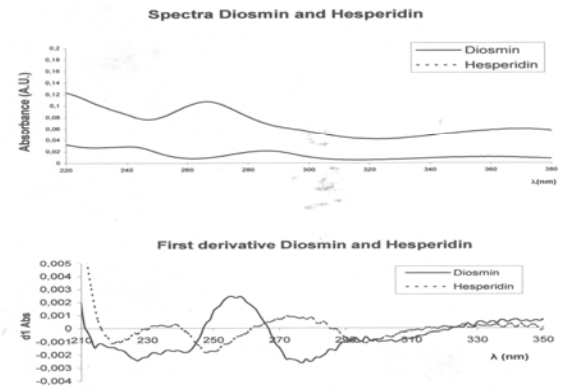

Figure 4. Spectra of different derivative order (zero, first) of the Diosmin and Hesperidin at basic pH (12.0).

Calibration curves (dA/dλ vs concentration) were plotted at the reported zero crossings wavelengths as

a way to choose the suitable wavelength to carry out the dissolution assay. Solutions of each separated active principle were 2.5 , 5, 10, 15 and 25 mg l^{-1} at pH 12 and the wavelength selection was made on the basis of the higher slope and correlation coefficients. Selected values for further work were 286 and 248 nm for Diosmin and Hesperidin measurements, respectively.

Different solvent mixtures (water-methanol and water-acetonitrile) were also tested to find better differences in zero crossings. However, experimental obtained results were not better than the obtained results in pure aqueous media.

Dissolution Tests

Mixture Paracetamol-Methocarbamol

The dissolution profiles for the formulation Robaxisal Compuesto, (from FAES FARMA, S.A.) with a label claiming: Paracetamol 300 mg and Methocarbamol 380 mg; were carried out at the following wavelengths: 213 nm for Paracetamol, 216 for Methocarbamol and 254 nm for the "global" profile [1]. Experimental results allowed us to obtain three solution profiles, shown in Figure 5. Results were successively recorded ten independent times (with freshly prepared solutions) and they were analysed by regression to calculate the corresponding equations. The results obtained using the three-parameters equation Higuch equation are illustrated in Table 2.

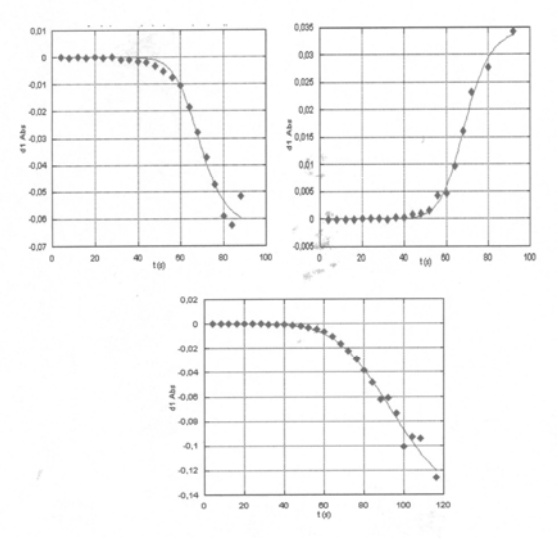

Figure 5. Dissolution profiles of Robaxisal compuesto Paracetamol 213 nm (top left); Methocarbanol, 216 nm (top right); and Global, 254 nm (bottom).

Table 2. Results from dissolution assays of the commercial formulation Robaxisal Compuesto (Higuchi equation).

Dissolution assays	Paracetamol (213 nm)			
	a	b	c	R^2
1	-0.08056	62.023	9.3161	0.9163
2	-0.05831	61.597	11.0820	0.9841
3	-0.06328	68.936	11.3670	0.9926
4	-0.05958	55.995	5.2591	0.9513
5	-0.07606	90.937	6.4477	0.9827
6	-0.08384	80.339	7.8338	0.8132
7	-0.09599	82.463	6.753	0.9822
8	-0.05002	52.342	15.4550	0.9003
9	-0.05659	65.260	8.5319	0.9563
10	-0.06843	57.907	8.8393	0.9970

Dissolution assays	Methocarbamol (286 nm)			
	a	b	c	R^2
1	0.1065	100.010	6.670	0.9590
2	0.0222	79.703	144.820	0.9580
3	0.0204	91.141	103.610	0.9939
4	0.0682	112.900	112.620	0.9951
5	0.1062	94.282	46.986	0.8850
6	0.1059	116.170	139.210	0.8305
7	0.0640	72.033	22.947	0.9976
8	0.0727	70.799	23.947	0.9922

Dissolution assays	Global (254 nm)			
	a	b	c	R^2
1	-0.13344	75.872	8.7164	0.9880
2	-0.06007	67.634	10.7470	0.9889
3	-0.16450	98.041	5.9530	0.9941
4	-0.06076	68.680	5.1809	0.8241
5	-0.20628	146.510	4.3156	0.9662
6	-0.19408	107.940	6.2440	0.9717
7	-0.08163	88.383	7.2504	0.9670
8	-0.10893	71.439	6.1004	0.9920
9	-0.21887	97.443	7.4159	0.9915
10	-0.195.7	90.278	4.8268	0.9874

Mixture Diosmin-Hesperidin

Tested formulation was DAFLON 500 mg from Laboratŏrios Servier, S.L. Madrid, and three simultaneous profiles were obtained; individual profiles were at 286 and 248 nm, and the global at 254 nm. See Figure 6 for details. According to the reported solubility characteristics of both formulations in aqueous solutions. It forced us to study the dissolutions directly at pH 12 instead of the officially recommended value. As reported the assembly complied with the type recommended by pharmacopoeia as no changes in solution were required from solution vessel to the required for absorbance measurements. The results were analysed by regression to calculate the corresponding equations. Regression curves fitting better with the obtained plots were of the polynomial type instead of with the Higuchi equation, as shown in Table 3

.

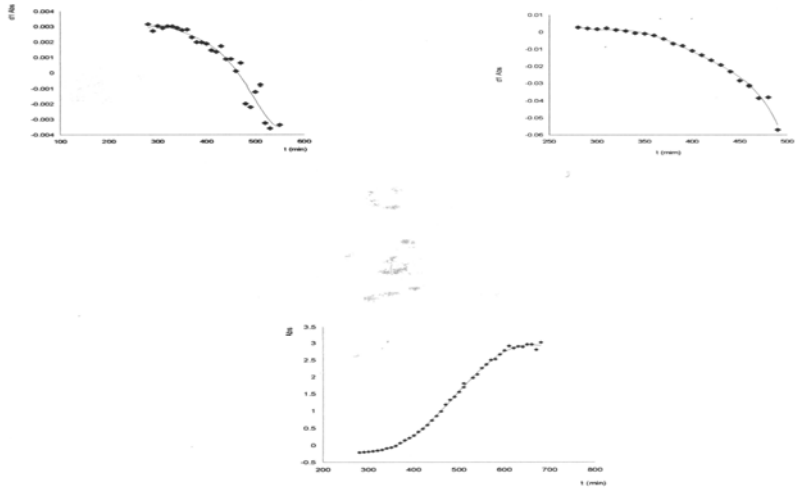

Figure 6. Dissolution profiles of Daflon Hesperidin, 248 nm (top left ; Diosmin, 286 nm (top right); and Global, 254 nm (bottom).

Table 3. Results from dissolution assays of the commercial formulation Daflon (Polynomial equation).

Hesperidin (248 nm)	M0	M1	M2	M3	M4	M5	R^2
Assay 1	-21.788	0.31308	-0.00172	4.40E-6	-5.10E-09	2.15E-12	0.9942
Assay 2	-28.986	0.35784	-0.00171	3.89E-06	-4.14E-09	1.65E-12	0.9950
Assay 3	-44.001	0.67956	-0.00402	1.13E-05	-1.49E08	7.46E-12	0.9987
Assay 4	-21.757	0.33014	-0.00191	5.21E-09	-6.57E-09	3.10E-12	0.9989
Assay 5	-16.014	0.23358	-0.00131	3.46E-06	-4.26E-09	1.99E-12	0.9980

Diosmin (286 nm)	M0	M1	M2	M3	M4	M5	R^2
Assay 1	14.466	-0.23460	0.00149	-4.60E-09	6.98E-09	-4.15E-012	0.9955
Assay 2	3.7623	-0.06432	0.00043	-1.42E-06	2.29E-09	-1.45E-12	0.9934
Assay 3	9.6765	-0.13327	0.00073	-1.97E-06	2.63E-09	-1.40E-12	0.9950
Assay 4	2.4284	-0.03911	0.00025	-7.50E-07	1.11E-09	-6.51E-13	0.9799
Assay 5	8.0732	-0.14296	0.00099	-3.41E-06	5.75E-09	-3.19E-12	0.9975
Assay 6	4.6322	-0.07342	0.00045	-1.35E-06	1.97E-06	-1.11E-12	0.9979

Global (254 nm)	M0	M1	M2	M3	M4	M5	R^2
Assay 1	2.4284	-0.03911	0.00024567	-7.50E-07	1.12E-09	-6.51E-13	0.9799
Assay 2	-0.18422	0.00334	-2.35E-05	8.20E-08	-1.41E-10	9.53E-14	0.9752
Assay 3	-0.45831	0.00601	-3.10E-05	7.92E-08	-1.00E-10	5.01E-14	0.9709
Assay 4	4.605	-0.06919	0.00040271	-1.14E-06	1.56E-09	-8.25E-13	0.9290
Assay 5	0.38522	-0.00718	5.30E-05	-1.93E-07	3.47E-10	-2.47E-13	0.9983
Assay 6	-0.74433	0.01053	-5.61E-05	1.39E-0.7	-1.55E-10	5.78E-14	0.9482

4. Conclusion

This paper is dealing with how to obtain simultaneously three dissolution profiles in formulations containing two active principles with overlapping spectra by means of the standard proposed assembly provided with a diode array spectrophotometer. In previous papers these three simultaneous profiles were obtained by means of a FIA or a Multicommutation manifold. Our results showed that the whole process can be per formed following a simple and cost-effective procedure .

The 3-parameters models and polynomial equation were proposed to describe the dissolution test curve.

References

[1] United States Pharmacopoeia (USPXXI), (National Formulary),p 1291, 1421.

[2] British Pharmacopoeia, Her Majesty′s Stationary Office, London 1993, p 547, 586.

[3] Real Farmacopoea Española. Ministerio de Sanidad y Consumo, Madrid 1997, p 1601, 1720.

[4] Mangin, D.; Garcia, E.; Gerard, S.; Hoff, C.; Klein, J. P.; Vessler, S., J. Crystal Growth, 2006, 286, 121.

[5] Bertocchi, P.; Antoniella, E.; Valvo, L.; Alimonti, S.; Memoli, A., J. Pharm. Biomed. Anal., 2005, 37 679.

[6] Moreno Gálvez, A.; Garcia Mateo, J. V.; Martĭnez Calatáyud, J., J. Pharm. Biomed. Anal., 2002, 27, 1027.

[7] Moreno Gálvez, A.; Garcĭa Mateo, J. V.; Martĭnez Calatáyud, J., J. Pharm. Biomed. Anal., 2002, 30, 535.

[8] Ferraro, M. C. F.; Castellano, P. M.; Kaufman, T. S.; J. Pharm. Biomed. Anal., 2002, 30, 1121.

[9] Tomšů, D.; Catalá Icardo M.; Martĭnez Calatáyud, J. Pharm. Biomed Anal., 2004, 36, 549.

[10] Vranic, E., Catala Icardo, M., Martĭnez Calatáyud, J., J. Pharm. Biom. Anal., 2003, 33, 1039.

[11] Martindale, The extra Pharmacopoeia, 31 edit.; J. E. F. Renolds Eds.; Royal Pharmaceutical Society, ISBN 0 85369 342 0

[12] http://www.nlm.nih.gov/medlieplus/druginfo/medmaster/a682579.html

[13] http://www.pharmweb.net/pwmirror/pwy/paracetamol_/pharmwebpic.html

[14] http://www.diseasedatabase.com/umlsdef.asp?glngUserChoice=29984

[15] Martindale; The complete Drug Reference; 34 ed.; Pharmaceutical Press; 1688.2

[16] The Merck Index, http://library.dialog.com/bluesheets/html/b10304.html

[17] Martĩnez Calatáyud, J., Flow Injection Analysis of Pharmaceuticals. Automation in the laboratory; Taylor and Francis; Cambridge 1996.

[18] Lŏpez Paz, J. L.; Martĩnez Calatáyud, J., Pharm. Technol. Europe, 1998, 10, 16.

[19] Solich, P.; Polydorou, C. K.; Koupparis, M. A.; Efstathiou, C. A.; Biomed-Chromatogr. 2000, 22,781.

[20] Gőrőg, S., Ultraviolet-Visible Spectrophotometery in Pharmaceutical Analysis; CRC Press, Boca Raton, Fl-(USA), 1995.

[21] Sachan, A.; Trivedi, P., Indian Drugs 1998, 35, 762.

[22] de Micalizzi, Y. C., Pappano,N. B., Debattista, N. B., Talanta, 1998, 47, 525.

[23] Berzas Nevado, J. J.; Rodriguez Flores, J.; Guibereau-Cabanillas, C., Villasenor-Llerena, M. J.; Contento-Salcedo, A., Talanta, 1998, 45, 933.

[24] Rivas, G. A.; Laredo Ortiz, S.; Martĩnez Calatáyud, J., Ana. Lett., 1996, 29, 2115.

[25] Encyclopedia of Pharmaceutical Technology, Swanbrick J. and J. C. Boylai; Eds., 12.

Arabian J. Chem. Vol. 1, No. 3, 239-253 (2008)

Diphosphine Compounds: Part II. UV/Visible Spectroscopy and Routes to Functionalized Diphosphine-$M(CO)_6$ Complexes (M = W, Mo, or Cr)

Fatma S. M. Hassan, Ahmed F. El-Hossainy* and Adila E. Mohamed

South Valley University, Faculty of science, Department of Chemistry, Aswan, Egypt.

****Author to whom correspondence should be addressed: E-mail:al_hossainy73@yahoo.com***
Department of Chemistry, Aswan Faculty of Science, South Valley University, Aswan P O: 81528, Egypt.

Abstract

Reaction of (diphenylphosphino)methane and different ketones or aldehydes have been characterized by $^{31}P\{H^1\}$-NMR, $^{1}H\{^{31}P\}$-NMR and UV/vis spectroscopy in dichloromethane. Group VI hexacarbonyl metals [$M(CO)_6$, where M =Cr, Mo and W] reacted with (diphenylphosphino)methane, $[(Ph_2P)_2CH_2]$[1-2] to give $[(OC)_4M\{(Ph_2P)_2CH_2\}]$ depending on the reaction conditions. The reaction of $[(CO)_4M\{(Ph_2P)_2CH_2\}]$ with different ketones or aldehydes undergo condensation reactions to give $[(CO)_4M\{(Ph_2P)_2C{=}CR_1R_2\}]$. Complexes of the type $[(OC)_4M\{(Ph_2P)_2C{=}CR_1R_2\}]$ with hydrazine underwent Michael's addition to give $[(CO)_4M\{(Ph_2P)_2CHC(R_1R_2)NHNH_2\}]$(1.3a-e), which condensated with different types of ketones and aldehydes to give complex of the type $[(CO)_4M\{(Ph_2P)_2CHC(R_1R_2)NHN{=}C(R_1)\}]$ (1.4a-e). The structures of the complexes are discussed on the basis of elemental analysis, IR, ^{1}H-NMR, ^{31}P-NMR spectroscopic data and FAB mass spectra. The UV/vis spectra showed two absorption bands with the low energy band moving to lower energy by introducing substitution on the (Diphenylphosphino) methane (dppm) ligand.

1. Introduction

Our attention has been centered on substitution reaction involving loss of carbon monoxide from the hexacarbonyl metal complexes $[M(CO)_6]$ by the bidentate phosphine ligand $[(Ph_2P)_2CH_2]$[3]**.** In last two decades there has been a great deal of interest in the preparation and properties of transition metal carbonyl complexes stabilized with multidentate ligands [4-13].

The vinylidine double bond in complexes (1.2a-1.2e) was highly activated towards nucleophilic attack (Michael addition) by a variety of amines, hydrazines and amino acids, yielding adducts of the type (1.3a-1.3e) $[(OC)_4Cr\{(Ph_2P)_2CHCNHNH_2R_1R_2\}]$ where R_1=CH_3, H, CH_3, H, H and R_2= CH_3, Ph(o-OH), CH=C(OH)CH_3, CH_3, Ph. We found that the free diphosphine $(Ph_2P)_2C{=}CH_2$, does not react with hydrazine either after prolonged heating 72 h with or without addition of hydrazine hydrochloride,

or with amine after prolonged heated (48 h) with or without addition of concentrated hydrochloric acid.

Also, we found that the diphosphine complexes $[M(CO)_4(Ph_2P)_2C=CH_2]$ where $M(CO)_4$ (M = Cr, Mo, and W), does react with hydrazine, acetone, salicylaldehyde and acetylacetone after heating 80 ^oC for 5-20 min. Relatively weakly electron withdrawing group, $M(CO)_4$ (M = Cr, Mo, and W) is sufficient to render the double bond ($C=CH_2$) reactive toward Michael's type addition, and also, we found that the hydrazine, acetone, salicylaldehyde and acetylacetone react with $[(OC)_4M\{(Ph_2P)_2CHC(R_1R_2)\text{-}NHNH_2\}]$ (M= Cr, Mo and W) after heating 80 ^oC for 5-20 min, to obtain (1.4a-1.4e) complexes.

2.Results and Discussion

Synthesis and characterization of the new derivatives of (diphenylphosphino)ethane metal complexes have been illustrated in Scheme 1.

The metal complexes can be prepared by treatment of the complexes (1) with acetone, salicylaldehyde, acetylacetone acetaldehyde and benzaldehyde (formed by condensation reaction) to give complexes of the type $[(OC)_4M\{(Ph_2P)_2C=CR_1R_2\}]$ (1.2(a-e)) in toluene. Complexes (1.2a) to (1.2e) of the types $[(OC)_4M\{(Ph_2P)_2C=CR_1R_2\}]$ underwent Michael's addition with hydrazine yielded $[(CO)_4M\{(Ph_2P)_2CHC(R_1R_2)\text{-}NHNH_2\}]$. Alkyl- and aryl-hydrazines have a very extensive chemistry and we found that compound $[(OC)_4Cr(Ph_2P)_2CHC(R_1R_2)NHNH_2\}]$ (1.3(a-e)) readily under condensation reactions with organic carbonyl compounds [$(CH_3)_2CO$, CHOPh(o-OH), $OC(CH_3)CH=C\text{-}(OH)CH_3$, $OCHCH_3$ and OCHPh] to give adducts of the type $[(CO)_4M\{(Ph_2P)_2CHC(R_1R_2)NHN=C(CH_3)_2\}]$(1.4a), $[(CO)_4M\text{-}\{(Ph_2P)_2CH\text{-}C(R_1R_2)NHN=CHPh(o\text{-}OH)\}]$(1.4b), $[(CO)_4M\{(Ph_2P)_2CHC(R_1R_2)NHN=C(CH_3)CH=C(OH)CH_3\}]$ (1.4c), $[(CO)_4M\{(Ph_2P)_2CHC(R_1R_2)NHN=CHCH_3\}]$(1.4d) and $[(CO)_4M\{(Ph_2P)_2CH\text{-}C(R_1R_2)NHN=CHPh)\}]$(1.4e) which investigated by spectroscopic techniques. Complexes (1.4c) and (1.5c) formed as pyrazole derivatives and the spectroscopic techniques applied.

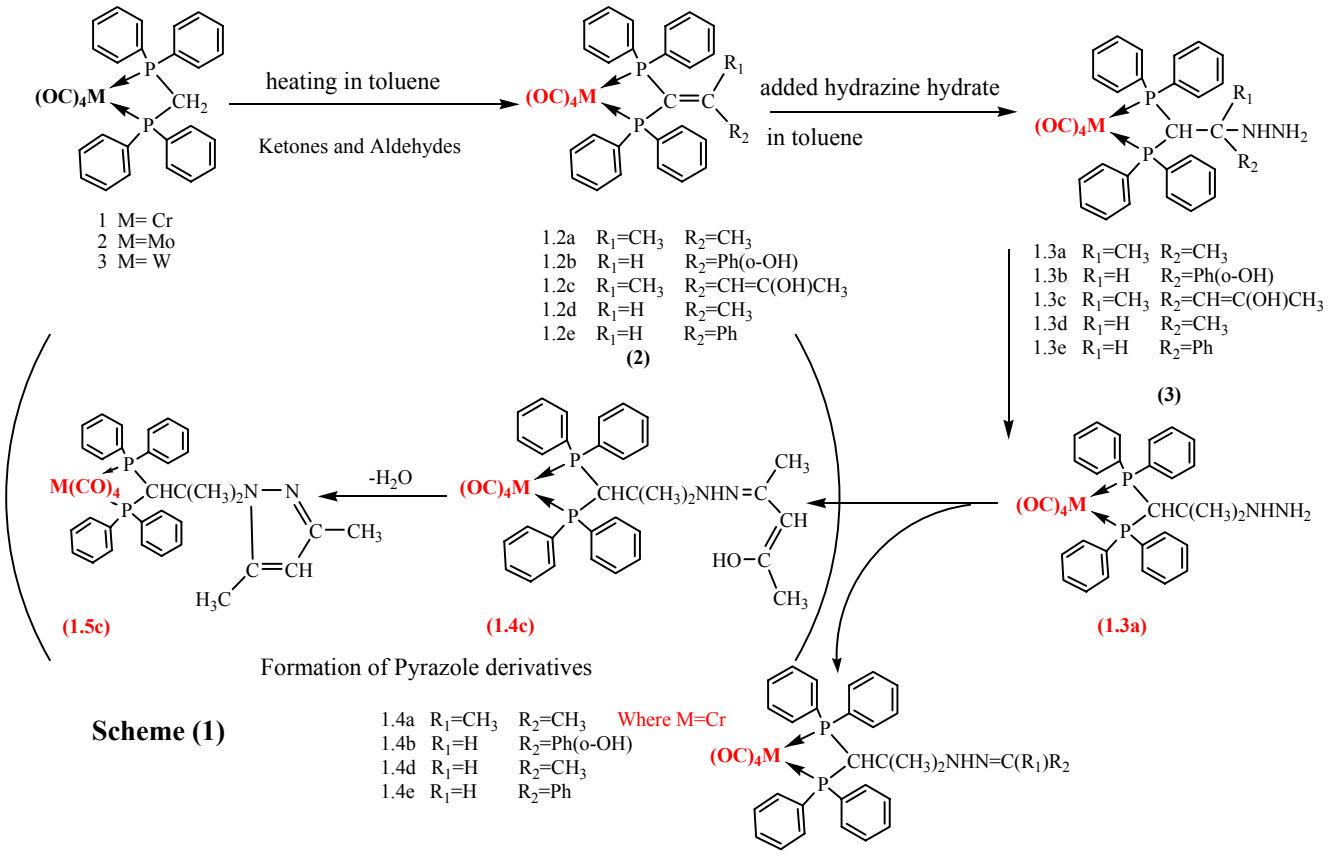

Scheme (1)

Condensation with acetone

Treatment of the tungsten-hydrazine adduct in benzene with a slight excess (20%) of acetone gave $[(OC)_4W\{(Ph_2P)_2CH^1C(CH_3^2)_2NH^3N=C(CH_3)_2{}^4\}]$ (3.4a) after heating ca. 1h under dinitrogen, yellow crystals of the tungsten actonadimine adduct in >70% yield. We assigned the structure of this adduct on the basis of (i) satisfactory elemental analysis; (ii) The $^{31}P-\{^1H\}$NMR spectrum showed a singlet at δ (Chemical shift)=-4.23ppm with ^{183}W satellites, $^1J(WP)/Hz$ (coupling constant) =205; (iii) the ^1H and $^1H-\{^{31}P\}$NMR spectra which showed four signals (excluding aromatic hydrogen). At δ=3.73ppm a triplet of relative intensity 1H is observed and assigned to CH^1.

A singlet is centered at δ=1.64 ppm of relative intensity 6H, assigned to $CH_3{}^2$ protons. A singlet at δ= 1.91 ppm of relative intensity 6H is observed, assigned to $CH^4{}_3$ proton. Finally a broad signal is observed at δ= 1.72 ppm of relative intensity 1H, assigned to NH^3 proton. These signal due to NH disappeared on addition of D_2O. In the ^1H NMR spectrum coupling to phosphorus is shown by the protons

CH^1, $^2J(\underline{P}C\underline{H}^1)$=10Hz; (iv) the infrared spectrum showed υ(NH) at 3300cm^{-1}.

Condensation with salicylaldehyde:

Treatment of the tungsten-hydrazine adduct in benzene with a slight excess (20%) of salicylaldehyde gave $[(OC)_4W\{(Ph_2P)_2CH^1C(CH_3{}^2)_2NH^3N{=}CH^4(Ph(o\text{-}OH^5)\}]$ (3.4b) after heating ca. 1h under dinitrogen, brown crystals of the tungsten salicyladimine adduct in >80% yield. We assigned the structure of this adduct on the basis of (i) satisfactory elemental analysis; (ii) The $^{31}P\text{-}\{^1H\}$ NMR spectrum showed a singlet at δ=-4.08 ppm with ^{183}W satellites, $^1J(WP)/Hz = 203$; (iii) the ^1H and $^1H\text{-}\{^{31}P\}$ NMR spectra which showed five signals (excluding aromatic hydrogen). At δ = 5.44 ppm a triplet of relative intensity 1H is observed and assigned to CH^1. A singlet is centered at δ = 1.66ppm, of relative intensity 6H, assigned to $CH_3{}^2$ protons, coupling with the CH^1 proton. A singlet at δ=8.01ppm of relative intensity 1H is observed, assigned to CH^4 proton. Another singlet at δ= 10.67 ppm of relative intensity 1H, is observed and assigned to the OH^5 proton. Finally a broad signal is observed at δ= 1.49 ppm of relative intensity 1H, assigned to NH^3 proton. These signals due to OH and NH disappeared on addition of D_2O.

In the ^1H NMR spectrum coupling to phosphorus is shown by the protons CH^1, $^2J(\underline{P}C\underline{H}^1)$ = 10Hz (iv) the infrared spectrum showed υ(OH) at 3240 cm^{-1} and υ(NH) at 3300cm^{-1}.

Formation of a pyrazole derivative

Hydrazine complexes of the type $[(OC)_4W\{(Ph_2P)_2CHC(CH_3)_2NHNH_2\}]$ was treated with acetylacetone to prepare a pyrazole derivates, and on heating the tungsten- hydrazine adduct with one mole equivalent of acetylacetone in toluene for a prolonged period (*ca.* 16 h), a pale brown crystalline product formed, which we formulated as the pyrazole derivative (3.4c) and $[(OC)_4W\{(Ph_2P)_2CH^1C(N{*}N{=}C(CH_3)^2CH^3{=}C{*}CH_3{}^4)(CH_3)_2{}^5\}]$ (3.5c). This complex was formulated on the following basis of: (i) satisfactory elemental analysis [Found: C, 54.40; H, 4.25; N, 3.42%]. (ii) The $^{31}P\text{-}\{^1H\}$ NMR spectrum showed a singlet at δ = -4.23 ppm with ^{183}W satellites. $^1J(WP)/Hz$ = 205 Table(1) for data. (ii) The $^1H\text{-}\{^{31}P\}$ and ^1H NMR spectra, Figure (1) showed five signals. At δ = 6.35 ppm a triplet of relative intensity 1H is observed and is assigned to CH^1 proton. A singlet of relative intensity 1H at δ = 5.43 ppm is observed and is assigned to (–N-N=C-CH^3) proton coupling with CH_3 protons, $^4J(C\underline{H}\text{-}C\text{-}C\underline{H}_3{}^4)$ = 2.5 Hz.

Table(1) ^{31}P-{^{1}H} NMR[a], and Infrared[b] data for some condensation products of $[(OC)_4W\{(Ph_2P)_2CHC(CH_3)_2NHNH_2\}]$ with acetone, acetylacetone or salicylaldehyde.

Complex	M	δ(P)[a] ppm	$^{1}J(WP)$ Hz	(υ(CO)/cm^{-1})[ν(P-C)][b]	υ(NH)/cm^{-1}
3.5c	W	-4.23	205	(2005s,1960w, 1885w, 1865sb)[715s]	-
3.4c[f]	W	-4.93	207	(2005s, 1930w, 1885w, 1865sb) [692s]	3300
3.4b	W	-4.08	203	(2005s, 1940w, 1890w, 1870sb) [721s]	3300
3.4a	W	-1.7	205	(2010s,1984w,11891w,1865sb) [682s]	3250
3.4d	W	-2.6	205	(2017s, 1942w, 1893w, 1852sb) [702s]	3300
3.4e	W	-4.20	203	(2000s, 1981w, 1892w, 1860sb) [695s]	3300

(a) In $CDCl_3$ (b) In KBr discs (f) υ(OH)= 3240 cm^{-1}
(s) Strong, (w) Weak, and (sb) Strong board

A strong signal is observed at δ = 2.67 ppm of relative intensity 6H, assigned to $2CH_3^5$ protons. Two singlet are observed at δ = 1.39 ppm and δ = 2.17 ppm of relative intensity 3H each, assigned to two methyl protons CH_3^2 and CH_3^4. It is difficult to distinguish between the two. It showed coupling to phosphorus by the CH^1 proton, the signal being a triplet of triplets, $^{3}J(PCH)$ = 12 Hz, (iii) The infrared spectrum was characteristic of a *cis*-chelated tetracarbonyl complex. The υ_{N-H} band was disappeared.

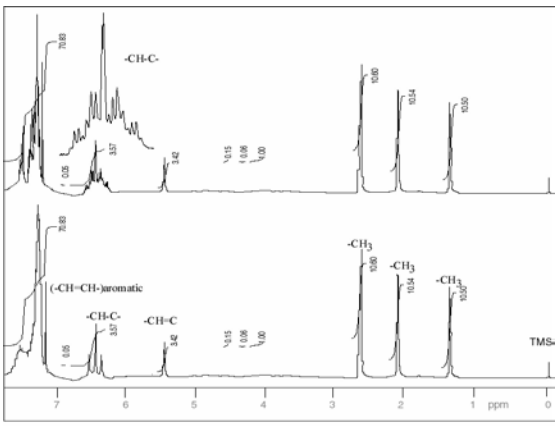

Figure (1) ^{1}H-{^{31}P} and ^{1}H NMR spectra for the complex $[(OC)_4W\{(Ph_2P)_2CHC(CH_3)_2N\text{-}N{=}C(CH_3)CH{=}C(CH_3)\}]$

Relation between molecular structure and electronic spectra of synthesized diphosphine derivatives complexes

The difference in energy between the lowest unoccupied orbital (LUMO) and the highest occupied orbital (HOMO) is considerably greater than the activation energy (A) for the transition from the singlet ground state S_o to the singlet excited state S_1. The difference rises from the different electronic interactions (Coulomb term J, exchange term 2K). The singlet-triplet splitting in this approximation is 2K. Since K>0 the lowest triplet state T_1 is always below S_1. As a result of the configurational interaction the HOMO-LUMO transition is not necessarily the lowest transition $S_o \longrightarrow S_1$[14]. The long wavelength absorption energy corresponds to the energy of the HOMO-LUMO gap [15-17]. However, solvent effects and transitions involving the SHOMO and SLUMO (and potentially other MOs), as well as changes in relative orbital energies and electron configurations, can significantly complicate the

situation to the extent that one can generally only get meaningful information by comparing closely related compounds[18].

A classification of the electronic transitions (bands) can be made from a knowledge of the molecular orbitals (MO's) involved. From occupied bonding σ or π orbitals or from non-bonding n-orbitals (lone pairs electrons) an electron can be raised to an empty anti-bonding σ*- or π*-orbitals. Correspondingly the electronic transitions (bands) are indicated as $\sigma \longrightarrow \sigma^*$, $\pi \longrightarrow \pi^*$, $n \longrightarrow \sigma$, $n \longrightarrow \pi$. If the absorbance is determined for all λ or υ and from that the substance-specific value ε, the absorption plot ε(υ) or ε(λ) can be obtained and thus the UV or UV/vis spectrum. As a consequence of the width (in energy terms) of the electronic states it is a band spectrum. The individual bands are characterized by their properties of position, intensity, shape, and fine structure.

The electronic absorption spectral data λ_{max} and ε_{max} values for the synthesized diphosphine derivatives chromium complexes as an example (1, 1.2a, 1.3a, 1.4c, 1.5c) in dichloromethane are presented in Table (5). The visible absorption spectra of these chromium complexes exhibit various absorption bands within the wavelength range (λ=350-700 nm). These absorption bands depend primarily on the terminal group (hydrazine derivatives), their linkage position [19-20], and the type of the transient metal complex. The visible absorption maxima of diphosphine derivatives chromium (dppm) complexes in CH_2Cl_2 undergo bathochromic or hypsochromic shifts depending on the nature of the alphatic and aromatic aldehydes and ketones (undergo condensations reaction) gave complexes of the type $[(OC)_4Cr\{(Ph_2P)_2C=C(CH_3)\text{-}CH_3\}]$(1.2a). Thus, substituting A= acetonyl group in compound (1) typically exhibit two UV/vis absorption bands (with extinction coefficients of between 250 and 880 L $mol^{-1}cm^{-1}$), one near 410 nm and the other near 550 nm. These bands are likely to be d–d transitions since the HOMO is largely metal-based and the extinction coefficients are less than 1,000 L mol^{-1} cm^{-1}. It has been observed that for methyl substitution the UV/vis spectra vary by only 15 nm (546–561 nm)(a bathochromic shift).

Table(5) UV/vis data for phosphino-substituted hydrazine chromium complexes in CH_2Cl_2.

compound	λ_{max}/nm (ε/L $mol^{-1}{}_{Cm}{}^{-1}$)	λ_{max}/nm (ε/L $mol^{-1}{}_{Cm}{}^{-1}$)
$C_{29}H_{22}CrO_4P_2$ (1)	-	546 (340)
$C_{33}H_{26}CrO_4P_2$ (1.2a)	420 (655)	561 (280)
$C_{32}H_{30}CrN_2O_4P_2$ (1.3a)	440 (860)	570 (330)
$C_{37}H_{36}CrN_2O_5P_2$ (1.4c)	453 (1132)	594 (450)
$C_{37}H_{34}CrN_2O_4P_2$ (1.5c)	442 (740)	581 (350)

For[$(OC)_4W\{(Ph_2P)_2CHC(NHN=C(CH_3)CH=C(OH)CH_3)(CH_3)_2\}$](3.4c), we found that the UV/vis absorption peaks change by (15–24 nm) whereas for pyrazole (3.5c), all of the UV/vis absorption peaks shift to lower wavelength by (11-13 nm). Apparently, the σ* orbitals of the tetra carbonyl transition metals groups have a significant influence on the pyrazole ring MOs, thus affecting the bands in the UV/vis spectra. Table(3) gives the absorptions for the phosphino derivatives illustrated in Scheme 1 and typical UV/vis spectra (Hyrazine- and Pyrazole-) are shown in Figure (2). It can be seen from Figure (2) that the hydrazine (1.4c) and pyrazole substituted (1.5c) both exhibit two bands in the UV/vis spectra and that these occur at similar energies. Although some extinction coefficients for the high energy band are over 1000 L mol^{-1} cm^{-1}, it should be noted that these absorptions overlap with a charge transfer band. Unfortunately, we were unable to obtain meaningful UV/vis spectra for the sterically congested, and consequently sensitive, complex 1(band at near 420 nm).

a: chromium hydrazone diphenylphosphine (1.4c)
b: chromium pyrazole diphenylphosphine (1.5c)
c: Chromium diphenylphosphine (1.3a)
d: Derivatives chromium diphenylphosphine (1.2a)
e: Chromium diphenylphosphine methane(1) complex

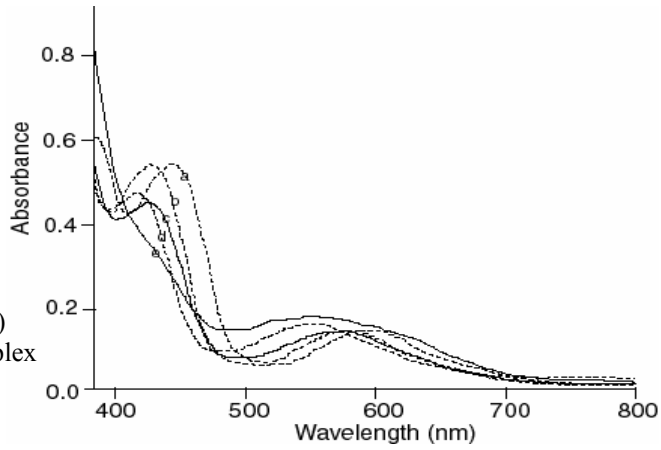

Figure (2) Typical UV/vis spectra of phosphino-substituted transition metals (group VI) complexes in CH_2Cl_2:

The UV/vis spectroscopy provides information on the HOMO–LUMO gap in both derivatives (1.4c and 1.5c), it is assigned to a ligand to metal charge transfer (LMCT) process from diphenylphosphino to a d^0 metal centre in the complexes rather than a d–d transition of the Chromium atom. One must be careful, therefore, when making comparisons between these derivates. $[(OC)_4W\{(Ph_2P)_2CHC(NHN=C-(CH_3)CH=C(OH)CH_3)-(CH_3)_2\}]$(3.4c) typically exhibit two UV/vis absorption bands (with extinction coefficients of between 300 and 900 L mol^{-1} cm^{-1}), one near 450 nm and the other near 590 nm. For pyrazole derivates (1.5c) exhibit two UV/vis

absorption bands, one near 420 nm and the other near 550 nm. These bands are likely to be d–d transitions since the HOMO is largely metal-based [21-22] and the extinction coefficients are less than 1,000 L mol^{-1} cm^{-1}.

3.Experimental

Apparatus

Elemental analyses were carried out at the Micro Analytical center (Assiut University). The IR spectra (KBr) were determined on Shimadzu corporation Chart 200-91527 spectrophotometer. ^{1}H-NMR spectra were recorded with a Bruker AMX-250 spectrometer. Mass spectra were recorded on HpMs 6988 spectrometer and electron-impact (EI). Visible spectra (300-999 nm) were recorded on Shimadzu UV/vis 160-A spectrophotometer at the Aswan Faculty of Science. All reagents and solvents were obtained from Aldrich Chemical Company (Milwaukee, WI, USA).

Preparation of organometallic compounds:

Novel method for the synthesis of complexes of the type $[(OC)_4M\{(Ph_2P)_2C=CH_2]$(M = Cr, Mo and W) complexes. A formalin gas (CH_2O) was bubbled into a stirred hot solution of dppm complexes (dppm = (diphenyl-phosphino)methane) under dinitrogen in *n*-decane (20cm^2); stirring under reflux at 100-150 ^oC was continued for 40 minutes. The resultant solvent was evaporated under reduced pressure and ethanol added. The product was separated as crystalline solid and the yield was 65-87% [23].

Preparation of $[(OC)_4Cr\{(Ph_2P)_2C=CR_1R_2\}]$ (1.2a)-(1.2e) [where (R_1=CH_3, H, CH_3, H, H and R_2= CH_3, Ph(o-OH), $CH=C(OH)CH_3$, CH_3, Ph)], respectively.

Acetone, salicylaldehyde, acetylacetone, acetaldehyde and benzaldehyde in toluene (0.5 cm^3), were added to a suspension of $[(OC)_4Cr\{(Ph_2P)_2CH_2\}]$ (0.15g, 0.28 mmol) respectively. The mixture was then heated to *ca.* 80 ^oC for 5-20 min a period over which the chromium complexes dissolved and a new crystalline precipitate formed. These were filtered off, washed with Et_2O and dried giving the required product $[(OC)_4Cr\{(Ph_2P)_2C=C(CH_3)_2\}]$ (brown) (1.2a), $[(OC)_4Cr\{(Ph_2P)_2C=CHPh(o\text{-}OH)\}]$ (yellow) (1.2b), $[(OC)_4Cr\{(Ph_2P)_2C=C(CH_3)CH=C(OH)CH_3\}]$ (pale brown) (1.2c), $[(OC)_4Cr\{(Ph_2P)_2C=CHCH_3\}]$ (brown) (1.2d) and $[(OC)_4Cr\{(Ph_2P)_2C=CHPh\}]$ (dark brown) (1.2e), respectively**.** The final products were recrystallized from ether-methanol. The obtained data are listed in Table (2)

Preparation of $[(OC)_4W\{(Ph_2P)_2C=C(CH_3)_2\}]$(3.2a).

Acetone in toluene (0.5 cm^3) was added to a suspension of $[(OC)_4W\{(Ph_2P)_2CH_2\}]$ (0.19 g, 0.28mmol). The mixture was then heated to *ca.* 80 ^oC for 5 min a period over which the tungsten complex dissolved and a new pale brown crystalline precipitate formed. This was filtered off, washed with Et_2O and dried giving a pale brown precipitate the yield was 0.17g (83%). The required product is

$[(OC)_4W\{(Ph_2P)_2C=C(CH_3)_2\}]$,which$[(OC)_4W\{(Ph_2P)_2C=C(CH_3)_2\}]$ was recrystallised from ether-methanol to give a pale brown crystals.

Preparation of $[(OC)_4W\{(Ph_2P)_2C=CHPh(o\text{-}OH)\}]$ (3.2b).

Salicylaldehyde [Ph(o-OH)CHO] in toluene (0.5 cm^3) was added to a suspension of $[(OC)_4W\{(Ph_2P)_2CH_2\}]$(0.19 g,0.28 mmol). The mixture was then heated to *ca.* 80 ^oC for 14 min a period over which the tungsten complex dissolved and a brown crystalline precipitate formed. This was filtered off, washed with Et_2O and dried giving brown precipitate, the yield was 0.17g, (76%). The required product $[(OC)_4W\{(Ph_2P)_2C=CHPh(o\text{-}OH)\}]$, was recrystallised from ether-methanol give brown crystals.

Preparation of $[(OC)_4W\{(Ph_2P)_2C=C(CH_3)CH=C(OH)CH_3\}]$(3.2c).

Acetylacetone $[CH_3COCH=C(OH)CH_3]$ in toluene (0.5 cm^3) was added to a suspension of $[(OC)_4W\{(Ph_2P)_2CH_2\}]$(0.19 g, 0.28 mmol). The mixture was then heated to *ca.* 80 ^oC for 10 min period over which the tungsten complex dissolved and a brown crystalline precipitate formed. This was filtered off, washed with Et_2O and dried giving brown precipitate, yield 0.17 g, (83%). The required product was recrystallised from ether-methanol to give brown crystals with Ca chemical structure as$[(OC)_4W\{(Ph_2P)_2C=C(CH_3)CH=C(OH)CH_3\}]$.

Preparation of $[(OC)_4W\{(Ph_2P)_2C=CHCH_3\}]$ (3.2d).

Acetaldehyde $[(CH_3CHO]$ in toluene (0.5cm^3) was added to a suspension of $[(OC)_4W\{(Ph_2P)_2CH_2\}]$ (0.19g, 0.28 mmol). The mixture was then heated to *ca.* 80 ^oC for 5 min period over which the tungsten complex dissolved and a pale brown crystalline precipitate formed. This was filtered off, washed with Et_2O and dried giving a pale brown precipitate; yield 0.16 g, (79%). The required product $[(OC)_4W\{(Ph_2P)_2C=CHCH_3\}]$ was recrystallised from ether-methanol to give pale brown crystals.

Preparation of $[(OC)_4W\{(Ph_2P)_2C=CHPh\}]$(3.2e).

Benzaldehyde [(PhCHO] in toluene (0.5cm^3) was added to a suspension of $[(OC)_4W\{(Ph_2P)_2CH_2\}]$ (0.19 g, 0.28 mmol). The mixture was then heated to *ca.* 80 ^oC for 5 min period over which the tungsten complex dissolved and a new pale yellow crystalline precipitate formed. This was filtered off, washed with Et_2O and dried giving a pale yellow precipitate, yield 0.15g (76%). The required product $[(OC)_4W\{(Ph_2P)_2C=CHPh\}]$ was recrystallised from ether-methanol to give pale yellow crystals.

Preparation of $[(OC)_4Cr\{(Ph_2P)_2\text{-}CHCNHNH_2R_1R_2\}]$ (1.3a-1.3e) [where ($R_1=CH_3$, H, CH_3, H, H and $R_2 = CH_3$, Ph(o-OH), $CH=C(OH)CH_3$, CH_3, Ph)], respectively.

Hydrazine hydrate (0.5cm^3), was added to a suspension of $[(OC)_4Cr\{(Ph_2P)_2C=C(CH_3)_2\}]$ (1.2a), $[(OC)_4Cr\{(Ph_2P)_2$-

C=CHPh(o-OH)}](1.2b), [$(OC)_4Cr\{(Ph_2P)_2C=C(CH_3)$-$CH=C(OH)CH_3\}$] (1.2c), [$(OC)_4Cr\{(Ph_2P)_2C=CHCH_3\}$] (1.2d) and [$(OC)_4Cr\{(Ph_2P)_2C=CHPh\}$] (1.2e) (0.28 mmol) in toluene respectively. The mixture was then heated to ca. 80 ^oC for 15 min. over which period the chromium complex dissolved and crystalline precipitate formed. These were filtered off, washed with Et_2O and dried giving the required product [$(OC)_4Cr\{(Ph_2P)_2CHC(NHNH_2)(CH_3)_2\}$] (1.3a), [$(OC)_4Cr\{(Ph_2P)_2CHCH(NHNH_2)(Ph(o\text{-}OH)\}$] (1.3b), [$(OC)_4Cr\{(Ph_2P)_2CHC(CH_3)(NHNH_2)(CH=C(OH)CH_3\}$] (1.3c), [$(OC)_4Cr\{(Ph_2P)_2CHCH(NHNH_2)(CH_3)\}$] (1.3d) and [$(OC)_4Cr\{(Ph_2P)_2CHCH(NHNH_2)(Ph)\}$] (1.3e),; respectively. The final products were recrystallied from ether-methanol. The obtained data are listed in Table (2).

Preparation of [$(OC)_4W\{(Ph_2P)_2CHCNHNH_2(CH_3)_2\}$] (3.3a).

Hydrazine hydrate (0.5 cm^3), was added to a suspension of [$(OC)_4W\{(Ph_2P)_2C=C(CH_3)_2\}$] (0.2 g, 0.28 mmol) in toluene. The mixture was then heated to *ca.* 80 ^oC for 15 min. over which period the tungsten complex dissolved and a brown crystalline precipitate formed. This was filtered off, washed with Et_2O and dried giving a brown precipitate, yield 0.17 g (81%). The required product [$(OC)_4W$-$\{(Ph_2P)_2CHC(NHNH_2)(CH_3)_2\}$], was recrystallised from ether-methanol to give brown crystals.

Preparation of [$(OC)_4Cr\{(Ph_2P)_2CHC(NHN=CR_1R_2)$-$(CH_3)_2\}$] (1.4a-1.4e) [where ($R_1$=$CH_3$, H, CH_3, H, H and R_2= CH_3, Ph(o-OH), $CH=C(OH)CH_3$, CH_3, Ph)]; respectively.

Acetone, salicylaldehyde, acetaldehyde and benzaldehyde (0.5 cm^3), respectively, were heated under reflux with a suspension of [$(OC)_4Cr\{(Ph_2P)_2CHC(NHNH_2)(CH_3)_2\}$] (0.17 g, 0.28 mmol) in toluene (10cm^3) for 10-25 min period over which the chromium complex dissolved and a new dark brown, brown, brown and brown crystalline precipitate formed, respectively. These were filtered off, washed with Et_2O and dried giving the required products [$(OC)_4Cr\{(Ph_2P)_2CHC(NHN=C(CH_3)_2)(CH_3)_2\}$] (dark brown) (1.4a), [$(OC)_4Cr\{(Ph_2P)_2CHC(NHN=CH(Ph(o\text{-}OH))(CH_3)_2\}$] (pale brown) (1.4b), [$(OC)_4Cr\{(Ph_2P)_2CHC(NHN=CH(CH_3))(CH_3)_2\}$] (brown) (1.4d) and [$(OC)_4Cr\{(Ph_2P)_2CHC(NHN=CH(Ph))(CH_3)_2\}$] (1.4e) (brown), respectively. The final products were recrystallied from ether-methanol. The obtained data are listed in Table (2).

Formation of pyrazole derivative with acetylacetone [$(OC)_4Cr\{(Ph_2P)_2CHC(N*N=C(CH_3)CH=C*CH_3)(CH_3)_2\}$] (1.5c).

A suspension of [$(OC)_4Cr\{(Ph_2P)_2CHCNHNN_2(CH_3)_2\}$] (1.3a) (0.18 g, 0.28 mmol) in toluene (1cm^3) and acetylacetone (0.028 g, 0.28 mmol) was heated under reflux for 15 h. The resultant pale yellow solution was evaporated to a low volume under reduced pressure and then ethanol was added. The product obtained was

separated as a yellow prism. Yield, of the separated product was, 0.12 g, (53%).

Formation of pyrazole derivative with acetylacetone[$(OC)_4W\{(Ph_2P)_2CHC(N*N=C(CH_3)CH=C*CH_3)(CH_3)_2\}$] (3.5c).

A suspension of $[(OC)_4W\{(Ph_2P)_2CHC(CH_3)_2NHNN_2\}]$ (3.3a) (0.23 g, 0.28 mmol) in toluene ($1cm^3$) and acetylacetone (0.028 g, 0.28 mmol) was heated under reflux for 15 h. The resultant pale yellow solution was evaporated to a low volume under reduced pressure and than ethanol was added. The product obtained was separated as a yellow prism. Yield, of the separated product 0.16 g, (71%). Molybdenum complexes have been prepared in a similar fashion to chromium and tungsten complexes. Data obtained are listed in Table (3). and Table (4)

Keywords: Electronic spectra; Condensation reactions, Diphenylphosphine derivatives; Organo-metallic; Transitions metal complexes.

Table (2): Characterization data of the newly synthesized (diphenylphosphino)ethene derivative complexes.

Compd. No	Mol. formula (mol. wt.)	Calcd.%,(Found) % C	H	N	Yield%	m.p., ºC	IR (ν^{KBr} max), cm^{-1}	$^1H\{^{31}P\}$-NMR($CDCl_3$) δ, ppm, Assignment	M^+
1.2a	$C_{32}H_{26}CrO_4P_2$ (588.49)	65.31 (64.98)	4.45 (4.50)	- -	73	201-211	2010s, 1980,1892w,1860sb (νCO) 720s, 690s single band (ν P-C)	1.73(s, 6H, CH_3 methyl), {7.25(s, 4H, p-CH)}, {7.11(s, 8H, o-CH)} {7.53(s, 8H, m-CH)}aromatic ring	588.7
1.3a	$C_{32}H_{30}CrN_2O_4P_2$ (620.54)	61.94 (62.05)	4.87 (4.85)	4.51 (4.63)	77	211-219	2000s, 1985,1892w,1860sb (νCO) 720s, 690s single band (ν P-C) 3300w, (ν (NH))	2.48(w, 1NH, $2NH_2$, amine), 3.72(w, 1H, methine, 1 beta -N), 1.56 (s, 6H, methyl –CH), {6.85-7.57(s, 4H, 8H, 8H)}aromatic ring	621
1.4a	$C_{35}H_{34}CrN_2O_4P_2$ (660.54)	63.64 (63.60)	5.19 (5.20)	4.24 (4.29)	75	205-210	2010s, 1980,1890w,1860sb (νCO) 725s, 690s single band (ν P-C) 3350w, (ν (NH))	1.65(s, 6H, methyl,1alpha -N), 1.89(s, 6H, methyl,1alpha -N), 3.73(m, 1H,methine, 1beta –N), 1.73(w, 1ÑH, hydrazid), {6.80-7.57(s, 4H, 8H, 8H)} aromatic ring	661
1.4b	$C_{36}H_{30}CrN_2O_5P_2$ (724.64)	64.64 (64.53)	4.73 (4.89)	3.87 (3.90)	73	201-207	2020, 1985,1890w,1865sb (νCO) 720s, 695s single band (ν P-C) 3400w, (ν (NH))	1.45(s, 6H, methyl,1beta -N), 3.26(m, 1H,methine, 1beta –N), 7.92(m, 1H,benzylidenimin, 1alpha –N), 8.85(w, 1ÑH, amine), 8.85(m, aromatic C-OH), {6.80-7.58(s, 5H, 10H, 9H)} aromatic ring	724
1.4c	$C_{37}H_{36}CrN_2O_5P_2$ (702.15)	63.25 (62.98)	5.16 (5.15)	3.99 (4.02)	85	172-187	2000s, 1980w,1890w,1860sb (νCO) 720s, 690s single band (ν P-C) 3400w, (ν (NH)) 3200wb, (ν (OH))	1.31(s, 6H, methyl,1beta -N), 3.304(w, 1H,methine, 1beta –N), 4.93(m, 1H, 1-ethylene, 1alpha –C=C), 8.11(w, 1ÑH, hydrazid) 11.86(w, enol (C-OH)), 1.82(s, 3H, methyl, 1alpha –C=CH) 0.97(s, 3H, methyl, 1gama C=CH-),{6.80-7.57(m, 4H, 8H, 8H)} aromatic ring	702
1.4d	$C_{34}H_{32}CrN_2O_4P_2$ (646.57)	63.16 (63.24)	4.99 (4.85)	4.33 (4.39)	88	209-215	2020s, 1980w,1890w,1865sb (νCO) 725s, 680s single band (ν P-C) 3200w, (ν (NH))	1.34(s, 6H, methyl,1beta -N), 3.304(w, 1H,methine, 1beta –N), 6.59(s, 1H, 1-hydrazid, 1alpha –N), 2.53(w, 1ÑH, hydrazid), 0.96(s, 3H, methyl, 1alpha –N), {6.53-7.55(m, 4H, 8H, 8H)} aromatic ring	646
1.4e	$C_{39}H_{34}CrN_2O_4P_2$ (708.64)	66.10 (66.05)	4.84 (4.95)	3.95 (4.08)	86	169-175	2000s, 1985,1890w,1860sb (νCO) 720s, 690s single band (ν P-C) 3320w, (ν (NH))	1.54(s, 6H, methyl,1beta -N), 3.304(w, 1H,methine, 1beta –N), 8.09(s, 1H, 1-benzylidenimin, 1alpha –N), 2.09(w, 1ÑH, amine), {6.53-7.55(m, 4H, 8H, 8H)} aromatic ring	709
1.5c	$C_{37}H_{34}CrN_2O_4P_2$ (684.62)	64.91 (65.08)	5.01 (5.12)	4.09 (4.25)	80	208-214	2020s, 1980,1895w,1860sb (νCO) 720s, 690s single band (ν P-C)	1.94(s, 6H, methyl,1beta -N), 4.094(w, 1H,methine, 1beta –N), 5.89(s, 1H, 1-pyrazole, 1alpha –N-N=C-C1), 2.35(s, 3H, methyl, 1 alpha –N-N=C-1), 2.13(s, 3H, methyl, 1 alpha –N-N=C-CH=C-1), {6.80-7.55(m, 4H, 8H, 8H)} aromatic ring	685

IR (ν^{KBr} max), cm^{-1} spectra: (s) Strong (sb) Strong board (w) Weak (wb) weak board

$^1H\{^{31}P\}$-NMR($CDCl_3$) spectra (δ) Chemical shift (m) Mediam (s) Strong (wb) Weak board (w) Weak (p-) Para Position (o-) Ortho position (m-) Meta position (ppm) Part per million (enol) Hydroxyl group

Table (3): Characterization data of the newly synthesized (diphenylphosphino)ethene derivative complexes.

Compd. No	Mol. formula (mol. wt.)	Calcd.%,(Found) %			Yield%	m.p., ºC	IR (ν^{KBr} max), cm^{-1}	$^1H\{^{31}P\}$-NMR($CDCl_3$)	M^+
		C	H	N				δ, ppm, Assignment	
2.2a	$C_{32}H_{26}MoO_4P_2$ (632.43)	60.77 (60.21)	4.14 (4.25)	- -	76	225-233	2005s, 1980,1892w,1865sb (νCO) 720s, 690s single band (ν P-C)	1.71(s, 6H, CH_3 methyl), {7.20(s, 4H)}, {7.12(s, 8H)} {7.55(s, 8H)}aromatic ring	634.04
2.3a	$C_{32}H_{30}MoN_2O_4P_2$ (664.48)	57.84 (57.80)	4.55 (4.55)	4.22 (4.20)	73	234-242	2010s, 1980,1892w,1865sb (νCO) 720s, 690s single band (ν P-C) 3310w, (ν (NH))	2.46(w, 1NH, $2NH_2$, amine), 3.70(w, 1H, methine, 1 beta -N) 1.53(s, 6H, methyl –CH), {6.81-7.59(s, 4H, 8H, 8H)}aromatic ring	663.07
2.4a	$C_{35}H_{34}MoN_2O_4P_2$ (704.54)	59.67 (59.60)	4.86 (4.85)	3.98 (4.00)	78	213-221	2010s, 1980,1890w,1860sb (νCO) 720s, 690s single band (ν P-C) 3320w, (ν (NH))	1.60(s, 6H, methyl,1alpha -N), 1.89(s, 6H, methyl,1alpha -N) 3.71(m, 1H,methine, 1beta –N), 1.70(w, 1ÑH, hydrazid) {6.80-7.57(s, 4H, 8H, 8H)} aromatic ring	703.11
2.4b	$C_{39}H_{34}MoN_2O_5P_2$ (724.64)	60.95 (60.90)	4.46 (4.43)	3.64 (3.60)	77	231-240	2020, 1980,1890w,1865sb (νCO) 720s, 690s single band (ν P-C) 3350w, (ν (NH))	1.47(s, 6H, methyl,1beta -N), 3.25(m, 1H,methine, 1beta –N) 7.90(m, 1H,benzylidenimin, 1alpha –N), 8.85(w, 1ÑH, amine) 8.70(m, aromatic C-OH), {6.80-7.58(s, 5H, 10H, 9H)} aromatic ring	768.10
2.4c	$C_{37}H_{36}MoN_2O_5P_2$ (746.58)	59.52 (59.50)	4.86 (4.90)	3.75 (3.74)	81	217-228	2010s, 1985w,1890w,1860sb (νCO) 720s, 695s single band (ν P-C) 3400w, (ν (NH)) 3200wb, (ν (OH))	1.33(s, 6H, methyl,1beta -N), 3.354(w, 1H,methine, 1beta –N) 4.90(m, 1H, 1-ethylene, 1alpha –C=C), 8.11(w, 1ÑH, hydrazid), 11.85(w, enol (C-OH)), 1.86(s, 3H, methyl, 1alpha –C=CH), 0.95(s, 3H, methyl, 1gama C=CH-), {6.80-7.57(m, 4H, 8H, 8H)} aromatic ring	745.12
2.4d	$C_{34}H_{32}MoN_2O_4P_2$ (690.52)	59.14 (60.00)	4.67 (4.65)	4.06 (4.05)	83	197-204	2010s, 1980w,1890w,1860sb (νCO) 720s, 680s single band (ν P-C) 3200w, (ν (NH))	1.35(s, 6H, methyl,1beta -N), 3.30(w, 1H,methine, 1beta –N) 6.60(s, 1H, 1-hydrazid, 1alpha –N) 2.53(w, 1ÑH, hydrazid) 0.99(s, 3H, methyl, 1alpha –N) {6.53-7.55(m, 4H, 8H, 8H)} aromatic ring	690.09
2.4e	$C_{39}H_{34}MoN_2O_4P_2$ (752.59)	62.24 (62.25)	4.55 (4.55)	3.72 (3.70)	80	183-189	2010s, 1980,1890w,1860sb (νCO) 725s, 690s single band (ν P-C) 3350w, (ν (NH))	1.55(s, 6H, methyl,1beta -N) 3.31(w, 1H,methine, 1beta –N) 8.10(s, 1H, 1-benzylidenimin, 1alpha –N) 2.09(w, 1ÑH, amine) {6.53-7.55(m, 4H, 8H, 8H)} aromatic ring	751.11
2.5c	$C_{37}H_{34}MoN_2O_4P_2$ (728.56)	61.00 (61.08)	4.70 (4.74)	3.85 (3.91)	80	237-244	2010s, 1980,1890w,1860sb (νCO) 720s, 690s single band (ν P-C)	1.95(s, 6H, methyl,1beta -N) 4.09(w, 1H,methine, 1beta –N) 5.90(s, 1H, 1-pyrazole, 1alpha –N-N=C-C1) 2.30(s, 3H, methyl, 1 alpha –N-N=C-1) 2.15(s, 3H, methyl, 1 alpha –N-N=C-CH=C-1) {6.80-7.55(m, 4H, 8H, 8H)} aromatic ring	727.11

IR (ν^{KBr} max), cm^{-1} spectra: (s) Strong (sb) Strong board (w) Weak (wb) weak board

$^1H\{^{31}P\}$-NMR($CDCl_3$) spectra (δ) Chemical shift (m) Mediam (s) Strong (wb) Weak board (w) Weak (p-) Para Position (o-) Ortho position (m-) Meta position (ppm) Part per million (enol) Hydroxyl group

Table (4): Characterization data of the newly synthesized (diphenylphosphino)ethene derivative complexes.

Compd. No	Mol. Formula (mol. wt.)	Calcd.%,(Found) % C	H	N	Yield%	m.p., ºC	IR (ν^{KBr} max), cm^{-1}	$^1H\{^{31}P\}$-NMR($CDCl_3$) δ, ppm, Assignment	M^+
3.2a	$C_{32}H_{26}WO_4P_2$ (720.33)	53.36 (53.41)	3.64 (3.62)	- -	75	183-188	2020s, 1980,1895w,1860sb (νCO) 725s, 690s single band (ν P-C)	1.75(s, 6H, CH_3 methyl) {7.23(s, 4H)}, {7.12(s, 8H)} {7.55(s, 8H)}aromatic ring	722.08
3.3a	$C_{32}H_{30}WN_2O_4P_2$ (752.38)	51.08 (51.05)	4.02 (4.11)	3.72 (3.75)	82	200-206	2000s, 1980,1892w,1860sb (νCO) 720s, 690s single band (ν P-C) 3310w, (ν (NH))	2.49(w, 1NH, $2NH_2$, amine), 3.73(w, 1H, methine, 1 beta -N) 1.56(s, 6H, methyl –CH), {6.85-7.57(s, 4H, 8H, 8H)}aromatic ring	754.12
3.4a	$C_{35}H_{34}WN_2O_4P_2$ (792.44)	53.05 (53.13)	4.32 (4.40)	3.54 (3.49)	82	234-237	2010s, 1980,1890w,1865sb (νCO) 720s, 690s single band (ν P-C) 3350w, (ν (NH))	1.65(s, 6H, methyl,1alpha -N), 1.90(s, 6H, methyl,1alpha -N) 3.74(m, 1H,methine, 1beta –N), 1.71(w, 1ÑH, hydrazid) {6.80-7.57(s, 4H, 8H, 8H)} aromatic ring	794.14
3.4b	$C_{39}H_{34}WN_2O_5P_2$ (724.64)	54.69 (54.53)	4.00 (4.09)	3.27 (3.30)	73	214-217	2020, 1980,1890w,1860sb (νCO) 720s, 690s single band (ν P-C) 3410w, (ν (NH))	1.44(s, 6H, methyl,1beta -N), 3.29(m, 1H,methine, 1beta –N) 7.95(m, 1H,benzylidenimin, 1alpha –N), 8.81(w, 1ÑH, amine) 8.75(m, aromatic C-OH), {6.80-7.58(s, 5H, 10H, 9H)} aromatic ring	858.15
3.4c	$C_{37}H_{36}WN_2O_5P_2$ (834.48)	53.25 (52.98)	4.35 (4.29)	3.36 (3.40)	85	193-198	2020s, 1985w,1895w,1860sb (νCO) 720s, 690s single band (ν P-C) 3410w, (ν (NH)) 3220wb, (ν (OH))	1.30(s, 6H, methyl,1beta -N), 3.32(w, 1H,methine, 1beta –N) 4.90(m, 1H, 1-ethylene, 1alpha –C=C), 8.11(w, 1ÑH, hydrazid) 11.86(w, enol (C-OH)), 1.89(s, 3H, methyl, 1alpha –C=CH) 0.99(s, 3H, methyl, 1gama C=CH-), {6.80-7.57(m, 4H, 8H, 8H)} aromatic ring	836.17
3.4d	$C_{34}H_{32}WN_2O_4P_2$ (778.42)	52.46 (52.24)	4.14 (4.15)	3.60 (3.59)	82	249-255	2010s, 1980w,1890w,1860sb (νCO) 725s, 680s single band (ν P-C) 3210w, (ν (NH))	1.35(s, 6H, methyl,1beta -N) 3.31(w, 1H,methine, 1beta –N) 6.60(s, 1H, 1-hydrazid, 1alpha –N) 2.53(w, 1ÑH, hydrazid) 1.00(s, 3H, methyl, 1alpha –N) {6.53-7.55(m, 4H, 8H, 8H)} aromatic ring	778.13
3.4e	$C_{39}H_{34}WN_2O_4P_2$ (840.49)	55.73 (55.66)	4.08 (3.95)	3.33 (3.35)	76	172-175	2000s, 1980,1890w,1865sb (νCO) 720s, 690s single band (ν P-C) 3310w, (ν (NH))	1.52(s, 6H, methyl,1beta -N) 3.34(w, 1H,methine, 1beta –N) 8.13(s, 1H, 1-benzylidenimin, 1alpha –N) 2.04(w, 1ÑH, amine) {6.53-7.55(m, 4H, 8H, 8H)} aromatic ring	842.15
3.5c	$C_{37}H_{36}WN_2O_4P_2$ (818.48)	54.30 (54.28)	4.43 (4.51)	3.42 (3.45)	84	218-220	2010s, 1985,1895w,1865sb (νCO) 725s, 690s single band (ν P-C)	1.93(s, 6H, methyl,1beta -N) 4.14(w, 1H,methine, 1beta –N) 5.87(s, 1H, 1-pyrazole, 1alpha –N-N=C-C1), 2.33(s, 3H, methyl, 1 alpha –N-N=C-1), 2.15(s, 3H, methyl, 1 alpha –N-N=C-CH=C-1) {6.80-7.55(m, 4H, 8H, 8H)} aromatic ring	820.17

IR (ν^{KBr} max), cm^{-1} spectra: (s) Strong (sb) Strong board (w) Weak (wb) weak board

$^1H\{^{31}P\}$-NMR($CDCl_3$) spectra (δ) Chemical shift (m) Mediam (s) Strong (wb) Weak board (w) Weak (p-) Para Position (o-) Ortho position (m-) Meta position (ppm) Part per million (enol) Hydroxyl group

References

[1] Cooper, G. R.; Hassan, F.; Shaw B. L.; Thornton-Pett, M. J. *Chem. Soc., Chem. Commun.,* **1985**, 614.

[2] Fontaine, X. L. R.; Hassan, F. S. M.; Higgins, S. J.; Jacobsen, G. B.; Shaw, B. L.; Thornton-Pett, M. *J. Chem. Soc., Chem. Commun.,* **1985**, 1635.

[3] Awad, I. M. A.; Hassan, F. S. M.; Mohamed, A. E.; Al-Hossainy, A. F. *Phosphorus, Sulfur, and Silicon*. **2004**, 179, 1251.

[4] Fatma, S. M. H.; Mahmoud, A. G.; Adila, E. M.; Al- Hossainy, A. F. *Arabian J. Chem.* **2008**, 1, 67-78.

[5] Badr, A. M., EL-Amin, A. A., Al-Hossainy. A. F., The European physical, J. B. **2006**, 53, 439–448.

[6] Allen, D. W.; Mifflin, J. P.; Skabara, P., J. J. *Organomet. Chem*. **2000**. 601: 2 293 – 298

[7] Bennett, M. A.; Edwards, A. J.; Harper, J. R.; Khimyak, T.; Willis, A. C., *J. Organomet. Chem*. **2001**, 629: 1-2 7 - 18

[8] Butler, I. R.; Coles, S. J.; Fontani, M.; Hursthouse, M. B.; Lewis, E.; Malik, K. L. M., Abdul; M., Marc; Z. P.,. *J. Organomet. Chem.* **2001**, 637: 538 – 548

[9] Huizhang, L.; Calhorda, M. J.; Felix, V.; Drew, M. G. B. *J. Organomet.Chem*. **2001**, 632: 1-2, 175 - 187

[10] Kasani, A.; Michael, F.; Ronajd, G. C., *J. Am. Chem. Soc*. **2000,** 722, 726-727

[11] Nagwa, N., *J. Organomet. Chem.* **2000,** 602(1-2), 137-143.

[12] Braunstein, P.; Galsworthy, J. R.; Hendan, B. J.; Marsmann, H. C., *J. Organomet. Chem.* **1998,** 551, 125.

[13] Araujo, M. H.; Hitchcock, P. B.; Nixon, J. F.; Vargas, M. D., *J. Braz. Chem. Soc*. **1998,** 9, 563.

[14] Enders, D.; Noyori, R.; Trost, B. M., Spectroscopic methods in organic chemistry, Georg Thieme Verlag Stuttgart., New York, 1997.

[15] Santi, S.; Carli, F.; Ceccon, A.; Crociani, L.; Gambaro, A.; Tiso, M.; Venzo, A., Extended Abstracts of the 201st Meeting of the Electrochemical Society, Philadelphia, USA, **2002**, 12-17.05., Ext. Abstr.1257.

[16] Atwood, C. G.; Geiger, W. E., *J. Amer. Chem. Soc.* **2000,** 122, 5477.

[17] Ward, M. D., *Chem. Soc. Rev.* **1995,** 24, 121.

[18] Loukova, G. V.; Strelets, V. V., *Collect. Czech. Chem. Commun.* **2001,** 66, 185.

[19] Abd El –Aal, R. M.; Belal, A. A. M., *Dyes and Pigments.* **2005,** 65, 129.

[20] Rajagopal, R.; Shenoy , V. U.; Padmanabhan, S.; Sequeira, S.; Seshadri, S., *Dyes and Pigments.* **1990,** 13, 167.

[21] O'Hare, D.; Green, J. C.; Marder, T.; Collins, S.; Stringer, G.; Kakkar, A. K.; Kaltsoyannis, N., Kuhn, A., Lewis, R.; Mehnert, C.; Scott, P.; Kurmoo, M.; Pugh, S., *Organometallics.* **1992,** 11, 48.

[22] Calhorda, M. J.; Veiros, L. F., *J. Organomet. Chemistry.* **2001**, 635, 197.

[23] Akhil, R., Chakravarty, F., Albert Cotton, and Willi S., *Inorganic Chimica Acta*. **1984**, 84, 2, pp 179.

Arabian J. Chem. Vol. 1, No. 3, 255-262 (2008)

Studying the Effect of Addition of Iron (III) Chloride During Acid Hydrolysis of Bagasse Viscose Pulp

Mona M. F. Fahmy

Department of Chemistry Faculty of Science,

Cairo University – Giza, Cairo, A.R. Egypt

Email: m.fahmy17@yahoo.com

Abstract

Bleached bagasse viscose pulp was subjected to mild acid degradation in absence and in presence of iron(III) chloride. The effects of these treatments on the yield, chemical, physical and submicroscopic characteristics of the degraded pulps were studied. The iron(III) chloride enhances the decrystallisation of the cellulose and resulted in higher leveling off the degree of polymerization (LODP) and improves the reactivity towards xanthation. The role of iron(III) chloride was greatly dependent upon the acid concentration. At higher acid concentration, iron(III) chloride results in a sharp initial degradation which is due to the increase in the susceptibility of the cellulose macromolecules and thereby creating the conditions under which severe degradation is to be expected. At lower acid concentration, intercrystalline degradation predominates in the less ordered domains that are created by iron(III) chloride.

1. Introduction:

The glucosidic linkages of the cellulose molecules are readily hydrolyzed by the action of mineral acids resulting in disintegration of the macromolecules. The rate of reaction of acid solutions with cellulose is not the same in different parts of the fibers. As a result, a complex mixture of products of incomplete decomposition of the cellulose, is formed and the composition of this mixture changes during the course of hydrolysis [1]. Bond cleavage by interaction with (H_3O^+) (acid hydrolysis) proceeds at random in a homogenous reaction system, but is selective with respect to the state of crystalline order in a heterophase reaction system [2]. The mechanism of hydrolysis of the cellulose is represented by the following scheme [3]. Iron(III) ions act as a catalyst for the cleavage of cellulose 1,4-β glycosidic bonds [4-6].

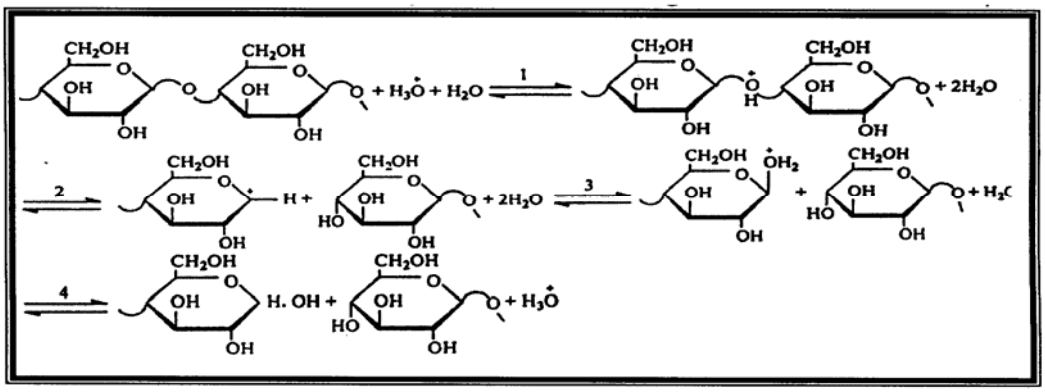

In the present work, acid hydrolysis of bagasse viscose pulp was carried out with and without addition of iron(III) chloride solution. The required amount (corresponding to 0.1% iron(III) chloride based on pulp), was added to the hydrolyzing solution. The effect of such addition on physical and super-molecular characteristics of bagasse viscose pulp and in particular on leveling off the degree of polymerization (LODP). Also, the effect of the acid concentration on the role of iron(III) chloride throughout the process of hydrolysis has been investigated.

2. Experimental

2.1 Raw material

The raw material used in this work was depithed Egyptian sugar cane bagasse, it was obtained from Egyptian sugar and distilling Co.

2.2. Prehydrolysis and pulping

Depithed bagasse was subjected to prehydrolysis followed by alkali treatments, both treatments were carried out under the prevailing atmospheric pressure for 6 h at 100°C and with a liquor ratio of 1: 10. The prehydrolysis was carried out with 6% sulphuric acid (based on depithed bagasse) and the pulping was done using 28% sodium hydroxide (based on prehydrolysed depithed bagasse). The pulp was then washed thoroughly and placed in dilute hydrochloric acid solution for 20 min, at room temperature with a consistency of 3% (based on pulp). The pulp was washed thoroughly till neutrality.

2.3 Bleaching

Multistage bleaching was applied on the prepared pulp as follows: after estimation of the natural chlorine requirement as stated earlier [7], the estimated amount of chlorine was added to the pulp in the form of chlorine water at 20°C for 1h at 3% consistency. This was followed by extraction with 16% sodium hydroxide (based on pulp) at 80°C for 2 h, at 7% consistency. In the third step, an alkaline hypochlorite solution was used; its active chlorine is corresponding to 30% of the amount of chlorine used in the first step. This treatment was carried out at 40°C for 2 h, at 3% consistency. In the fourth step, l g of sodium chlorite was used with 7.5 mL 10% acetic acid for 1.5 h at 80°C with a consistency of 5%.

2.4 Techniques of Acid Hydrolysis

An amount of bleached pulp corresponding to 15 g of dry sample was refluxed at 100°C with 750 mL of the required concentration of hydrochloric acid alone, and hydrochloric acid containing 0.1 % of iron(III) chloride solution (British Drug House, England). The reaction was carried out for various times as indicated in Tables (1 and 2). The samples were then washed with distilled water until they become neutral and dried at room temperature.

2.5 Analysis of hydrolyzed products

The chemical analysis of the degraded products for α-, β- and γ-cellulose % and pentosan % were measured according to American Tappi standard method [8,9]. The average degree of polymerization (DP) was determined according to Buchs and Mertes [10]. Jayme's method was used for the estimation of water retention value [11]. The degree of crystallinity was determined by iodine adsorption method of Hessle and Power [12]. The reactivity towards xanthation was determined according to the method of Fock [13].

3. Results and Discussion

When bagasse viscose pulp hydrolyzed with 0.5 N at 100 °C (Table 1), the loss in material increased slowly with hydrolysis till it become 2.2% only at the levelling off of the degree of polymerisation (LODP) (222) which was attained after 6 h . The effect of hydrolysis on the α-cellulose was more pronounced. Thus, it decreased from 91.92% to 52.1% at the beginning of the LODP stage. The long-chain α-cellulose macromolecules were hydrolysed to the shorter-chain β-celluloses which were still long enough to resist dissolution. Thus, the value of β-cellulose increased from 3.2% to 16.2%, while the shorter chain γ cellulose increased slightly from 0.99% to 1.2% after 6 h.

The degree of polymerization (D.P.) dropped from 1326 to 364 just after 20 min of hydrolysis, then it decreased more slowly and it leveled off at a value of 222 after 6 h. There was an initial decrystallization resulting from the acid attack on the cellulose chain which was followed by recrystallization till the LODP stage [14]. The pentosans decreased with hydrolysis and became more resistant to the hydrolytic action in the period of LODP. The chemical reactivity improved in spite of the increase in the crystallinity. Thus, the degree of crystallinity is not the only factor governing reactivity. The decrease in D.P. and α-cellulose, means shorter-chain macromolecules and hence better dissolution during xanthation i.e. better chemical reactivity.

In case of hydrolysis with 0.5N HCl-0.1% $FeCl_3$ mixture (Table 1, Fig. 1-6), the α-cellulose decreased from 91.92 to 66.6% at the beginning of the LODP stage. Whereas, β-cellulose and γ-cellulose increased from 0.99% to 2.5% at the LODP stage. The pentosans decreased with hydrolysis. The D.P. decreased and leveled off at a value of 243 which was attained after 6 h. Moreover all samples hydrolyzed with HCl-$FeCl_3$ mixture had lower crystallinity than the starting sample except at the LODP stage where crystallinity increased sharply.

A striking effect took place in the reactivity towards xanthation and the percent of insoluble cellulose in the xanthation reaction became zero (i.e. the pulp was completely reactive) after 20 min only of hydrolysis. The pulp remained completely reactive throughout the whole time of hydrolysis. It seems that the penetration of iron(III) chloride in between the cellulose chains increases the intermolecular distances to such an extent that the pulp becomes completely soluble during xanthation.

Table (1): Effect of Iron (III) chloride on the hydrolysis of bagasse viscose pulp at higher acid concentration.

Medium of hydrolysis	Start pulp	0.5 N hydrochloric acid					0.5 N hydrochloric acid + 0.1% iron (III) chloride				
Hydrolysis time (h)		0.33	0.67	3	6	9	0.33	0.67	3	6	9
Analysis of residues											
Yield (%)		99.6	98.4	97.5	96.8	94.8	99.14	98.8	96.6	94.7	94.5
Loss in weight (%)		0.4	1.6	2.5	3.2	5.2	0.86	1.2	3.4	5.3	5.5
α- cellulose (%)	91.92	78.76	76.1	59.2	52.1	61.0	80.04	80.9	64.5	66.6	64.3
β- cellulose (%)	3.2	10.3	10.2	18.1	16.2	15.2	5.6	8.1	15.5	13.3	14.1
γ- cellulose (%)	0.99	1.74	1.9	1.4	1.2	1.5	1.6	1.4	1.5	2.5	2.1
Pentosan (%)	8.6	8.3	8.1	7.3	7.2	6.9	8.3	7.2	6.2	5.8	4.9
D.P.	1326	364	326	233	222	185	655	470	275	243	223
W.R.V. (%)	86.2	70.9	82.4	85.4	81.8	81.8	75.3	71.8	92.9	86.2	84.7
Crystallinity (%)	83.6	63.5	65.6	65.6	80.7	77.7	61.0	60.2	68.1	74.0	77.4
Reactivity (% of insol. Cellulose)	48.8	48.1	42.1	31.1	23.5	18.7	00.0	00.0	00.0	00.0	00.0

When the hydrolysis of bagasse viscose pulp was carried out with lower acid concentration, namely, 0.05N HCl at 100°C (Table 2) it resisted the hydrolytic action as indicated by the loss in material which amounted to 1.5% only after 9 h of hydrolysis. After an initial small increase in α-cellulose, its value decreased with hydrolysis until it became 80.9% the sum of β- and γ-cellulose increased till it became about 9.9%. The D.P. decreased throughout the whole period of hydrolysis till it leveled off at 326 which attained after 9 h. The pentosans % decreased slowly at first with hydrolysis, then became constant at a value of 6.5% throughout the whole period of hydrolysis and the reactivity was improved and did not change at the LODP period.

In case of hydrolysis with 0.05N HCl-0.1% $FeCl_3$ mixture the loss in material amounted to 0.5% only after 9 h of hydrolysis (Fig. 1). The α-cellulose decreased with hydrolysis to a value of 81.9% at the LODP stage which was attained after 9 h (Fig. 2). The pentosans % decreased in the first hours and began to be constant at a value of (6.5-6.0%) at the LODP stage and the reactivity increased with hydrolysis.

Table (2): Effect of Iron (III) chloride on the hydrolysis of bagasse pulp at lower acid concentration.

Medium of hydrolysis	Start pulp	0.05 N hydrochloric acid					0.05 N hydrochloric acid + 0.1% iron (III) chloride				
Hydrolysis time (h)		0.67	1.5	3	6	9	0.67	1.5	3	6	9
Analysis of residues											
Yield (%)		99.9	98.9	98.7	98.6	98.5	99.9	99.8	99.6	99.5	99.5
Loss in weight (%)		0.1	1.1	1.3	1.4	1.5	0.1	0.2	0.4	0.5	0.5
α- cellulose (%)	91.92	94.0	89.6	85.4	85.5	80.9	90.2	88.6	88.0	83.0	81.9
β- cellulose (%)	3.2	2.5	3.2	5.2	6.9	7.9	3.5	3.9	4.4	6.6	8.2
γ- cellulose (%)	0.99	2.1	2.1	1.9	2.1	2.0	1.5	1.6	1.7	1.4	1.4
Pentosan (%)	8.6	6.6	6.5	6.5	6.5	6.5	7.1	6.7	6.5	6.5	6.0
D.P.	1326	755	539	494	408	326	774	576	543	490	371
W.R.V. (%)	86.2	82.0	77.6	78.2	80.1	72.2	75.3	108.9	83.1	90.2	81.7
Crystallinity (%)	83.6	55.9	56.8	51.8	60.2	63.1	60.2	62.7	63.6	65.6	62.7
Reactivity (%) of insol. Cellulose	48.8	36.3	41.1	44.4	35.9	35.6	24.4	15.8	13.3	10.5	10.2

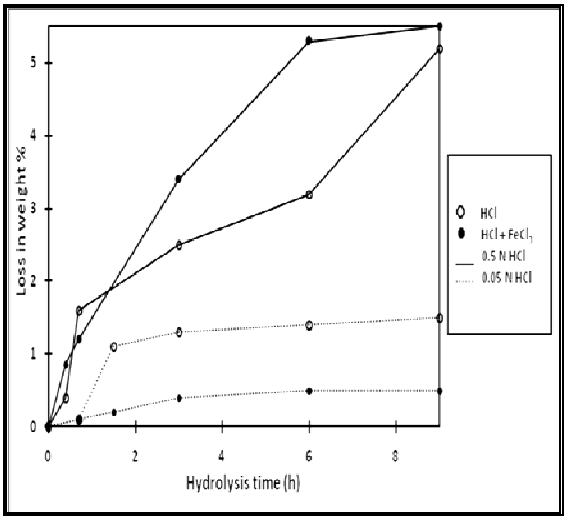

Figure 1. Loss in weight with time of acid treatment

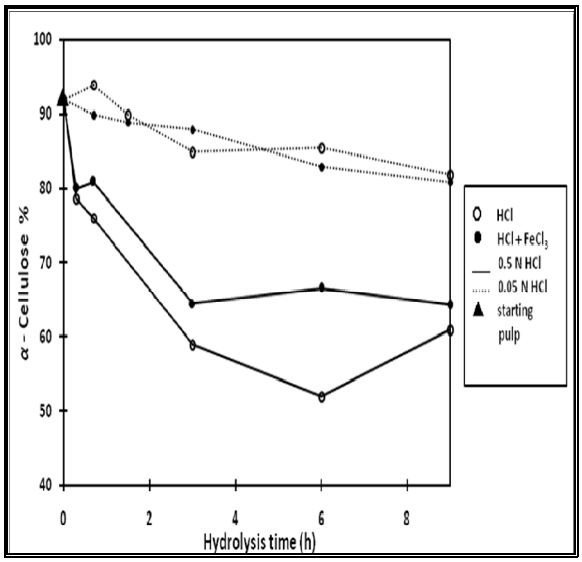

Figure 2. Change in α-Celluse with time of acid treatment

It is clear that iron(III) chloride reduced the rate of the hydrolysis reaction. This is indicated by the yield % and the degree of polymerization. The cellulose samples undergo intracrystalline degradation in which the reactant penetrates the crystallites. This results in a stronger degradation than in case of intercrystalline degradation, which is mostly restricted to the amorphous domains of the fibers [15]. Iron(III) chloride seems to reduce the intracrystalline degradation reaction of bagasse viscose pulp via its initial decrystallisation effect on the supermolecular structure of cellulose. This iron(III) chloride effect, together with the additional free chain ends resulting from the action of acid, may create relatively low-ordered domains and consequently intercrystalline degradation becomes more probable, resulting in a decrease in the rate of the acid degradation reaction.

It was noticed that iron (III) chloride does not affect the time required to reach the leveling off the D.P. (LODP), but it does result in a higher LODP. According to Philipp [2], the LODP depends to a slight extent upon acid concentration, but very much on the state of the supermolecular order of the substrate as well as the state of swelling; higher swelling caused by changing the medium increases the LODP. Thus the higher LODP in the presence of iron(III) chloride is mostly due to its decrystallisation effect on cellulose.

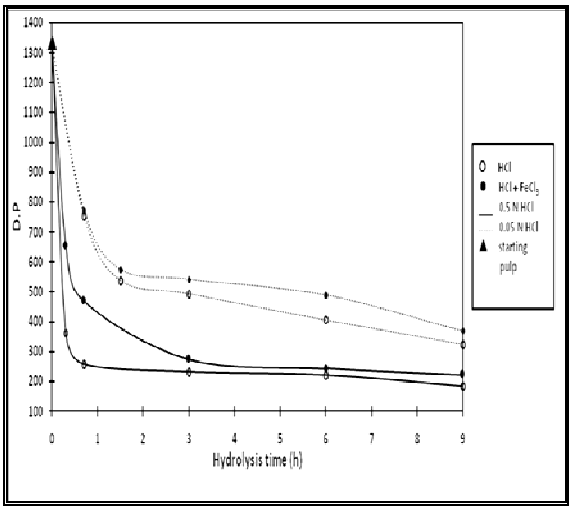

Fig. 3. Change in D.P with time of acid treatment

The decrystallisation effect of iron(III) chloride may be further deduced from the degree of crystallinity of the resulting products, the value of which remains lower than in the presence of acid alone, as shown by Fig. (4). It

is clear that the change in behaviour of the degree of crystallinity is unaffected by iron(III) chloride, i.e. the degradation process involves initial decrystallisation followed by crystallization. Crystallinity measures the difference between the rate of decrystallisation and that of the digestion of the more susceptible fractions.

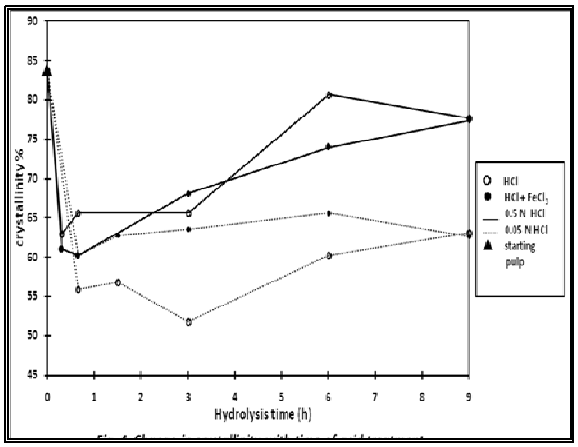

Fig. 4. Change in crystallinity with time of acid treatment

The acid degradation of bagasse viscose pulp cellulose results in residues having lower W.R.V. than the original pulp as shown in Fig. (5). Iron(III) chloride increases the W.R.V., i.e., increases the accessibility of the celluosic fibres.

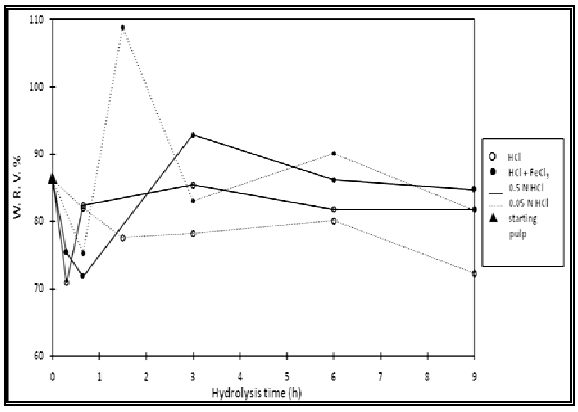

Fig. 5. Change in W. R. V. % with time of acid treatment

Increasing the concentration of the acid to 0.5 N increased the rate of degradation and reduced the time of the LODP. As shown in Fig. (4,5) the changes in the supermolecular characteristics of bagasse viscose pulp cellulose during degradation were also affected by increasing the concentration of the acid. The higher values of degree of crystallinity and lower W.R.V. is due to the greater digestive action of the acid on the more susceptible fractions which was reflected in the rate of weight loss (Fig. 1).

Comparison of the results in tables 1 and 2 reveals a remarkable change in the role of iron(III) chloride throughout the process on increasing the acid concentration. With the higher acid concentration, the presence of iron(III) chloride results in a sharper initial degradation. This is mostly due to the increase in the susceptibility of the cellulose macromolecules, thereby creating conditions under which severe degradation is to be expected. As the reaction proceeds towards the LODP, the rate of the reaction decreases. The shorter fragments have a higher affinity towards the iron(III) chloride effect. Thus, intercrystalline degradation becomes more probable which results in higher LODP. This is accompanied by a sharp decrease in weight and an increase in the degree of crystallinity which is due to the preferential digestion of the lower-order domains. Generally, iron(III) chloride results in higher LODP, lower crystallinity and higher W.R.V. and much better reactivity independently on the acid concentration.

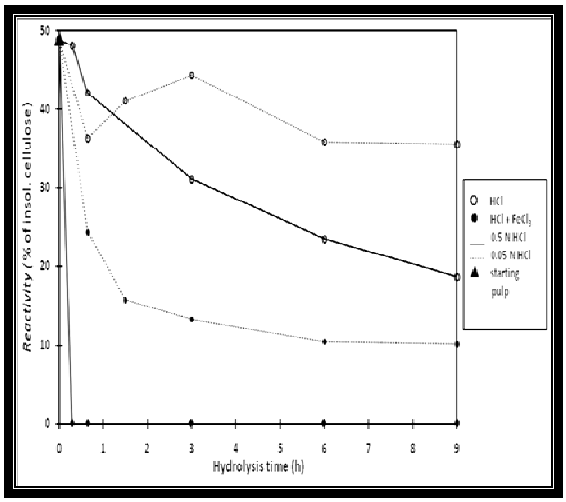

Fig. 6. Change in reactivity % with time of acid treatment

References

[1] F. Sadov, M. Korchagin and A. Matetsky, Chemical Technology of Fibrous Materials, Mir Publisher, Moscow 1973: 31.

[2] B. Philipp, Pure & Appl. Chem., 1984; 56: 391.

[3] T.P. Nevell and W.R. Upton. Carbohydrate Research, 1976; 49: 163.

[4] M. Bicchieri and S. Pepa., Laboratory Chemistry, Istituto Centrale Patologia del Libro I-00184 Rome (Italy), Rastaurator 1996; 17(3): 165 (Eng) Chem. Abst. 1997; 126 (1): 9370.

[5] P. Calivini, A. Gorassini, Rastaurator, (2002); 23, 205.

[6] V.S. Salih, M. Stric, J. Kolar and B. Pihlar, Poly. Deg. & Stab,(2007); 92, 1476.

[7.] M.A. Aboustate, S.A. Helmy and N.Y.S. Mostafa. Dissolving pulps from wheat straw by sulphate anthraquinone and alkaline sluphite-anthraquinone pulping, Pira international straw Conf. Cambridge, UK, 1987; 2: 135.

[8] Tappi Standards, Technical Association of the Pulp and Paper Industry, Atlanta, G.a., T. 2036 OS 61.

[9] Tappi Standards, TS 223 to -63.

[10] L. Buchs and F. Mertes, Milliand Text. Ber., 45, 275 (1964).

[11] G. Jayme, Tappi, 41, 180 A (1958).

[12] L.E. Hessler and E. Power, Text. Res. J., (1954), 24, 822.

[13] W. Fock, Papier (Darmstadt) (1959); 13, 92.

[14] G. Jayme and E. Roffael Papier., (Darmstdt), 23 (1) (1969).

[15] S.A. Helmy, Poly. Deg. & Stab, (1993); 39, 155.

Arabian J. Chem. Vol. 1, No. 3, 263-269 (2008)

Reaction of Ozone with Cobalt(II) Acetate: Formation of μ-Hydroxo-diacetato Cobalt(III) Dimer

Mutasim I. Khalil
Department of Chemistry, College of Science, King Saud University,
P.O. Box 2455 , Riyadh 11451, Saudi Arabia

Abstract

Cobalt(II) acetate tetrahydrate in glacial acetic acid is readily oxidized by ozone at room temperature. The reaction is followed by UV spectroscopy. The elemental analysis, molecular weight determination, I. R. and UV spectroscopic measurements of the dark green product obtained suggests the formation of hydroxo-diacetato cobalt(III) complex. Solubility, reactivity, oxidative ability and speculative mechanism of formation and structure of the complex are described.

1-Introduction

Cobalt(III) salts, in general, play an important role in the oxidation of aromatic hydrocarbons[1,2] and are extensively used as catalysts in the autoxidation of aldehydes and saturated as well as unsaturated hydrocarbons[3]. Their catalytic activity might reside in the higher-valency cobalt(III) state formed during the oxidation or within their readiness to undergo electron transfer with a wide variety of organic molecules forming free radicals [3-5].

Cobalt(III) acetate in particular plays an important role in several processes as an aerobic one-electron oxidizing agent. For example, cobalt acetate catalyzed oxidation of alkylbenzenes to the corresponding mono-and di-carbylic acids forms the basis of several commercial processes [6].

It also oxidizes toluene in acetic acid to benzyl acetate and benzaldehyde, in 50-90%, yield based on the consumption of cobalt(III) ions, and it oxidizes 2-methynaphthalene at 70° in acetic acid to 2-naphthaldehyde, 1-acetoxy-2-methyl naphthalene and 2-acetoxy-methyl naphthalene[7].

Although several authors have claimed the preparation of cobalt(III) acetate, either by reaction of cobalt(III) sulphate with an acetate or by oxidation of cobalt(II) acetate[8-10], no pure product corresponding to $Co(OAc)_3$ has yet been obtained. For example, the electronic method reported by sharp[9] affords a crude product containing only 10-15% cobalt(III). Attempts to purify the product either by solvent extraction or ion-exchange chromatography were unsuccessful although the latter technique resulted in a product containing 20% cobalt(III). Hill [11] investigated the kinetics and mechanism of the cobalt(II)-catalyzed decomposition of ozone in perchloric acid and acetic acid solution and reported a value of $Co(OAc)^{2+}$ / Co^{2+} ratio in solution of 7.0, and measured ratio of $Co(OH)^{2+}$ / Co^{2+} in solution without acetic acid was 0.8. However, no product was separated. Solutions of cobalt(III) acetate prepared by Heiba [7] by bubbling oxygen into an aqueous mixture of $Co(OAc)_2.4H_2O$ and glacial acetic acid contained only 55% cobalt(III) content.

Recently, we have reported a different route and mechanism for the formation of cobalt(III) acetate based on a peroxyacetate intermediate formed by the reaction of cobalt metal with acetic acid or its anhydride under reflux in the presence of an oxidizing nitrate group. A dimmer with either four hydroxyl groups or with a peroxidic as well as hydroxyl groups bridging the two cobalt atoms was proposed[12,13].

Because there exists some controversy concerning the constitution and mechanism of formation of cobalt(III) acetate, we have investigated the products of the

reaction of ozone with acidified cobalt(II) solution at room temperature. From these studies, it was apparent that neither solution of cobalt(II) sulfate, nitrate, nor chloride in the corresponding acid show any tendency towards oxidation. However, in contrast, a solution of cobalt(II) acetate in acetic acid is smoothly oxidized to cobalt(III) species.

In this paper we report the isolation, properties and proposed mechanism of formation of hydroxo-diacetatocobalt(III) complex obtained from this reaction.

2-Experimental

0.04 M Solutions of cobalt(II) salts ($CoSO_4$; $CoCl_2$; $Co(NO_3)_2$. $2H_2O$ and $Co(OAc)_2$. $4H_2O$) in their corresponding acids, H_2SO_4 , HCl (pH ~ 1.6) HNO_3 and CH_3COOH acid (pH = 4.8) respectively, were prepared. In each of the experiment, ozone (generated by Fisher 500 M ozone generator) was bubbled at room temperature through 50 cm^3 of the cobalt(II) solutions. The reactions were followed by recording the UV spectra at intervals of 5 min using a Beckman Du 70 spectrometer. No change in the color and spectra of the former three solutions was observed even after 20 hours of bubbling ozone. However, the pink cobalt(II) acetate solution has changed gradually into the dark green color (Fig. 1).

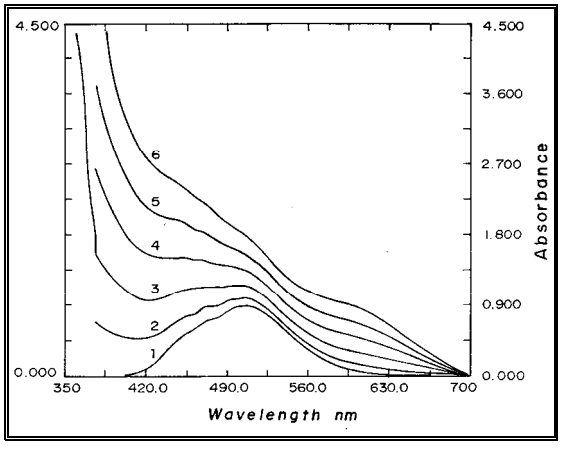

Figure 1: Visible spectra of solutions of $Co(Oac)_2$ in acetic acid reacted with O_3, measured after 5 (1) , 10 (2) , 15 (3) , 20 (4) , 25 (5) and 30 (6) minutes.

The dark green solid, obtained in a separate experiment, by bubbling ozone through 0.12 M solution of cobalt acetate tetrahydrate in acetic acid was dried under vacuum at room temperature. Excess of the acetic acid was washed out with CCl_4. The crude product was recrystallized from ethanol, washed with ether and dried under vacuum giving dark green shiny crystals. The product is soluble in water, ethanol and acetic acid giving very deep green solutions which are stable for periods of several months.

Visible spectra of the product in acetic acid, ethanol and water are presented in Figure 2, and infra red spectrum (KBr disc) was obtained by using a Perkin-Elmer 457 spectrometer and is presented in (Figure 3).

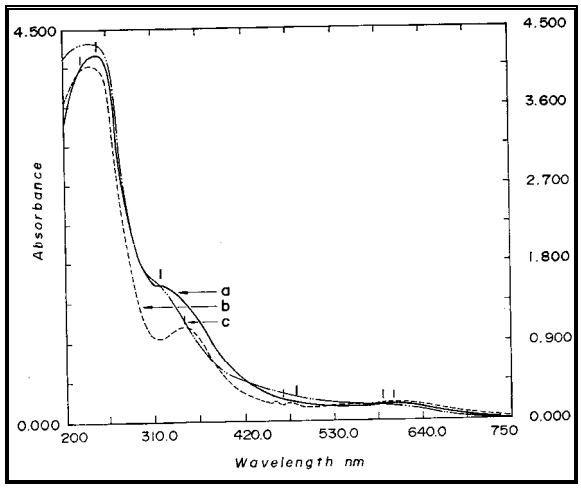

Figure 2: Visible spectrum of the product in : (a) _ alcohol ; (b) -- water ; (c) ___ acetic acid

The cobalt content was determined by atomic absorption using a Perkin-Elmer atomic absorption spectrophotometer. Elementary analysis of the product gave the following; Co, 29.05 % ; C, 25.1 % and H, 4.1 %; (required for $Co(OAc)_3$: Co, 24.97 % ; C, 30.08 % ; H, 2.5

% and for $Co(OH)(OAc)_2$: Co, 30.38 %; C, 24.74 %, H, 3.6 %) .

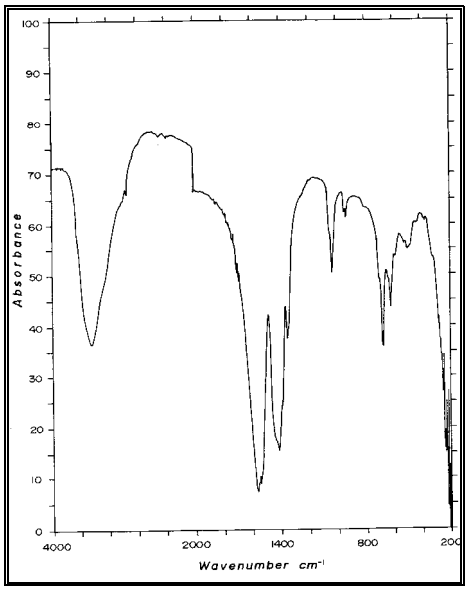

Figure 3: IR Spectrum of Co(OH)(Oac) disk

The cobalt(III) product exhibited a strong and a quantitative oxidizing power, where 0.0525 g of it liberated 0.00028 mole/L of I_2. The computation of cobalt(III) content and molar mass of the product according to the following reaction equation :

$$2\ Co^{3+} + 2\ I^- \longrightarrow I_2 + 2\ Co^{2+}$$

results in an average value of 31.09 % cobalt(III) and a molar mass of 189.45 g/mol of compound (molar mass of $Co(OH)(OAc)_2$ = 193.93 g/mole). Addition of ethylenediamine to an aqueous solution of the product gives a lighter green colour which changes to red clear solution on standing. Sodium hydroxide gives a voluminous brown precipitate, presumably $Co(OH)_3$ while mineral acids give reddish-brown colours instantaneously . The same colour is observed on addition of 0.88 ammonia to an acid solution. On the other hand, stable green solutions are obtained upon addition of KNO_3 and LiCl solutions. However, dark brown precipitate are obtained upon aging.

3. Results and Discussion

Visible spectra of the cobalt(II) acetate acetic acid solution shows a gradual change of cobalt(II) to cobalt(III) as the reaction with ozone proceeds, (Figure 1). Such an oxidation process is clearly supported by the visible spectra of the green separated product in aqueous, alcoholic and acid solutions. The spectra (Figure 2) are indicative of low spin octahedral cobalt(III) species in solution [9,14,15] (Table I).A perfect on symmetry is then tentatively assigned. Such low spin d^6 complexes, possessing the ground term $^1A_{1g}$ arising from the strong-field configuration t_{2g}^6 have several spin-allowed transition, eg.

$$^1T_{1g} \leftarrow {}^1A_{1g}$$

$$^1T_{2g} \leftarrow {}^1A_{1g}$$

$$^1E_g \leftarrow {}^1A_{1g}$$

The higher energy transition, $^1E_g \leftarrow {}^1A_{1g}$, is usually obscured by charge transfer bands. Hence, the bands at 16449 cm^{-1} and 28738 cm^{-1} are assigned to $^1T_g \leftarrow {}^1A_{1g}$, υ_1 and $^1T_{2g} \leftarrow {}^1A_{1g}$, υ_2, transitions, respectively.

Table 1. Energies (cm^{-1}) of Electronic Absorption Maxima of some Cobalt(III) Coplexes (Data from ref. 9,14 and 15)

Complex colour	$[CoF_6]^{3-}$ Yellow	$[Co(H_2O)_6]^{3+}$ Blue	$[Co(NH_3)_6]^{3+}$ Golden brown	$Co(Oac)_3$ Dark green	$[Co_2(C_2O_4)_4(OH)_2]^{4-}$ Green	$[Co(C_2O_4)_3]^{3-}$ Dark green	$[Co(CO_3)_3]^{3-}$ Dark green	$[Co(NO_3)_6]^{3-}$ Dark green	$[Co(en)_3]^{3+}$ Yellow	$[Co(CN_3)_6]^{3-}$ Yellow	Product Dark green	Assigment
High spin	11800											$^5E_g \leftarrow {}^5T_{2g}$
	14000											
Low spin		16500	21000	15300	15300	16600	15700	15200	21400	32400	16449	$^1T_{1g} \leftarrow {}^1A_{1g}$
		24950	29500	21350	21350	23800	22800	22500	24500	39000	28738	$^1T_{2g} \leftarrow {}^1A_{1g}$
					27500							$^1E_g \leftarrow {}^1A_{1g}$
$10Dq/cm^{-1}$		18200	22900	---	----	18000	--	16191	23200	33500	19513	
B/cm^{-1}		670	620	---	---	540	---	466	590	460	766	

Accordingly, the computed Racah parameters, B` and C`, are 766 cm^{-1} and 3064 cm^{-1}, respectively (where $\upsilon_2 - \upsilon_1 \approx 16B$; $C \approx 4B$)[10] .

Then, 10 Dq (= υ_1 + C) is found to be 19513 cm^{-1}. This is compared with a theoretical value of 18050 cm^{-1} calculated using the relation [16,17].

$$10\ Dq = g_{Co(III)} \cdot F_L$$

Where $g_{Co(III)} = 19$; $f_{OH} = 0.94$, $f_{Oac} = 0.96$ (f_L is taken as average of 0. 95).

The nephelauxetic ratio, β , is therefore

$\beta = 766 / 1065 = 0.71$

reflecting considerable covalency in the metal ligand bond. The strong band at 43103 cm^{-1} is assigned as a LMCT band. The corrected value , $\upsilon\ ^1CT$, is :

$\upsilon\ ^1CT = u_{CT}$ (obs) – 10Dq – SPE

where the change in spin pairing energy, SPE, from + 2D to D is – 5362 cm^{-1}, hence:

$\upsilon\ ^1CT = (43103 - 19513 + 5362)\ cm^{-1} = 28952\ cm^{-1}$.

The optical electronegativity, χ_{opt}, of the mixed ligands [$OH(Oac)_2$] is estimated as follow:

$28952\ cm^{-1} = 30{,}000\ (\chi L - \chi Co(III))$

$= 30{,}000\ (\chi L - 2.30)$

$\therefore = \chi L = 3.17$

Such a value is comparable to χ RNH_2 of 3.2 and place it at the light side of the nephelauxetic series[8].

The infra red spectrum (Figure 3). Exhibited bands at 3437 cm^{-1} v.s., (OH) str; 1560 cm^{-1} v.s. υ_{as} [COO] str; 1540 cm^{-1} sh, υ_{as} [COO] str; 1534 cm^{1} sh and 1411 cm^{-1} v.s. υ_s [COO] str; 1349 cm^{-1} s. and sharp, (CH_3) deform.; 1037 cm^{-1} s. and sharp, (CH_3) rock; 935-940 cm^{-1} m, (C-C) str.; 675 cm^{-1} s. and sharp (COO) sym deform.; 619 cm^{-1} s. and sharp (out of plane rock); 497 cm^{-1} w, (COO) rock.

Comparison with the infra red spectra modes of acetate bonding [19-23] it is apparent that bridging [Δ (υ_{as} - υ_{sym}) = 149 cm^{-1}] as well as bidentate modes of acetate bonding are evident in the product; (Table II). Hene two possible strictures, I and II could be investigated ; i.e. hydroxo cobalt(III) μ-tetra-acetato hydroxo cobalt(III), I; and, acetate cobalt(III) μ-diacetato-μ-dihydroxo acetate cobalt(III), II.

Table (II)

Symmetric (υ_s) and Antisymmetric (υ_{as}) stretching frequencies (cm^{-1}) of some cetate complexes :

Mode of acetate bonding	Example	(υ_{as}) [COO}]	(υ_s) [COO]	Δ^{*a}	References
Ionic	NaOAc	1575	1422	153	13
Unidenate	$Co(NH_3)_5Oac$	1603	1380	223	14
Bidenate	$Zn(Oac)_2\ 2H_2O$	1570	1452	118	15
Bridging	$Zn_4O(Oac)_6$	1639	1489	150	16,17
	$[Cr(Oac)_2]_2$	1571	1422	149	17
	Product	1560	1411	149	This work

Δ^{*a} = (υ_{as}) [COO] – (υ_s) [COO]

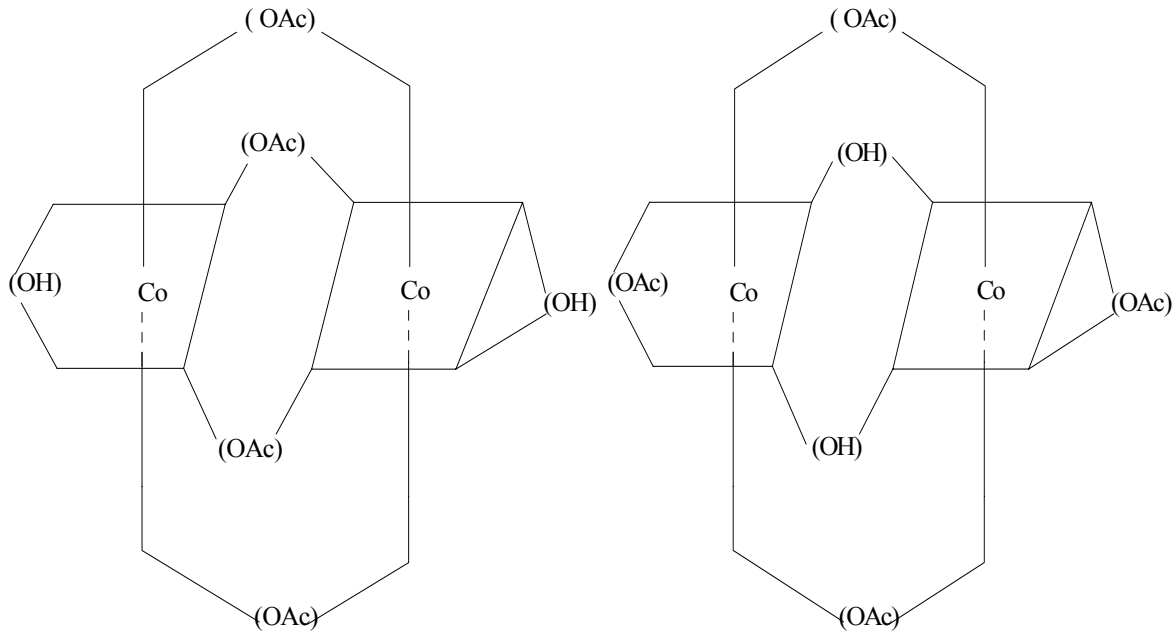

Since no oxidation of Co(II) takes place in the absence of the acetate ion, under the conditions of the reaction reported, it can be inferred that the presence of such an oxidizable ligand seems to be an important and determining factor besides the availability of a higher oxidation state of the metal ion. Hence, the mechanism of the reaction is proposed to involve the formation of a peroxyacetate anions $CH_3CO_3^-$ as a rate determining step in the reaction. The proposed steps are:

$$CH_3COO^- + O_3 \longrightarrow CH_3CO_3^- + O_2 \quad (1)$$

$$2\,Co^{2+} + CH_3CO_3^- \longrightarrow 2\,Co^{3+} + CH_3COO^- + O^{2-} \quad (2)$$

$$CH_3COOH + O^{2-} \longrightarrow CH_3COO^- + OH^- \quad (3)$$

Further hydroxylation could be brought about by peroxyacetic acid [24].i.e.

$$CH_3COOH + O_3 \longrightarrow CH_3CO_3H + O_2 \quad (4)$$

$$CH_3CO_3H + CH_3COO^- \longrightarrow (CH_3CO_2)_2O + OH^- + \tfrac{1}{2}\,O_2 \quad (5)$$

i.e, overall : reaction is :

$$2Co(CH_3COO)_2 + 2\,CH_3COOH + 2O_3 \longrightarrow Co_2(CH_3COO)_4(OH)_2 + (CH_3CO)_2O + 2.5\,O_2 \quad (6)$$

Detailed investigation of such a mechanism as well as the reaction of ozone with different transition metal salts are now in progress.

References

[1] T. A. Cooper, A. A. Clifford, D. J. Mills and W. A. Waters, J. Chem. Soc., (1966), 793.

[2] T. A. Cooper and W. A. Waters, J. Chem. Soc.(B), (1967), 464 and 687.

[3] C. E. H. Bawn and J. A. Sharp, J. Chem. Soc., (1957), 1854 and 1866.

[4] A. S. Hay, J. W. Eustance and H. S. Blanchard, J. Org. Chem., (1960), 25, 616.

[5] T. Morimoto and Y. Ogata, J. Chem. Soc., (B) (1967), 1353.

[6] W. F. Bril, Ind Eng. Chem., (1960), 52, 837.

[7] E. I. Heiba, R. H. Dessau and W. J. Koehl, Jr., J. Amer. Chem. Soc., (1969), 91, 6830.

[8] C. Shall and C. Theimewiedet marker, Z. Electronchem. (1929), 35, 337.

[9] J. A. Sharp and A. G. White, J. Chem. Soc., (1952), 110.

[10] E. Koubek and J. O. Edwards, J. Inorg. Nucl. Chem., (1963), 25, 140.

[11] G. R. Hill, J. Amer. Chem. Soc., (1948), 70, 1306; ibid, (1949), 71, 2434.

[12] Mutasim I. Khalil and Jamal A. Al-Shargawi, Inorg. Chemica Acta, (1986), L-27,121.

[13] Mutasim I. Khalil, Jamal A. Al-Shargawi and Hassan Daban, ibid, (1987), 95, 132.

[14] Mutasim I. Khalil, N. Logan and A. D. Harris, J. Chem. Soc., Dalton Trans, (1980), 314.

[15] N. N. Green wood and A. Eamshaw, Chemistry of the elements, Pergaman Press, (1984), 1308.

[16] James E. Huheey, Inorganic Chemistry, 3rd edition, Happer and Row Publishers, New York, (1983), 446.

[17] D. Sutton, Electronic Spectra of Transition Metal Complexes, Megraw Hill, New York, (1968).

[18] A. P. B. Lever Inorganic Electronic Spectroscopy, Sec. edition, Eleseveir, New York, (1984).

[19] K. J. Wilmshurts, J. Chem. Phys., (1955), 23, 2453.

[20] M. Linhard and B. Row, Z. Anorg. Chem., (1953), 271, 121.

[21] J. Tabot, Acta Crytalloogr., (1953), 6, 720.

[22] K. Nakamato, Y. Morimato and E. Mardell, J. Amer. Chem. Soc., (1961), 82, 4528.

[23] H. Koyama, Y. Saito and H. Kuroya, Bull. Chem. Soc., Jpn., (1954), 127, 113.

[24] R. T. Morrison and R. N. Boyd, Organic Chemistry, 5th edition, Ally and Bacon, Inc., Boston, 1987.

Arabian J. Chem. Vol. 1, No. 3, 271-280 (2008)

Synthesis and Properties of New Polyketones and Copolyketones based on Difurfurylideneacetone

Nayef S. Al-Muaikel

Chemistry Department , College of Education , Aljouf University, Al Jouf, P.O. Box 643, Sakaka, Al Jouf, Saudi Arabia.

E-mail: n_almuaikel@hotmail.com

Abstract

A new category of polyketones and copolyketones were synthesized via Friedel - Crafts reaction through the polymerization of the monomer **I** with different diacid chlorides. The model compound was synthesized by reacting **I** with benzoyl chloride and characterized by ^{1}H-NMR, IR and elemental analyses. The polyketones and copolyketones were soluble easily in protic solvents like H_2SO_4 and trifluroacetic acid. The thermal properties of these polyketones and copolyketones were evaluated and correlated to their structural units by TGA and DSC measurements, and had inherent viscosity 0.35-0.59 dI g^{-1}. The crystallinity of some polymers was tested by X-ray analyses; also the morphological properties of selected examples of poly-and copolyketones were detected by SEM.

Keywords: Polyketones; Friedel-Crafts; Synthesis; Characterization.

1. Introduction

Aromatic polyketones are an emerging family of materials that are currently attracting technical interest on account of their impressive thermal and mechanical properties and their chemical resistance [1, 2]. At present, several aromatic polyketones have been commercialized. The commercial utility of these polymers is based on a combination of properties, among which toughness and crystallinity are crucial [3]. The synthesis of these polymers is usually performed by Friedel-Crafts acylation or nucleophilic aromatic displacement, which has been a subject of research for a number of years [4-7]. As a result, the preparation of various aromatic polyketones and investigations of their properties have been reported by many workers [8-11].

Up to our knowledge, no work has been reported concerning the synthesis of polyketones containing bis-furfurylidene acetone moiety in the main chain.

The work reported in this paper, outlines the synthesis and characterization of some new polyketones and copolyketones based on bis-furfurylidene acetone. The major aim of this work has been to investigate the effect of inclusion of aromatic, and aliphatic chains on the polymer properties. In addition other characteristic of these new polyketones such as thermal stability, solubility, and crystallinity, were discussed.

2. Experimental Procedure

2.1. Instrumentation

Melting points were determined on a Perkin-Elmer 240C electrothermal melting point apparatus and are uncorrected. Infrared spectra were recorded on a Shimadzu 2110 PC Spectrophotometer with KBr pellets. The ^{1}H-NMR spectra were recorded on a varion EM-390 (90 MHz) NMR spectrophotometer at room temperature in DMSO or $CHCl_3$ using TMS as the internal reference. Viscosity measurements were made with 0.5% (w/v) solution of polymers in DMSO at 25^{o}C using an Ubbelohde suspended level viscometer. X-ray diffractographs of the polymers were obtained with a Philips X-ray Pw 1710 diffractometer, using Ni-filtered Cuk$_\alpha$ radiation.

TGA and DTG measurements were performed on V 5.1 A Du Pont 2000 thermal analyzer at a heating rate 10^{o}C/min in air. The solubility of the polymers was determined using 0.02 g of polymer in 3.5 ml of solvent. The morphology of polymers were examined by scanning electron microscopy (SEM) using a JEOL JSM-5400 LV instrument; images were recorded with a Pentax Z-50P Camera with Ilford film at an accelerating voltage of 15KV.

2.2. Reagents and Solvents:

Furfural (Fluka AG) (b.p. 162^{o}C) and benzoyl chloride (Aldrich) were used as purchased. Terephthaloyl chloride and isophthaloyl chloride (Aldrich) were recrystallized from n-hexane (m.p 83-84^{o}C and 40^{o}C, respectively). Adipoyl and sebacoyl dichlorides [12] were freshly distilled at 125^{o}C/11 Torr, and at 182^{o}C/16 Torr, respectively, were used. Acetone (Merck) was freshly distilled at b.p 58^{o}C. Anhydrous aluminum chloride (Merck) and all other solvents were of high purity and were further purified by a standard method [13].

2.3. Monomer Synthesis:

2.3.1. Synthesis of bis-furfurylidene acetone I :

A mixture of 0.1 mole acetone and 0.2 mole of furfural in warm ethanol was stirred, and few drops of NaOH (20% conc.) was added. The reaction mixture was stirred at room temperature for 1 hr, and the resulting solid was collected by filtration, washed with cold water, dried and recrystallized from ethanol, as yellow needles; yield 95%, m.p. 146-7°C. Calculated for $C_{13}H_{10}O_3$: C, 72.90; H,4.67%. Found: C, 72.35; H, 4.38. %. IR (KBr, cm^{-1}): at 1600 (s, C=C), at 1660 (s, C=O). ^{1}H-NMR ($CDCl_3$, ppm), at 7.2-8.0 (m, 6H of furfuryl moieties and 4H of 2CH=CH).

2.3.2. Synthesis of bis-benzylidene acetone II.

This monomer was prepared as described previously [14].

2.4. Synthesis of Model Compound III:

In a 100 ml round-bottomed flask equipped with a magnetic stirrer, and a nitrogen inlet and outlet, was placed a solution of 1 mmole bis-furfurylidene acetone I and 2 mmole of benzoyl chloride in 40 ml of dry carbon disulphide. The flask was purged with nitrogen while stirring and 20 mmole of anhydrous aluminum chloride was added portion wise to the solution. The solution was stirred for 24 hrs at 25°C, and the separated solid product was filtered off, washed with water and dried in a vacuum at room temperature. An analytical sample was obtained by recrystallization from benzene in yellow needles, yield 75%, m.p 225-7°C. Calculated for $C_{27}H_{18}O_5$: C, 76.78; H, 4.27; %. Found: C, 76.35; H, 4.51 %. IR (KBr, cm^{-1}): at 1665 (C=O of acetone), at 1700 (C=O of benzoyl group), at 1600 (C=C group). ^{1}H-NMR (DMSO-d_6, ppm), at 7.2-8.5 (m, 4H, furfuryl moiety, 10 H Ar-H, and 4H of 2CH=CH).

2.5. Synthesis of Polyketones IV a-d

Friedel-Crafts method was applied for the preparation of all the polymers. Typically, in a 100-ml round-bottomed flask equipped with a magnetic stirrer and, nitrogen inlet and outlet, was placed a solution of 1.284 g (6 mmole), bis-

furfurylidene acetone **I** and 1.218 g (6 mmole) of isophthaloyl chloride in 25 ml of dry carbon disulphide. The flask was purged with nitrogen while stirring, and 2.66 g (20 mmole) of aluminum chloride was added during the nitrogen flush. The reddish brown reaction mixture was stirred for 24 hrs then it was filtered off and the separated product was triturated three times with a large excess of methanol. The powdery material was again filtered off, washing with water, methanol, and acetone and dried under reduced pressure (1 mmHg) at 70°C for 2 days. This method was applied for the preparation of other polyketones; whose yields, elemental analyses, viscosity and colors are listed in Table 1.

Table 1. Elemental Analyses, Inherent Viscosity, Yield and Color of Polyketones IVa-d and Coployketones V and VI.

Polymer Code	Repeating unit	C%		H%		η_{Inh} (dl/g)	Yield %	Appearance of polymer
		Calcd.	Found	Calcd.	Found			
IVa	$C_{21}H_{12}O_5$	73.26	72.43	3.49	3.36	0.35	68	Powder-yellow
IVb	$C_{21}H_{12}O_5$	73.26	72.92	3.49	3.01	0.44	73	Powder-yellow
IVc	$C_{19}H_{16}O_5$	70.37	71.56	4.94	5.32	0.56	76	Powder-yellow
IVd	$C_{23}H_{24}O_5$	72.63	71.24	6.32	6.07	0.42	69	Powder- yellow
V	$C_{46}H_{28}O_8$	77.97	76.87	3.95	4.18	-	85	Powder- yellow
VI	$C_{42}H_{36}O_8$	75.45	74.72	5.39	5.05	0.59	81	Powder-yellow

*η Inherent viscosity measured in DMSO at 25°C.

2.6. Synthesis of Copolyketones Vand VI:

The same method, which applied in the synthesis of the polyketones, was also applied in the synthesis of the copolyketones.

Typically, in a 100-ml round-bottomed flask equipped with a magnetic stirrer and, nitrogen inlet and outlet, was placed a solution of 0.642 g (3 mmole), bis furfurylidene acetone I and 0.702 g (3 mmole) of bis-benzylidene acetone II and 1.208 g (6 mmole) of terephthaloyl chloride in 50 ml of dry carbon disulphide. The flask was purged with nitrogen while stirring, and 2.66 g (20 mmole) of aluminum chloride was added during the nitrogen flush. The reddish brown reaction mixture was stirred for 24 hrs then it was filtered off and the separated product was triturated three times with a large excess of methanol. The powdery material was again filtered off, washing with water, methanol, and acetone and dried under reduced pressure (1 mmHg) at 70°C for 2 days. This method was applied for the synthesis of copolyketone VI; whose yield, elemental analysis, viscosity and colors are also listed in Table 1.

3. Results and discussion

3.1 Synthesis of Monomer I.

Bis-furfurylidene acetone **I** monomer was synthesized in good yield by the basic catalyzed condensation of two moles of furfural with one mole of acetone, as shown in **Scheme I**.

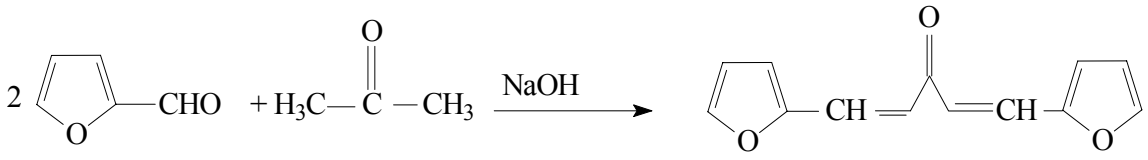

Scheme I. Synthesis of bis-furfurylidene acetone I.

3.2 Synthesis of Model Compound III:

Before attempting the polymerization, model compound was prepared by the reaction of monomer I with two equivalents benzoyl chloride. A typical reaction is depicted in Scheme II.

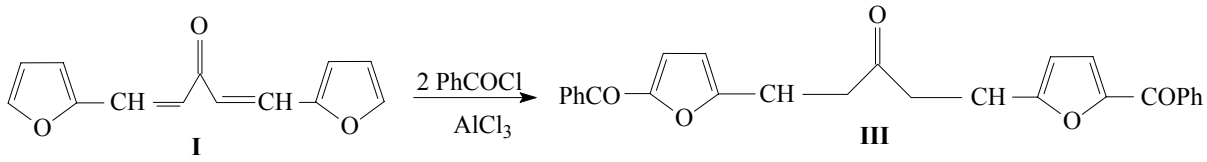

Sheme II. Synthesis of Model Compound III

3. 3. Synthesis of Polyketones IV a-d.

In order to determine an adequate catalyst for the synthesis of polyketones based on furfurylidene acetone in the main chain, Friedel-Crafts polycondensation of bis furfurylidene acetone **I** with terephthaloyl chloride (as an example) (polymer $\mathbf{IV_b}$) was carried out in the presence of various Lewis acids such as: $FeCl_3$, $SbCl_5$, and $AlCl_3$. It appeared that anhydrous $AlCl_3$ gave the best result with respect to yield and degree of polymerization. The favorable mole ratio of catalyst to each reactant was ca. 2.0.

On the basis of these results, Friedel-Crafts polycondensation of dicarbonyl chlorides including: isophthaloyl, terephthaloyl, adipoyl and sebacoyl dichlorides with bis -furfurylidene acetone **I** was carried out at room temperature for 24 hrs. These reactions are shown in **Scheme III.**

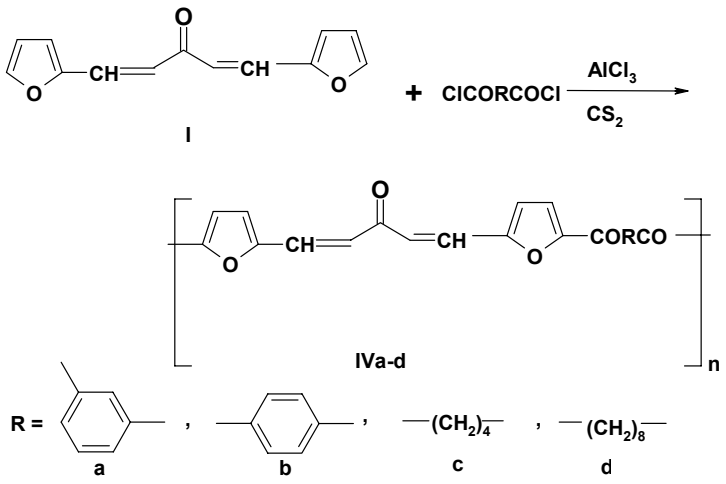

Scheme III. Synthesis of Polyketones IVa-d

3.4. Synthesis of Copolyketones V and VI.

Unreported copolyketones **V** and **VI** containing two different moieties e.g. bis-furfurylidene acetone, and bis-benzylidene acetone in the polymer main chain. These two copolyketones were synthesized from the copolymerization of monomer **I** and monomer **II** with two different diacid chlorides e.g. terephthaloyl or adipoyl as shown in **Schemes IV and V**.

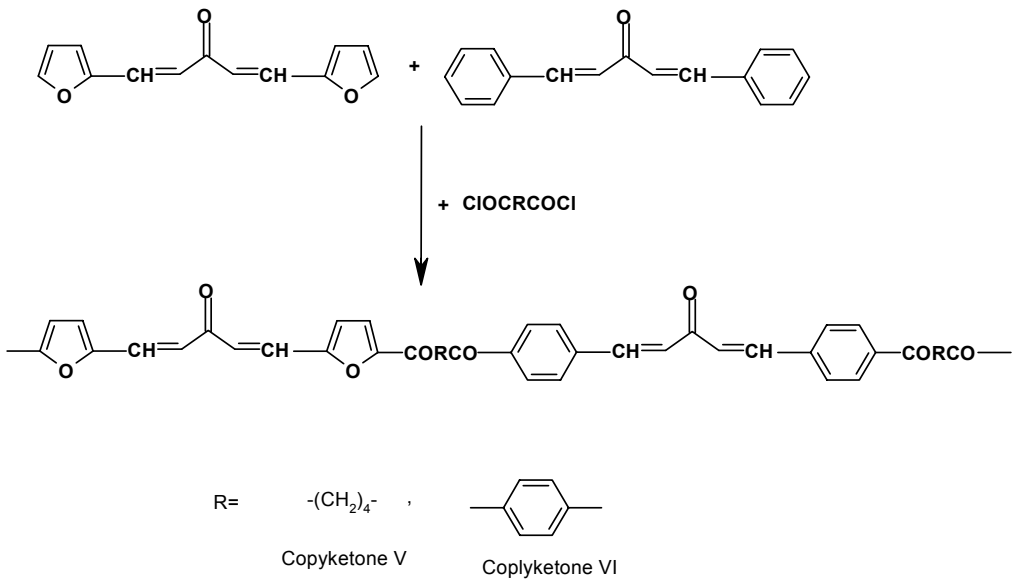

Scheme IV. Synthesis of Copolyketones V. VI

The polymerization and copolymerization reactions were carried out at room temperature in carbon disulphide as a solvent and anhydrous aluminum chloride as a catalyst. The reaction times varied from 20-24 hrs and the polymers and copolymers were immediately isolated when the reaction mixtures were poured into methanol/water mixture, with a yield in the range of 68-85 %. These polymers were characterized by elemental analysis, IR spectroscopy, solubility, viscometry, thermal analysis and morphological properties. The elemental data of all the polymers and copolymers coincided with the characteristic repeating units (Table 1).

Spectral analyses in (KBr disks) showed the appearance of new carbonyl absorption at 1690-1720 cm^{-1}, characteristic for the C=O of ketonic group besides the original C=O of acetone at 1650-1670 cm^{-1}, and at C=C at 1595-1610 cm^{-1}. Other characteristic absorption peaks for the rest of the groups in the molecules were also present, as shown in Fig. 1.

3.5. Properties of the Polyketones IV_{a-d} and Copolyketones V , VI.

The solubility characteristics of polyketones and copolyketones (**IV_{a-d}, V, VI**) were tested in various solvents (Table 2) including: dimethylsulfoxide (DMSO), N,N-dimethylformamide (DMF), N-methylpyrrolidone (NMP), tetrahydrofuran (THF), methylene chloride, $CHCl_3$-acetone (1:1) and concentrated sulphuric acid. It was found that all the polyketones and copolyketones dissolved readily in DMSO and in concentrated H_2SO_4 at room temperature giving deep red color due to the instability of the polymers. For halogenated solvents like CH_2Cl_2 and $CHCl_3$-acetone mixture, polymers **IVa-c** and copolymers **V, VI** were partially soluble. More particularly, polymer **IVd** and copoplymer **VI** (with n = 8 or 4, respectively) showed good solubility in most organic solvents, due the high flexibility of these polymers through the polymethylene spacers.

Table 2: Solubility Characteristics of Polyketones IVa-d and Copolyketones V and VI.

Polymer code	DMSO	DMF	NMP	Chloroform Acetone	THF	Methylene chloride	H_2SO_4
IVa	+	±	±	±	±	±	+
IVb	+	±	±	±	±	–	+
IVc	+	±	±	±	±	–	+
IVd	+	+	±	+	±	±	+
V	±	±	±	±	±	±	+
VI	+	±	±	±	±	±	+

(+) Soluble at room temperature RT.

(±) Partially soluble at RT.

(–) Insoluble.

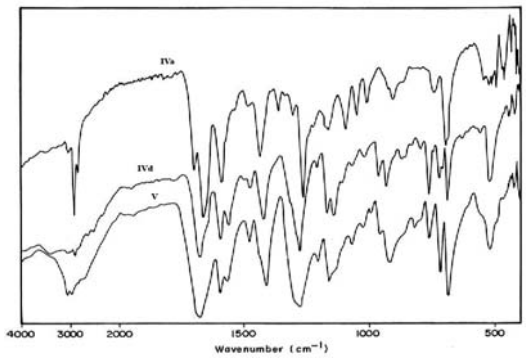

Figure 1. IR Spectra of Polyketones IVa,d and Coplyketone V.

X-ray diffractograms of selected examples of polyketones **IVa,d** and copolyketones **V and VI** in Figure 2 showed few sharpness peaks with an amorphous background, in the region 2θ = 5-60°, this indicating that there is a large class of structures, in polymer main chains, are intermediate in the ordered states between crystals (with pronounced long-range order) in the arrangement of their atoms and molecules. Moreover, the presence of C=O as polar group in addition to high C=C band levels chains in the polymer, leading to some extent of crystallinity [15]. Also, the diffractogram, indicated that polyketones **IVa,d** has a high degree of crystallinity in comparison with copolyketones **V and VI**.

The morphology of the synthesized polyketone **IVa** in Figure 3 was examined by SEM (Jeol-SM-5400 LV instrument). The SEM sample was prepared by putting a fine powder of the polyketone on a smooth surface of aluminum foil and coating it with gold-palladium alloy. The SEM (Camera) with Ilford film at an accelerating voltage of 15 kv using a low dose technique [16]. The SEM study of polyketone **IVa** in Figure 3 showed that the polymer had a polymorph globular and subglobular structures which appeared in a continuous chain with some coalescence present.

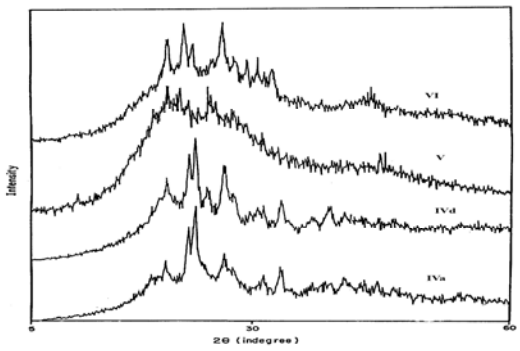

Figure 2 . X-Ray Diffractograms of Polyketones IVa,d and Copolyketones V,VI.

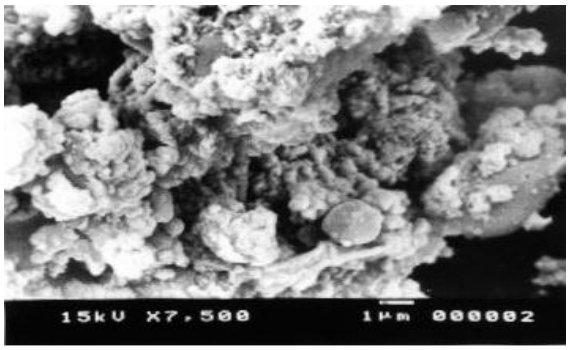

Figure 3. SEM image of Polyketone IVa.

The SEM for the polyketone **IVd** shown in Figure 4 showed that the polymer had aggregates like a kidney morphology (X= 3500).

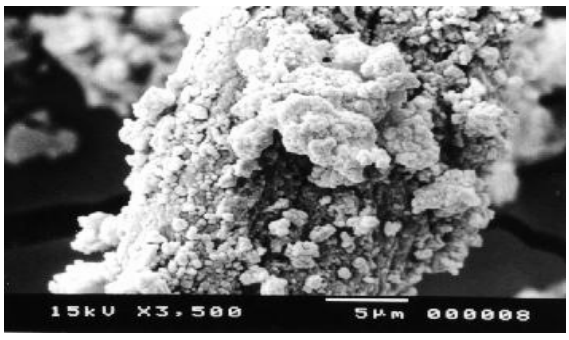

Figure 4. SEM image of Copolyketone V.

. The thermal behavior of polyketones **IVa-d** and copolyketones **V and VI** were evaluated by thermogravimetric analysis (TGA) in air at a heating rate of 10°C /min. The thermographs of these polymers are given in Figures 5 and 6, also Table 3 gives the temperature of various percentages of weight loss. In Figure 5, TGA curves of polyketones **IVa,d** show a small weight loss in the range 2-4% starting at 160°C until 190°C, which may be attributed to the loss of absorbed moisture and entrapped solvents. The thermographs also indicate, the polymers decompose in two stages. The first stage between 205°C and 310°C depends upon the nature of the polyketones. This result is in good agreement with the decomposition of ketone-linkage observed by Swedo and Marvel [17].

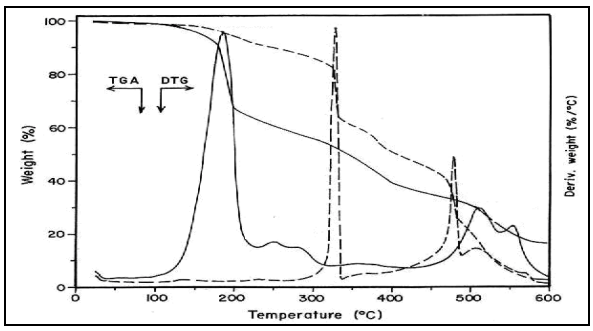

Figure 5. Thermogravimetric Curves of Polyketones IVa (-----) and IVd (—).

The second stage of degradation of polyketones occurred between 340°C and 590°C. The rate of degradation in the first stage is somewhat faster than in the second stage. A comparison of the T_{10} values of polyketones $\mathbf{IV_{a,b}}$ containing aromatic moiety showed better thermal stability than others based on aliphatic **IVc,d** . For copoyketones **V** and **VI** in Figure 6, showed that a small weight loss in the range 2-4% starting at 180°C until 220°C, which may be attributed to loss of absorbed moisture and entrapped solvents. In contrary to the decomposition of the polyketones, the decomposition of copolyketones occurred in one step only, and the T_{10} values are in the range 350-370°C. For copoyketones **V** and **VI**, Figure 6 showed a small weight loss in the range 2-4% starting at 160°C until 210°C, which may again be attributed to loss of absorbed moisture and entrapped solvents. In contrary to the decomposition of the polyketones, the decomposition of copolyketones occurred in one step only, and the T_{10} values are in the range 320-340°C. Moreover, the data indicated that the copolyketone **V** is more thermally stable than the copolyketone **VI** and this may be attributed to the presence of polymethylene groups $(CH_2)_4$ as flexible spacers in the polymer main chain in the latter copolyketone, these decreasing the stability.

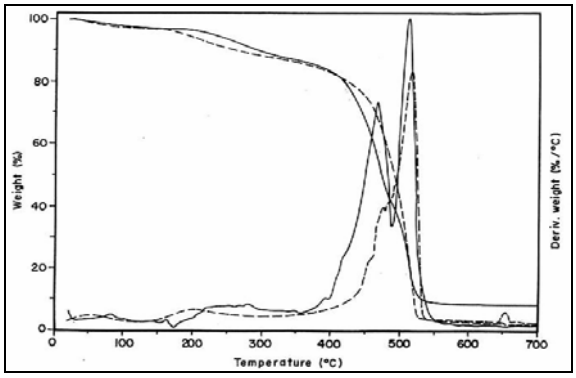

Figure 6. Thermogravimetric Curves of Copolyketones V(------)and VI(—).

Table 3: Thermal Properties of Polyketones IV_{a-d} and V, VI.

Polymer Code	Temperature (°C) for various decomposition levels				
	10%	20%	30%	40%	50%
IVa	290	340	350	390	440
IVb	250	265	280	310	370
IVc	215	255	280	310	355
IVd	210	215	230	290	390
V	340	450	480	495	510
VI	320	435	470	490	500

* Heating rate: 10°C min^{-1}.

4. Conclusion

Two novel series of polyketones and copolyketones based on bis-furfurylidene acetone were synthesized via Friedel-Crafts reaction. All the polyketones and coplyketones were soluble in concentrated H_2SO_4. Thermogravimetric analyses showed that the cyclohexanone based polyketones were somewhat less thermally stable than their copolyketones. X-ray diffraction analyses indicated that most of the polymers are semi crystalline. SEM images of polyketone **IVa** indicated that their surfaces possess globular and aggregates structure, and the polyketone **IVd** showed that the polymer had aggregates like a kidney morphology.

References

[1] Staniland PA, in "Comprehensive Polymer Scina", Allen. G, Bevington, J.C., Eds., Pergamon, Oxford (U.K.) Vol. 5, pp. 483-497, (1989).

[2] Rose, JB, in "High Performance Polymers: Their Origin and Development", Seymour, RB, Kirshenbaum. G.S., Eds., Elsevier Science Publishing, New York pp. 187-193, (1986).

[3] Zolotukhin MG, Rueda DR, Balta FJ, Bruix M, and Cagiao M E, Macromol. Chem. Phys., 188, 1131, (1997).

[4] Patel NZ, Patel JN, Ray RM and Patel RM; Angew Makromol. Chem., 192, 103 (1991).

[5] Patel BT, Solanki, YK, Patel PM and Patel RM; Res. J. Chem. Environ, 1(1) 21, (1997).

[6] Patel BT, Patel RT, Patel RM and Patel KC; Angew, Makromol. Chem. 263, 21, (1998).

[7] Lee J and Marvel CS, J. Polym. Sci., Polym. Chem. Ed., 21 (8) 2189 (1983).

[8] Lin S, Kriek G, and Marvel CS, J. Polym. Sci., Polym. Chem. E. D., 20 (2), 401, P. 572, (1970).

[9] Lee B, and Marvel C S, J. Polym. Sci., Prolym. Chem. Ed., 20 (2), 393 (1982).

[10] Patel BT and Patel RM; Intern. J. Polymeric Mater., 41, 199, (1998).

[11] Patel RM, Mehta, YN and Patel R.M., Res. J. Chem. Environ, 2(2), 29, (1998).

[12] Vogel A., Text Book of Practical Organic Chemistry, Vol.1, longmans, Green, 2nd, ed., Pergamon, Nedw York, (1980).

[13] Perrin, D.D., Armergo, W.L.F., and Perrin; D.R. Purification of loboratory chemicals, 2nd, ed., Pergamon, New York, (1980).

[14] Aly K. I., Khalaf, A. A. and Mohammed, I. A. Europ. Polym. J. 39, 1035, (2003).

[15] Mandelkern, Crystallization of Polymers, M.C. Graw-Hill, New York, (1964).

[16] Tager A., Physical Chemistry of Polymers, Mir Publishing, Moscow, (1972).

[17] Swedo, R.J. and Marvel C.S., J. Polym. Sci., Polym. Chem., Ed., 17. 2815, (1979).

Arabian J. Chem. Vol. 1, No. 3, 281-290 (2008)

Effect of The Heat Treatment on The Corrosion and Passivation of Tinplate in Synthetic Industrial Water

M'hammed Belkhaouda[a], Rachid Salghi [b], Lahcen Bazzi [a], Belkheir Hammouti [c*]

[a] Laboratoire Environnement et Matériaux, Faculté des Sciences, B.P 8106 Agadir, Morocco.

[b] Laboratoire d'Ingénierie des Procédés de l'Energie et de l'Environnement, Ecole Nationale des Sciences Appliquées, B.P: 1136 Agadir, Morocco

[c] Laboratoire de Chimie Appliquée et Environnement, Faculté des Sciences 60 000 Oujda, Morocco.

E-mail: hammoutib@yahoo.fr

Abstract

In this work we are interested in the impact of effect of the heat treatments on the corrosion and passivation of tinplate in synthetic industrial water. For the realisation of this work, we called on the electrochemical polarization techniques such as the polarisation curves and polarisation resistance measurement. The surface morphology and composition of the tinplate surface were studied using scanning electron microscopy (SEM), energy dispersive X-ray (EDX) and X-ray diffraction (XRD). The obtained results show that the corrosion resistance of tinplate in the studied medium depends on the annealing temperature and the thermal processing time. The best corrosion resistance is obtained when the sample is annealed for 4h at 140°C. This result is justified by the low corrosion current density and the high value of polarization resistance recorded at these conditions. The sensitivity to the pitting corrosion is also reduced by this treatment. These results are confirmed by SEM examination coupled with EDX microanalysis.

Keywords: Heat treatment; corrosion; tinplate; passivation; industrial water.

1. Introduction

Tinplate, which is a non-homogeneous material with a stratified structure [1], is composed essentially of a thin sheet of carbon steel rolled and coated on both faces with pure tin. In spite of the increasing use by the canning industry of new alternative materials such as aluminium and chromated steel, tinplate continues to be used in more than 80% of cases [2,3].

These diverse uses are related to its good properties such as the excellent formability, the solderability, the non-toxicity and its best corrosion resistance. This corrosion resistance can be assigned to the oxide and/or hydroxide film formed on the tinplate surface [2,4-7].

The study of the corrosion behaviour of tinplate is similar to that carried out for tin; indeed, an external layer of tin and an intermediate layer constituted the Sn-Fe layer cover steel, which presents a cathodic character compared to basic steel.

The corrosion process of continuous ideal layer tin coating is similar to what occurs for pure tin. However, the protective properties are affected by the presence of defects or discontinuities in the external layer. In presence of chloride solutions, tinplate exhibits localised corrosion as a consequence of defects or imperfections of the tin

passivation layer, which leaves the Fe-Sn layer exposed to the aggressive solutions [8]. Consequently, it involves the attack of the less noble sites. The pitting corrosion remains the most dangerous type of corrosion that affects the passivity of these materials [9-11].

To avoid corrosion problems, different methods have been used such as protective lacquers [12,13] and different types of corrosion inhibitors. The oxo-anionic compounds assure a better protection against the pitting corrosion of this material type [14-19]. Also, heat treatments of material significantly improved its corrosion resistance. The effect of heat treatment on the corrosion behaviour of aluminium alloy [20-31], and of amorphous alloy [32,33] can be found in the literature, and to our knowledge, no previous work has been published in case of tinplate.

The aim of this work is to study the effect of various heat treatments on the corrosion of tinplate.

2. Experimental

Preparation of the sample

Tinplate is composed of a thin sheet of carbon steel, laminated and coated by a layer of pure tin on both faces. Between the tin layer and the carbon steel, there is the formation of Fe-Sn and Fe_2Sn alloys. These layers are formed by diffusion from the tin to the steel. This material is provided by CARNAUD society with the following references: 0.19DR 550 2.8/2.8, the tinned rate is 2.8 g /m² on both faces.

Before the electrochemical study and the characterization, the sample undergoes suitable heat treatments, which are carried out in a programmable continuous pipe under inert atmosphere of nitrogen at temperatures varying between 70 and 220 °C for 1, 2 and 4h. For electrochemical tests, the commercial tinplate samples are in the form of a disc of 0.78 cm^2 used like working electrode that is rinsed with acetone then with distilled water before plunging the electrode in the solution.

Electrochemical tests

The electrochemical study is carried out using a potentiostat PGP 201 piloted by Voltamaster software. This potentiostat is connected to cell with three electrodes with double wall (Tacussel Standard CEC/TH). Saturated calomel electrode (SCE) and platinum electrode are used as reference and auxiliary electrodes, respectively. Potentiodynamic polarisation curves are ploted in the potential range from – 1000 to 200 mV vs. SCE at a scan rate of 1 mV/s and linear polarisation resistance (R_p) was applied using an interval of ± 10 mV from the corrosion potential (E_{corr}). In all experiments the potential is stabilized at a free potential for 30 min.

The experiments are carried out in synthetic industrial water (0.01M NaCl, 0.008 M Na_2SO_4 and 0.003 M $NaHCO_3$). All aqueous solutions are obtained from analytical grade chemicals and bidistilled water. The solution testes are freshly prepared before each experiment and adjusted at pH equal to 8.2 by addition of an appropriate volume of H_2SO_4 or NaOH. The test solutions are deaerated by bubbling nitrogen gas. Gas pubbling is maintained prior and through the experiments, which are repeated three times to ensure the reproducibility.

Characterization

The characterization and analysis of the surface state have been achieved using scanning electron microscopy (SEM), energy dispersive X-ray (EDX) and X-ray diffraction (XRD).SEM and EDX techniques were performed using a JEOL JSM – 5500 equipment with appropriate system for the EDX analysis. Identification of the tinplate phases was evaluated by X-ray diffraction (XRD) using a diffractometer Siemens D5000. The analysis of XRD diagrams is carried out using Winploter software.

3. Results and discussion

Potentiodynamic polarization curves

Samples annealing for 1 h

Fig. 1 represents the potentiodynamic polarization curves of untreated and treated tinplate. Heat treatment involved annealing the samples during 1h at temperatures from 70 to 220°C. The curves are recorded in the synthetic medium at pH 8.2 between -1000 and 200 mV/SCE. The electrochemical parameters related to these curves are gathered in Table 1.

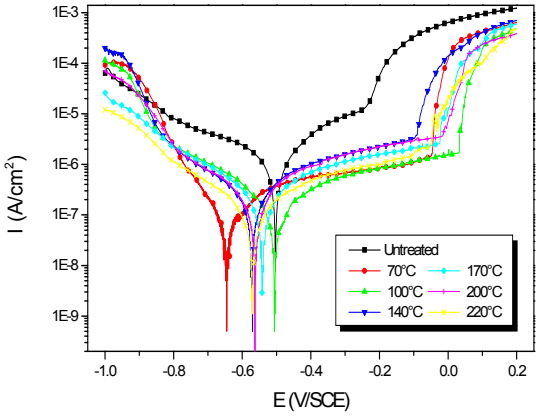

Fig. 1. Polarization curves of untreated and treated tinplate annealing at various temperatures for 1 h

Table 1. Electrochemical parameters of untreated and treated tinplate annealing at various temperatures during 1h.

T(°C)	E_{corr} (mV/SCE)	I_{corr} (μA/cm^2)	I_{pass} (μA/cm^2)	E_{pit} (mV/SCE)	$\Delta E = E_{pit} - E_{corr}$	R_p kΩ.cm^2
untreated	-504	1.56	8.95	-230	274	124.41
70	-644	0.06	1.01	-49	595	708.26
100	-505	0.22	0.66	+31	536	559.21
140	-572	0.21	1.76	-95	478	471.80
170	-542	0.24	1.26	-25	517	473.86
200	-563	0.21	1.76	-17	546	495.53
220	-570	0.12	0.85	-58	512	838.66

We note that the general shape of these curves is not affected by the heat treatment. They are characterized by parallel Tafel lines indicating that the water reduction reaction is activation controlled [34]:

$$2\,H_2O + 2e^- \longrightarrow 4OH^- + H_2 \qquad (1)$$

The examination of the anodic branch indicates that tinplate presents a passivation phenomenon with breakdown of passivity in the synthetic medium. This is further supported by the SEM image of the surface state of tinplate after electrochemical study (Fig. 2). Indeed, the anode current density increases with the electrode potential to reach a current plateau called passivation plateau. The passive current density I_{pass} remains almost constant and then increases abruptly when the pitting potential E_{pit} is exceeded denoting film breakdown and pitting corrosion phenomenon.

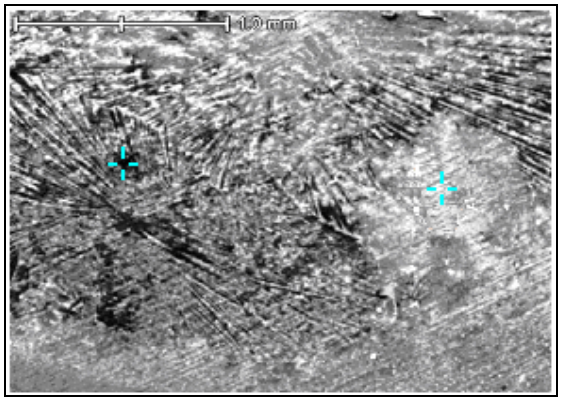

Fig.2. SEM micrograph for tinplate after sweeping from -1000 to 0 mV vs. SCE in synthetic industrial water.

For all annealing temperatures, we notice that the corrosion potential E_{corr} shifts to negative values, whereas the corrosion and passivation current densities undergo a clear reduction. The pitting potential E_{pit} is slightly modified by the variation of the annealing temperatures, while the difference ΔE between the pitting and corrosion potential increases for all temperatures of annealing. The highest value of ΔE is obtained for treated specimens at 70°C. At this same temperature, the lowest value of I_{corr} is obtained.

Samples annealing during 2 h

Fig. 3 represents the polarization curves recorded in a synthetic solution for untreated and treated tinplate at various temperatures and for 2 h. The electrochemical parameters are given in Table 2. We notice that the obtained cathodic curves after heat treatment show significant variation compared to untreated sample.

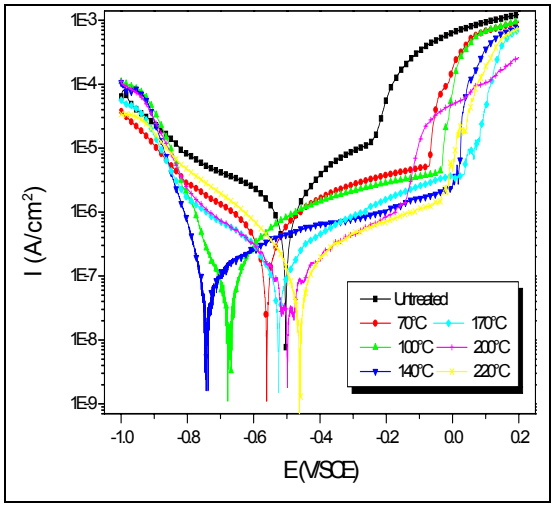

Fig. 3. Polarization curves of untreated and treated tinplate annealing at various temperatures for 2 h

Table 2. Electrochemical parameters of untreated and treated tinplate at various temperatures during 2 h

T(°C)	E_{corr} (mV/ SCE)	I_{corr} (μA/cm²)	I_{pass} (μA/cm²)	E_{pit} (mV/SCE)	ΔE= $E_{pit} - E_{corr}$	R_p kΩ.cm²
Untreated	-504	1.56	8.95	230	274	124.41
70	-558	0.41	2.73	-71	510	300.41
100	-677	0.04	2.18	-34	707	4316.63
140	-741	0.10	0.77	+9	750	281.04
170	-524	0.19	0.88	+34	499	681.56
200	-498	0.14	0.45	-144	481	845.06
220	-457	0.24	0.45	-39	399	483.24

We mentioned that the annealing temperature causes a remarkable reduction of the corrosion current density. The most important reduction is obtained for an annealing at 100°C. The shape of the anodic curves presents a passivation phenomenon with a rupture of passivity. The passivation current density decreases with the increasing of annealing temperature and is stabilized starting from 200°C. We observe also a reduction in the pitting sensitivity which is characterized by the increase in the difference ΔE between the pitting potential and the corrosion potential. The corrosion potential E_{corr} shifts towards more actives values for annealing at temperature lower than 200°C and to positive values for treated sample at 220°C.

Samples annealing during 4 h

Fig. 4 illustrates the polarization curves of untreated and treated tinplate annealing at various temperatures during 4h. The various electrochemical parameters deduced from these curves are given in Table 3. From the obtained results, the following conclusions can be drawn:

- The corrosion and passivation current densities undergo a reduction for all annealing samples. The lowest values of I_{corr} and I_{pass} correspond to the sample treated at 140°C.
- The corrosion potential E_{corr}, pitting potential and passivation domain are affected by annealing.
- The passivation of tinplate is promoted by heat treatment. The passivation domain represented by $\Delta E = E_{pit} - E_{corr}$ is more pronounced for the annealing temperature at 140 and 200°C

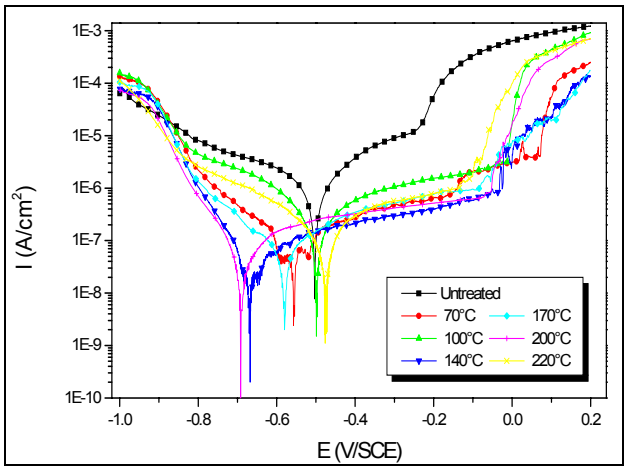

Fig. 4. Polarization curves of untreated and treated tinplate annealing at various temperatures during 4 h.

Table 3. Electrochemical parameters of untreated and treated tinplate at various temperatures during 4 h

T(°C)	E_{corr} (mV/SCE)	I_{corr} (μA/cm²)	I_{pass} (μA/cm²)	E_{pit} (mV/SCE)	$\Delta E = E_{pit} - E_{corr}$	R_p kΩ.cm²
untreated	-504	1.56	8.95	-230	274	124.4
70	-557	0.07	0.58	16	573	1046.6
100	-498	0.60	1.30	-12	486	251.9
140	-672	0.03	0.34	-33	639	1192.7
170	-581	0.06	0.63	-86	495	1192.8
200	-692	0.05	0.48	-72	620	801.1
220	-477	0.22	0.63	-134	342	594.4

Surface morphological characterization

X-ray diffraction analysis

The XRD patterns recorded on treated samples at different temperatures and various times of annealing and on the untreated sample are shown in Fig. (5). Peak identification is done by using the JCPDS files [35]. This identification shows the existence of a multiphase system for all samples. The analysis of untreated pattern (Fig. 5) indicates the presence of the following phases Fe, Sn, $FeSn_2$ and Sn_3O_4.

According to the obtained electrochemical results and the XRD analysis, the corrosion behaviour and the pitting sensitivity of tinplate are generally modified. The improvement of the corrosion resistance and the pitting sensitivity of tinplate are commonly observed for the treated samples at 100°C, 140°C, and 170°C. On the surface of these specimens, the tin oxides (SnO and/or SnO_2) are formed in addition to the indexed phases of untreated samples. The uniform dissolution rate increases for the heated samples and those containing iron oxide (Fe_2O_3) on the surface, without reaching the recorded value of the untreated samples. This result is observed for treated samples at 220°C during various times.

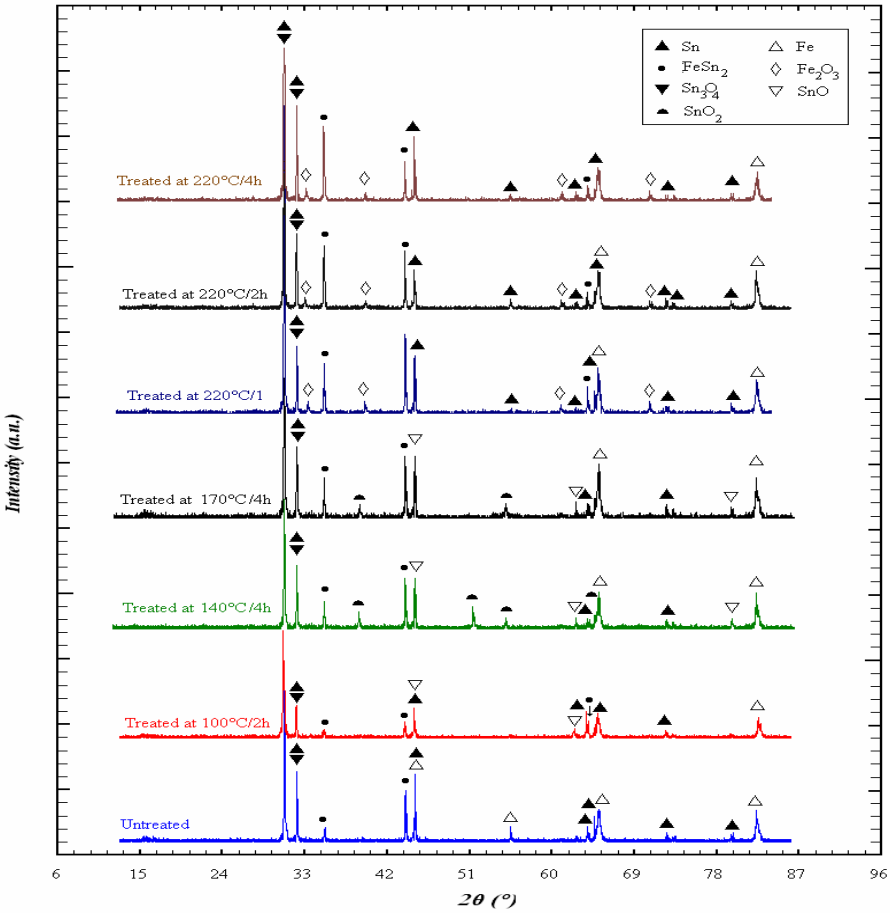

Fig. 5. XRD spectra of untreated and treated tinplate at different conditions

SEM and EDX Analysis

Fig. 6 represents the non-corroded surface state of untreated and treated tinplate samples. In the same figure the corresponding EDX analysis results are also represented.

It is noted that the homogeneity of the tinplate surface state is influenced by the heat treatment. Also, the heterogeneities observed for the untreated sample is completely eliminated by annealing at a temperature of 140°C during 4 hours. This could be attributed to the formation of a homogeneous protective layer on the tinplate surface, due to annealing.

The analysis of tinplate surface by SEM before and after annealing indicates the presence of oxygen, tin and iron elements in the analysed surface layer (Fig.6).

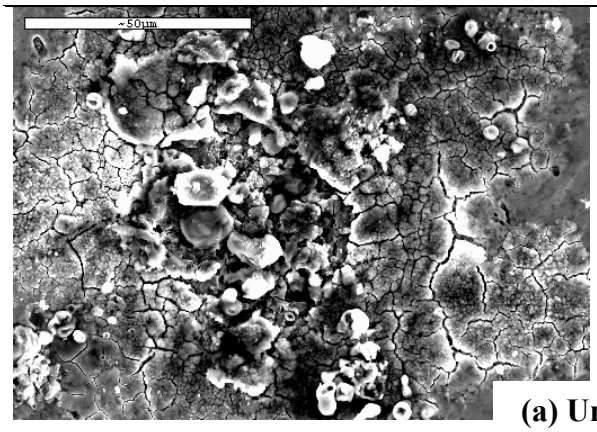

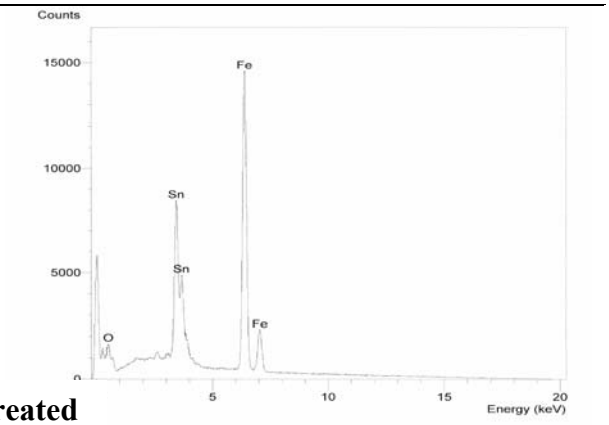

(a) Untreated

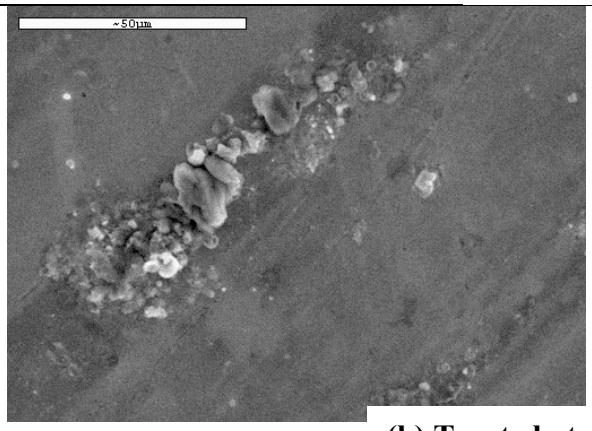

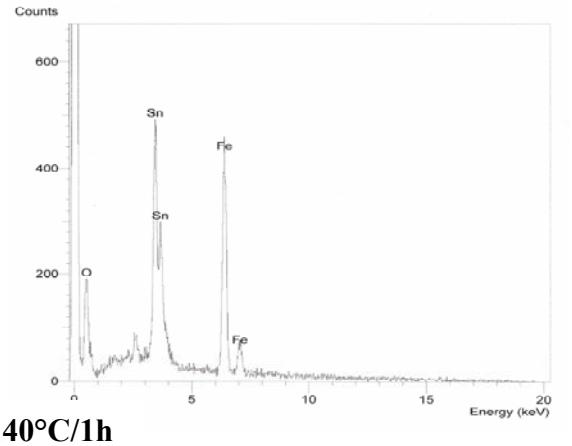

(b) Treated at 140°C/1h

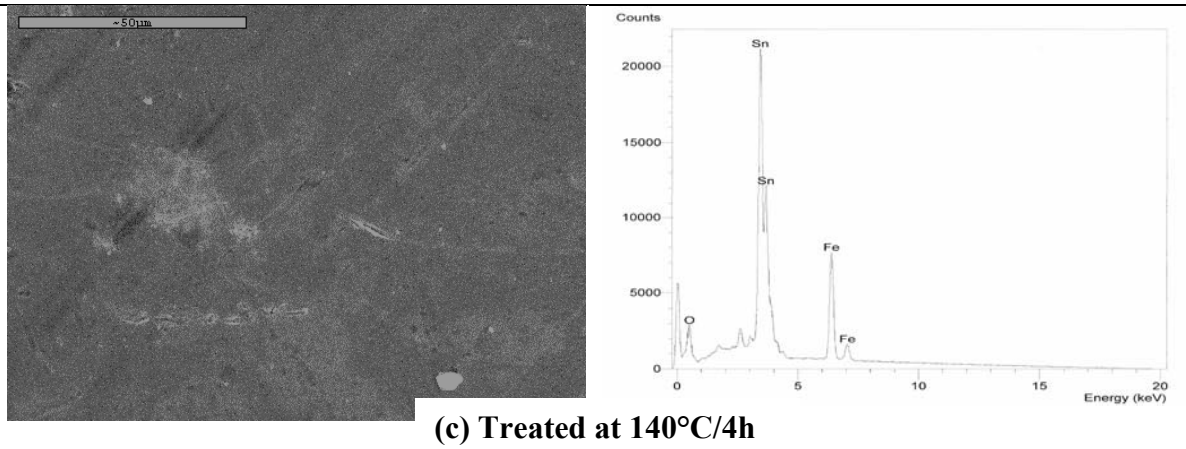

(c) Treated at 140°C/4h

Fig. 6. SEM and EDX results for the untreated (a) and treated tinplate (b and c).

The existence of the oxygen peajk justifies the presence of tin oxide SnO and/or SnO_2 at tinplate surface. The tin peajk can be assigned to the Sn^{2+} or Sn^{4+} ions coming from the passive layer. The increase of the atomic percentage of the tin and oxygen after annealing favours the formation of the tin oxides which are responsible for forming the passivation layer (Table 4.). The iron detected is probably situated under the tin layer because of the thinness of the superficial analysed layer.

Table 4. Atomic % elements for untreated and treated tinplate

	Untreated	Treated at 140°C/1h	Treated at 140°C/4h
Element	Atomic %	Atomic %	Atomic %
O	62.54	69.91	74.50
Fe	28.01	19.04	9.66
Sn	7.8	8.84	16.85

Tests of long time

During the survey dedicated to the effect of the heat treatment the electrochemical techniques are used as efficient and fast means for the tests accelerated of the corrosion and the passivation of tinplate. Prolonged exposure tests were undertaken for 1 week to establish an interrelationship between laboratory and field experiments. After every attack, the surface state of sample has been examined by SEM in order to see the effect of the attack after immersion for one week in synthetic medium (Fig. 7) compared to the surface state of the untreated and treated sample annealing during 140°C for just 1h. We again notice a destruction of the passive layer in the untreated sample, whereas the annealing sample presents a less

corroded surface.

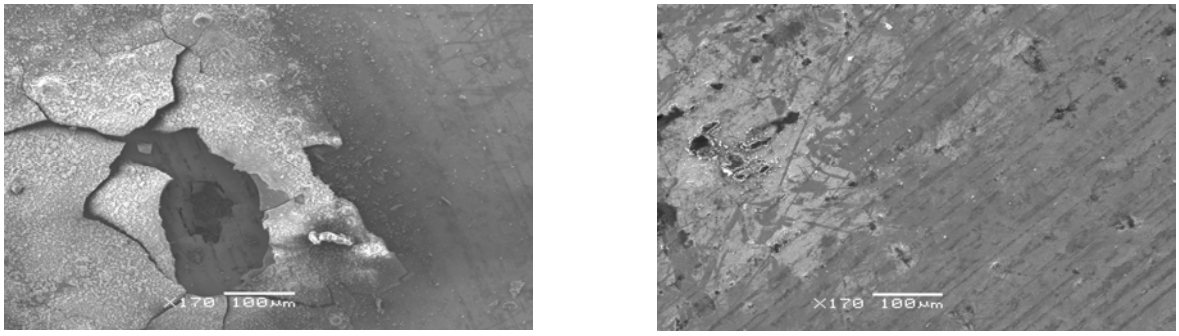

A **B**

Fig. 7. SEM micrograph for untreated (A) and treated at 140°C/1h (B) tinplate with immersion in synthetic water during one week.

4. Conclusion

In this work, the effect of heat treatment on the corrosion and the passivation of tinplate in synthetic industrial water has been studied.

From the obtained results, we can have the following conclusions:

- Tinplate presents a passivation phenomenon with rupture of passivity in synthetic industrial water.
- The sensitivity of pitting corrosion is influenced by heat treatment duration and temperature of this material.
- The best resistance of pitting corrosion is obtained for heat treatment at 140°C during 4h. This is justified by the value of the difference between the pitting potential and corrosion potential ($\Delta E = E_{pit} - E_{corr}$) which is maximum for heat treatment at 140°C during 4h.
- The electrochemical results are confirmed by prolonged exposure tests:

for treated sample, the SEM shows that the passivation layer persists after immersion for one week. We notice that for untreated tinplate, the film is completely destroyed during one week.

Acknowledgements: The authors gratefully thank Prof. E.E. Oguzie of the Federal University of Technology Owerri, Nigeria for his reading.

References

[1] Harrison and Landriault, F. W., Electrochemical Aspect of Tinplate corrosion, Proc. Iith int. Tinplate conference, London, 1990, 278.

[2] Mora, N., Cano, E., Polo Puente, J. L. and Bastidas, J. M., Corros. Sci. 2004, 46, 563.

[3] Kamm, G., Progress in materials for can stock and futur trends, ISII International. 1990, 29, 614.

[4] Hinton, B. R. W., Ryan, N. E. and Arnott, D. R., Mater. Australas. 1987, 19, 18.

[5] Da venport, A. J., Issaacs, H. S. and Kending, M. W., Corros. Sci. 1991, 32, 653.

[6] Hinton, B. R. W., Arnott, D. R. and Ryan, N. E., Mater. Forum. 1986, 9, 162.

[7] Hghes, A. E., Taylor, R. J., Hinton, B. R. W. and Wilson, L., Surf. Interface. Anal. 1995, 23, 540.

[8] Britton, S. C., Tin versus corrosion. International Tin Research Institute, England, 1975, 510, 7.

[9] Shreir, L. L., Jarman, R. A. and Burstein, G. T., Corrosion Metal Environment Reaction, Butterworth-heinemann, London, 1994, 1, 4.

[10] Rafaey, S. A. M.and AbdElrehim, S. S., Electrochem. Acta 1996, 42 (4), 667.

[11] Drogowska, M., Brossard, L. and Menard, H., J. Electrochem. Soc. 1991, 138(5), 1243.

[12] Zumelzu, E. and Rull, F., Sci. Eng. Compos. Mater. 2002, 10(1), 71.

[13] Bastidas, J. M., Cabañes, J. M. and Catalá, R., Prog. Org. Coat. 1997, 30, 9.

[14] Arenas, M. A., Conde, A. and Damborenea, J. J., Corros. Sci. 2002, 44, 511.

[15] Refaey, S. A. M.; Abd El-Rehim, S. S., Taha, F.; Saleh, M. B. and Ahmed, R. A., Appl. Surf. Sci. 2000, 158, 190.

[16] Foad El-Sherbini, E. E., Abd-El-Wahab, S. M., Amin, M. A. and Deyab, M. A., Corros. Sci. 2006, 48, 1885.

[17] Abdel Rehim, S. S., Sayyah, S. M. and El Deeb, M. M., Mater. Chem. Phys. 2003, 80, 696.

[18] Foad El-Sherbini, E. E., Corros. Sci. 2006, 48, 1093.

[19] Ait Addi, E. H., Bazzi, L., Elhilali, M.; Salghi, R.; Hammouti, B. and Mihit, M., Appl. Surf. Sci. 2006, 253, 555.

[20] Ambat, R., Krishna Prasad R. and Dwarakadasa, E.S., Corros. Sci. 1995, 37(8), 1253.

[21] Cabot, P. L., Garrido, J. A., Pérez, E., Moreira, A. H.; Sumodjo, P. T. A. and Benedetti, A. V., J. Appl. Electrochem. 1995, 25, 781.

[22] Andreatta, F., Terryn, H. and Dewit, J. H. W., Electrochim. Acta 2004, 49, 2851.

[23] Andreatta, F., Terryn, H. and Dewit, J. H. W., Corros. Sci. 2003, 45, 1733.

[24] Winkler, S. L., Ryan, M. P. and Flower, H. M., Corros. Sci. 2004, 46, 893.

[25] Andreatta, F., Lohrengel, M. M., Terryn, H. and Dewit, J. H. W., Electrochim Acta 2003, 48, 3239.

[26] Gundersen, J. T. B.; Aytac, A., Ono, S., Nordlien, J. H. and Nisancioglu, K., Corros. Sci. 2004, 46, 265.

[27] Kaplanoglou, I. T., Theohari, S.; Dimogerontakis, T., Wang, Y., Kuo, H. H. and Kia, S., Surf. Coat. Tech. 2006, 200, 2634.

[28] Lin, J. C., Liao, H. L., Jehng, W. D.; Chang, C. H. and Lee, S. L., Corros. Sci. 2006, 48, 3139.

[29] Ambat, R., Davenport, A. J. , Scamans, G. M. and Afseth, A., Corros. Sci. 2006, 48, 3455.

[30] Afseth, A., Nordlien, J. H., Scamans, G. M. and Nisancioglu, K., Corros. Sci. 2001, 43, 2359.

[31] Belkhaouda, M., Bazzi, L., Benlhachemi, A.; Salghi, R.; Hammouti, B. and Kertit, S., Appl. Surf. Sci. 2006, 252, 7921.

[32] Aride, J.; Ben-Bachir, A.; Elkacemi, K.; Etman, M.; Kertit, S. and Srhiri, A., J. Chim. Phys. 1991, 88, 63.

[33] Afseth, A., Nordlien, J. H., Scamans, G. M. and Nisancioglu, K., Corros. Sci. 2002, 44, 145.

[34] Bazzi, L., Kertit, S. and Hamdani, M., J. Chim. Phys. 1997, 94, 93.

[35] Powder Diffraction File, JCPDS-ICDD, Swarthmore, PA, USA, 2000.

Arabian J. Chem. Vol. 1, No. 3, 291-294 (2008)

Solar Thermochemical Reactions III[1]: A Convenient One-pot Synthesis of 1,2,4,5-tetrasubstituted Imidazoles Catalyzed by High Surface Area SiO_2 and Induced by Solar Thermal Energy

Ramadan A. Mekheimer, Afaf M. Abdel Hamid, Seham A. A. Mansour and Kamal Usef Sadek*

Chemistry Department, Faculty of Science, El-Minia University, El-Minia- 61519, A.R. Egypt

**E-mail: Kusadek@yahoo.com*

Abstract

A simple, convenient and efficient method for the synthesis of 1,2,4,5-tetrasubstituted imidazole derivatives using benzoin, an aromatic aldehyde, an aromatic amine in the presence of ammonium acetate catalyzed by high surface area SiO_2 and induced by free solar thermal energy was reported.

Keywords: One-pot synthesis, SiO_2, Solar thermal energy, Tetrasubstituted imidazole.

1. Introduction

Multi-component reactions (MCRs) are powerful tools in generating products in a single synthetic operation [1,2]. It enables straight forward access to structurally related, drug like compounds and therby facilitating lead generation. Such reactions have constituted an increasingly valuable approach to drug discovery efforts in recent years [3,4]. The developing of new MRCs [5] and improving known multi-component reactions are an area of considerable recent interest.

One such reaction is the synthesis of tetrasubstituted imidazoles. Tetrasubstituted imidazoles scaffold is a core constituent in many biological systems such as Olmesartan [6] as well as many natural products and pharmacologically active compounds [7]. Despite of extensive synthetic approaches to such molecules, only few attempts to comprise a general method have been reported. This involves the reaction of benzyl or benzoin, aromatic aldehyde and an aromatic amine in the presence of ammonium acetate and catalyzed by silica gel/$NaHSO_4$ [8], silica gel or Zeolite Hg [9], molecular iodine [10], heteropolyacids [11], $K_5COW_{12}O_4.\ 3H_2O$ [12], $HClO_4$-SiO_2 [13]. Very recently a solvent free convenient method has been reported using a silica-supported boron triflouride [$BF_3.SiO_2$] as a catalyst at 140°C [14].

However, the use of high temperature, expensive metal precoursers and catalysts that may be harmful to the environment are disadvantages of such syntheses. Therefore, green chemistry has received considerable attention [15] and we have recently reported the first attempt to synthesize polyhydroquinoline derivatives induced by free solar thermal energy [16]. Nowadays, there is an increasing interest towards a new and economic energy sources particularly those green ones. There is no

need to convince researchers by the necessity to shift towards greener techniques. Innovative chemical reactions have to make the green concepts happen. An important parameter for the economical and green chemical techniques is the energy efficiency. Free solar thermal energy was regarded as a clean energy and almost no side effects could be detected in using such energy [17]. High surface area fumed silica, sigma product, have a surface area equals to 390 (± 40) m^2/g with particle size of 0.007μ and a refractive index of 1.46 is a top reagent which is easy to handle, reusable with a better accessibility of the reactants to the active sites.

As a part of our efforts toward the developing of useful environmentally friendly and efficient methodology for the synthesis of biologically active heterocycles [18, 19] we report herein the synthesis of tetrasubstituted imidazoles catalyzed by high surface area SiO_2 and induced by free solar thermal energy. To the best of our knowledge the combination of reusable catalyst with the free solar thermal energy to accomplish such transformation has not been reported in the literature.

Exposing a solution of benzoin, ammonium acetate, aromatic amine and aromatic aldehyde in dichloromethane to direct sunlight for 2-2.5 hrs (determined by TLC control). After completion of the reaction, the mixture was cooled to room temperature. Chloroform was added to the mixture which was filtered to remove the catalyst. After evaporation of the solvent, a solid was obtained which was crystallized using a proper solvent.

The generality of the method is demonstrated by using different aldehydes and amines bearing both electron donating and electron withdrawing groups as cited in Table 1. In both cases, the reaction proceeds smoothly to afford the corresponding tetrasubstituted imidazoles in high yields (80-93%) with a little bit increase when R or Ar is electron withdrawing groups. To optimize the reaction conditions, different molar ratios of reactions and catalyst were used and our study revealed that the best molar ratio of aldehyde/amine/benzoin/ammonium acetate/SiO_2 is 1:1:1:0.1. The structure of imidazoles were confirmed by comparison with an authentic specimens (^1H NMR, ^{13}C NMR and IR) spectra and melting points.

Table 1: Solar thermal energy/SiO_2 synthesis of 1,2,4,5-tetrasubstituted imidazoles 4a-h

Compound[a]	Ar	R	Time (h)	Yield %	M.p. °C	Lit. M.p. °C	Ref.
4a	C_6H_5	C_6H_5	2	88	218-220	216-218	13
4b	C_6H_5	$C_6H_5CH_2$	2	80	163-165	163-165	14
4c	4-Cl-C_6H_4	C_6H_5	2	93	160-161	160-162	14
4d	4-OH-C_6H_4	C_6H_5	2	85	281-282	280-281	14
4e	4-CH_3-C_6H_4	C_6H_5	2	90	185-178	185-188	14
4f	3-NO_2-C_6H_4	4-CH_3-C_6H_4	2.5	89	149-151	149-150	8
4g	4-OH-C_6H_4	4-CH_3-C_6H_4	2	84	>280	>270	10
4h	4-Cl-C_6H_4	4-Cl-C_6H_4	2	90	188-189	187-189	8

[a] All compounds were characterized by IR, NMR, Mps.

The possibility of recycling the catalyst was detected. For this purpose, the reaction of benzoin, benzaldehyde, aniline and ammonium acetate as a model reaction was restudied. Our study revealed that the catalyst was reusable without appreciable reduction (82-93%) in its catalytic activity.

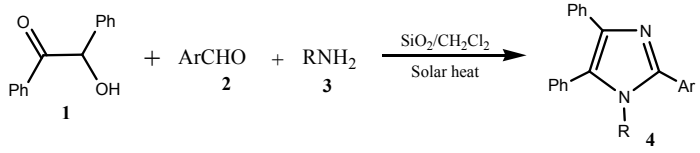

2. Experimental

High surface SiO_2 is commercially available from sigma products.

Typical procedure for the synthesis of tetrasubstituted imidazoles:

To a solution of benzoin (1 mmol), aldehyde (1 mmol), amine (1 mmol) and amm. acetate (1 mmol) in dichloromethane (10 ml) was added high surface SiO_2 (0.1 mol%). The reaction mixture was exposed to direct sunlight for about 2-2.5 hrs by (TLC control). The mixture was filtered to separate the catalyst which was washed with dichloro-methane (5 ml) and dried to be reused. The combined solvent was removed under reduced pressure to afford the crude product which was purified by crystallization from EtOH-H_2O (10:1). The obtained products were characterized by IR, NMR and through comparison of their physical properties with those reported in literature.

1-Benzyl-2,4,5-triphenyl-1H-imidazole **(4b)**

IR (KBr): ν_{max} = 1600, 1580, 1480 cm^{-1}; ^{1}H NMR (DMSO-d_6, 300 MHz): δ = 5.25 (s, 2H, CH2), 6.71-6.88 (m, 20H, Ar-H).

1,2-Di(4-chlorophenyl)-4,5-diphenyl-1H-imidazole **(4h)**

IR (KBr): ν_{max} = 1598, 1496 cm^{-1}; ^{1}H NMR (DMSO-d_6,300 MHz): δ = 6.92-7.66 (m, 18H, Ar-H); ^{13}C NMR (DMSO-d_6, 75 MHz): δ = 127.1, 127.5, 127.9, 128.3, 128.4, 130.0, 130.2, 130.4, 131.1, 131.3, 133.3, 133.8, 134.7, 137.6, 138.7, 145.6.

2-(3-nitrophenyl)-4,5-diphenyl-1-(4-tolyl)-1H-imidazole **(4f)**

IR (KBr): ν_{max} = 1588, 1506, 1334 cm^{-1}; ^{1}H NMR (DMSO-d_6, 300 MHz): δ = 2.13 (s, CH_3), 6.95-8.22 (m, 18H, Ar-H); ^{13}C NMR (DMSO-d_6, 75 MHz): δ = 21.22 (CH_3), 122.7, 123.2, 126.8, 127.1, 128.7, 128.8, 129.1, 130.4, 130.4, 131.5, 132.2, 132.7, 134.1, 134.3, 134.4, 137.7, 139.2, 144.1, 148.1.

3. Conclusion

we have developed an efficient, simple and environmentally friendly process for the synthesis of the interesting 1,2,4,5-tetrasubstituted imidazoles, with expected biological activity, with a good yield and an economical gain. The catalyst is recoverable and several runs without loss of its activity were achieved.

References

[1] Mekheimer, R. A.; Ameen, M. A.; Sadek, K. U., *Chinese Chem. Lett.,* **2008**, *19***,** 788; is considered part 2.

[2] (a) Eilbracht, P.; Bärfachen, L.; Buss, C.; Hollmann, C.; Kitsos-Rzychan, B. E.; Kranemann, C. L.; Rische, T.; Roggenbuck, R.; Shimdt, A., *Chem. Rev*., **1999**, *99*, 3329; (b) Bora, M.; Saikia, A.; Boruah, R. C., *Org. Lett*., **2003**, *5*, 435.

[3] Weber, L., *Curn. Med. Chem*., **2002**, *9*, 2085.

[4] Chang, L. C. W.; Von Fritag Drabbe Künzel, J. K.; Mulder-Krieger, T.; Spanjersherg, R. F.; Brussee, J.; Iizermann, A. P., *J. Med. Chem*., **2004**, *47*, 2045.

[5] Weber, L.; Illgen, K.; Almstetter, N., *Synlet*., **1999**, 366.

[6] Wolkenberg, S. E.; Wisnoski, D. D.; Leister, W. H.; Wang, Y.; Zhao, Z.; Lindsley, C. W., *Org. Lett*., **2004,** *6*, 1453.

[7] (a) Sisko, J., *J. Org. Chem*., **1998**, *63*, 4529; (b) Shilcrat, S. C.; Mokhallalati, M. K.; Fortunak, J. M. D.; Pridgen, L. N., *J. Org. Chem*., **1997**, *62*, 8449; (c) Horne, D. A.; Yakushijin, K.; Büchi, G., *Heterocycles*, **1994,** *39*, 139; (d) Reiter, L. A.; *J. Org. Chem*., **1987**, *52*, 2714.

[8] Karimi, A. R.; Alimohammadi, Z.; Azizan, J.; Mohammadi, A. A.; Mohmmadizadeh, R. R., *Catal. Commun*., **2006**, *7*, 728.

[9] Balalaei, S.; Arabanian, A., *Green Chem*., **2000**, *2*, 274.

[10] Kidwai, M.; Mothsro, P.; Bansal, V.; Somvanshi, R. K.; Ethayathulla, A. S.; Dey, S.; Singh, T. P.; *J. Mol. Catal. A: Chem.,* **2007**, *265*, 177.

[11] Heravi, M. H.; Derikvand, F.; Bamoharram, F. F., *J. Mol. Catal. A: Chem.,* **2007**, *263*, 112.

[12] Nagarapu, L.; Apuri, S.; Kantevari, S.; *J. Mol. Catal. A: Chem.*, **2007**, *266*, 104.

[13] Kantevari, S.; Vuppalapati, S. V. N.; Birdar, D. O.; Nagarapu, L., *J. Mol. Catal. A: Chem.*, **2007**, *266*, 109.

[14] Sadeghi, B.; Mirjalili, BiBi F.; Hashemi, M. M., *Tetrahedron Lett*., **2008**, *49*, 2575.

[15] (a) Li, C.-J.; Chen, L., *Chem. Soc. Rev*., **2006**, **5**, 68; (b) Varma, R. S., *Org. Chem. High.,* **2007**, *Clean Chemical Synthesis in water*, *MRL*: http://www. *Organic Chemistry.Org/highlights/2007/01 February. Shtm.*; (c) Kappe, C. O.; Dallinger, D., *Nat. Rev. Drug Disc*., **2005**, *5*, 51.

[16] Mekheimer, R. A.; Abdel Hameed, A.; Sadek, K. U., *Green Chem*., **2008**, *10*, 592.

[17] Funken, K. H., *Sol. Energy Mater*., **1991**, *24*, 370.

[18] Barsy, M. A.; Abdel Latif, F. M.; Aref, A. A.; Sadek, K. U., *Green Chem*., **2002**, *4*, 196.

[19] Sadek, K. U.; Mekheimer, R. A., *Arabian J. Chem*., **2008**, *1*, 79.

Arabian J. Chem. Vol. 1, No. 3, 295-306(2008)

DETECTION OF ADENOSINE RELEASED FROM BIOLOGICAL CELLS AT NANOSTRUCTURED CARBON FIBER SENSORS

Mohammed A. Al-Omair

Department of Chemistry, College of Science, King Faisal University

P.O. Box 380, Hufof, Al-Ahsa, Saudi Arabia

E-mail: malomair@yahoo.com

من المعروف علميا انه فى الأنظمة الحيوية وبخاصة فى الخلايا المكونة للجدار الخارجى اللقلب ينكون مركب الأدينوسين نتيجة التفكك السريع لمركب ادينوسين ثلاثى الفوسفات عند نقص الأكسجين الداخل للقلب.وبالتالي إذا كان تركيز الادينوسين المتحرر من هذه الخلايا عالى يكون هذا دليل على احتمالية الاصابة بالسكتة القلبية وعليه فان قياس تركيز هذا الأدينوسين المتحرر يمكن من الاكتشاف المبكر لأمراض القلب

بناء على ما تقدم فإن هذا البحث يهدف إلى قياس تركيز الادينوسين بالخلايا عند حدوث التفكك السريع لمركب ثلاثى فوسفات الأدينوسين وقد تمت الدراسة على خلايا حية من حيوان الهامستر. وتم القياس باستخدام تقنية النانو والمتمثلة فى استخدام حاسات بيولوجية مصنعة من الياف الكربون ذات القطر المتناهى فى الصغر بعد عمل تنشيط لهذه الحاسات مع تقنية فولنامتر المسح السريع التى توفر امكانية القياس السريع والدقيق لأقل كمية من الأدينوسين حيث ان زمن العمر له قصير داخل الخلايا و يتفكك بسرعة الى مواد اخرى. وقد أوضحت النتائج امكانية تقدير تركيز الأدينوسين المتحرر من الخلايا الحية بدقة وانتقائية عالية .

Abstract

Adenosine may be formed from the rapid degradation of extracellular adenosine triphosphate (ATP) by acetonucleotidase which is present on the extracellular surface of vascular smooth muscle cells and endothelium. Thus by monitoring the extracellular concentration of adenosine, total amounts of adenosine in a biological system can be determined. Adenosine released from the hamster ductus defenes cloned tumor cell line (DDT_1 MF-2 cells) was measured amperometrically at carbon fiber sensor (CFS) using fast scan voltammetry (FSV). Amperometric methods provide the advantages of fast and accurate measurements with a little sample preparation as adenosine has a rapid turn rate in tissues.

For high sensitivity measurements of adenosine, the carbon fiber sensor was activated by the method of electrochemical pretreatment (ECP) in which the electrode potential was continuously cycled, for 30 min, in Hanks' Balanced Salts (HBSS) buffer pH 7.4 at a scan rate of 10 Vs^{-1} in the potential window from –1.0 to 1.5 V vs SCE. As a result of the ECP for the carbon fiber sensor, a nanostructured carbon fiber surface was formed and also a stable background current was achieved which is needed in FSV for background subtraction. Adenosine released from the DDT_1 MF-2 cells can be measured with good sensitivity and selectivity at the activated carbon fiber sensor .

1. Introduction

Adenosine participates in many important cell functions such as production of cellular energy, intra and extracellular communications, modulation and other cellular functions [1,2]. The concentration of adenosine in biological systems is always controlled by means of a fast responding feedback system in order to maintain cellular functions [3]. This feedback system in the cell maintains the balance between intra and extracellular concentration of adenosine. The extracellular adenosine concentration is determined by the diffusion rate from the cells and uptake rate by cell or deactivation from the extracellular fluid by adenosine deaminase [3].

Within the cell, adenosine is formed by two metabolic routes [4]. (A) By degradation of ATP via ADP and AMP to adenosine. (B) By hydrolysis of ATP via s-adenosylmethionine to a-adenosylhomocystien which in turn hydrolyzes to adenosine. Adenosine diffuses through the cellular membrane between the extracellular and intracellular space, and this process is facilitated by a nucleoside transporter which is located in the plasma membrane of many cells such as endothelial cells, erythrocytes, cardiomyocytes and vascular smooth muscle cells[5].

Adenosine formation may occur from the rapid degradation of extracellular ATP by acetonucleotidase that is present on the extracellular surface of vascular smooth muscle cells and endothelium [6]. In normal oxygenation, the concentrations of intracellular adenosine and AMP are low. For this reason, extracellular adenosine will be transported rapidly to the intracellular space where it is phosphorylated to AMP or deaminated to inosine. Thus, by monitoring the extracellular concentration of adenosine, total amounts of adenosine in a biological system can be determined [1]. Because of the rapid turn rate of adenosine in tissues, fast measurements of adenosine are important. For this reason, amperometric techniques with fast scan voltammetry at miniaturized carbon fiber sensors are applicable.

Carbon fiber sensors with 7μm diameter, which allows small current to generate at these sensors [7] and also reduces the double layer capacitance, thus resulting in rapid voltammetric determinations [8-11] as well as monitoring kinetic processes [12] were used for the determination of adenosine released from the DDT_1 MF-2 cells which are the hamster ductus deferens cloned tumor cell line. The wild type DDT_1 MF-2 smooth muscle tumor cell line was derived from an estrogen/androgen-induced leiomyosarcoma that arose in the ductus deferens of a Syrian hamster. This cell line expresses receptors for both androgens and glucocorticoids, and its proliferation is differentially sensitive to these classes of steriod hormones. Growth of DDT_1 MF-2 cells is stimulated by androgens and inhibited by glucocorticoids.

DDT_1 MF-2 cells were used for the determinations of the released adenosine because of their ability of fast and easy growing. Also, these cells are capable of living for a long time. The measurements reported in this work were done by using fast scan voltammetry (FSV) technique which offers many advantages over conventional electroanalytical techniques. One of these advantages is its high temporal resolution that allows determinations in real-time [7, 13]. Also, allows using of signal averaging to improve signal-to noise ratio [14]. FSV allows acquisition of a large number of scans in a short period of time [15] hence, an improvement in signal-to-noise ratio can be achieved [14, 16]. Additionally, in FSV, rapid scan reversal occurs [17, 18] which can also contribute to the increase in the sensitivity and stability of the CF sensor.

The sensitivity as well as the limit of detection (LOD) in FSV is limited by the background current interferences. The background current results from the

double layer capacitance and the oxidation-reduction reaction of the surface-bound species [11]. However, background subtraction allows for sensitive FSV determinations that are also depend on the stability of the background current [18]. Previously, it was found that a stable background current was obtained after the electrochemical pretreatment of the CF sensor by continuous cycling of the electrode potential, for 30 minutes, in the potential window from -1.0 to 1.5 V vs SCE [16]. This process improves the sensitivity and selectivity of the surface of the CFE for the determination of biological molecules such as uric acid and adenosine [16, 19-20].

Furthermore, treatment of the CFE surface in different physiological buffers was investigated, and was found that the surface of the graphite fiber has a structure that is largely independent of the buffer used in the treatment [20]. On the other hand, the composition of the buffer has some effect on the sensitivity and LOD in the determination of adenosine [20].

In this work the activation of the carbon fiber sensor was done by the same procedure discussed above for a sensitive measurements of adenosine released from the DDT_1 MF-2 cells.

2.Experimental

Materials and Methods

Preparation of the working solutions

All chemicals used were of the analytical reagent grade and were used as received. Deionized water was used to prepare the solutions. Adenosine, potassium ferricyanide, potassium chloride and 2,4-dinitrophenol (DNP) were obtained from Sigma . Hanks' Balanced Salts was prepared from the highest purity materials from Sigma (HBSS; in mM: NaCl 137.0, KCl 5.0, $CaCl_2$ 1.0, $MgCl_2$ 0.4, $NaHCO_3$ 4.0, KH_2PO_4 0.4, Na_2HPO_4 0.4, d-glucose 5.0). Unless otherwise specified, the pH of HBSS buffers was 7.4. The pH was adjusted with HCl or NaOH.

The analyte solutions, adenosine and DNP, were freshly prepared in HBSS buffer pH 7.4 and the buffer solution was stored at 5^o C. Potassium ferricyanide was prepared in 0.5 M KCl. All determinations were performed at room temperature. All measurements were repeated at least in triplicate. The results from the determinations at several carbon fiber working electrodes were pooled. The reported results reflect the reproducibility of the measurements and fabrication of the carbon fiber electrodes. The sensitivity was measured from the slope of the calibration curve. At least eight points for each calibration curve and four determinations for each point were taken for three different electrodes.

DDT_1 MF-2 cells culture

Cells were cultured in Dulbecco's Modified Eagle Media (DMEM) [21-22]. The culture medium also includes 5% Fetal Bovine Serum, Penicillin, Streptomycin and Amphotericin. Cells were grown in 150-mm Petri dishes and were incubated at 37 ^{o}C with 5 % CO_2.

All experiments are performed on cells that are one day pre-confluent. The cells are not under stressful conditions such as depleted medium. The number of cells cultured per mL is 5.8 x 10^6 cells

Electrodes

Carbon fiber, 7 μm diameter, was used as the working electrode, and a saturated calomel electrode (SCE) was used as a reference electrode. Fabrication of the carbon fiber electrodes (CFEs) has been described previously [15, 20]. Electrode was polished using 600-grit silicon carbide paper and with a polishing cloth. The polished electrodes were cleaned by alcohol and doubly distilled water before use.

The response of the polished electrodes was tested in 5.0 mM potassium ferricyanide in 0.5M KCl by cyclic voltammetry at a scan rate of 50 mVs^{-1}. The electrodes which did not respond were polished again; and those which, did not respond after the second polishing were discarded.

Instrumentation

For slow-scan cyclic voltammetric measurements, a Bioanalytical Systems Electrochemical Analyzer, with a home-built preamplifier [11], interfaced to a PC, was used. Fast scan cyclic voltammetry (FSV) [16-17, 23] and the instrumental setup for FSV has been described previously [11, 16, 20]. A function generator was used to apply a triangular waveform to the SCE reference electrode in a two-electrode configuration potentiostat. A home-built current transducer was used to measure the current at the CFE [11]. The current was converted to voltage, amplified, and was recorded and stored by a digital oscilloscope. The stored data were transferred from the oscilloscope to a personal computer for analysis and display. A copper mesh Faraday cage was used in FSV to minimize the environmental noise.

The buffer and the analyte were injected into a ca. 80 μL electrochemical cell with a syringe which allowed the solutions to be pumped into the cell and provided a permanent contact between the solution and the electrode. Before each measurement, background current was recorded in the working buffer in the absence of the analyte, and was averaged and stored for digital background subtraction. The background current was recorded at the experimental scan rate, with the same number of scans as were used in the analytical determinations of the analytes, in the same potential window of -1.0 to 1.5 V vs SCE. In the determinations of the analytes, the same number of scans was recorded under the same experimental conditions as in the buffer alone, in the same potential window. The current measured in the analyte solutions was averaged, and then digitally subtracted from the stored background current.

The number of cycles that were recorded in FSV was 250, which allowed a high signal-to-noise ratio to be achieved in a short time [16].

Selection of Suitable Carbon Fiber Sensors for Electrochemical Measurements

As it was mentioned above the response of the polished electrodes was tested by cyclic voltammetry in ca. 5.0 mM potassium ferricyanide in 0.5 M KCl at a slow scan rate of 50 mVs^{-1} in a potential window from 500 to -200 mV vs SCE [19]. The selected CFE showed a slowly rising current plateau with a small separation between the forward and the reverse current traces of $Fe(CN)_6^{3-}$. Potassium ferricyanide limiting current of *ca*. 5.0 ± 0.5 nA and a half wave potential ($E_{1/2}$) of 135 ± 10 mV vs SCE were expected for a well fabricated CFE. The reproducibility of fabrication of CFE was also tested from the log-plot analysis of the voltammetric curve of ferricyanide.

Ferricyanide was used as the electroactive probe for selection of good quality electrodes, because of its well known redox properties as well as its limited adsorption at graphite [24]. The limiting current of ferricyanide obtained at 50 mVs^{-1} in 0.5 M KCl was used to determine the radius of the CFE using previously determined diffusion coefficient of ferricyanide of 7.7 X 10^{-6} cm^2 s^{-1} [25] and by assuming a disk equivalent area of the electrode [26].

Electrochemical Pretreatment (ECP) and Capacitance Measurements of The Carbon Fiber Sensor

The selected carbon fiber sensor which have good quality were electrochemically pretreated in HBSS buffer, pH 7.4, by continuous cycling of the electrode potential at a scan

rate of 10 Vs^{-1}, for 30 min, in a potential window from -1.0 to 1.5 V vs SCE. This electrochemical pretreatment under these conditions was used previously to produce a highly active CFE surface for the electrochemical measurements with a stable background current, which is the current that is recorded in the buffer solution (HBSS). All of the electrochemical measurements were done in HBSS buffer and for this reason it was used for the ECP of the carbon fiber sensor[15,19].

To confirm the success of the electrochemical pretreatment process, the CFE capacitance (C_{obs}) was measured before and after ECP. The apparent carbon fiber sensor capacitance was measured at 0.75 V vs SCE from the background current measured in HBSS buffer pH 7.4 at a scan rate of 10 Vs^{-1} in a potential window from -1.0 to 1.5 V which is the same potential that was used for ECP.

As it was explained previously [15], at a potential of 0.75 V, the background current which is due to surface faradaic reaction of graphite is low and the measured background current is due to the double layer charging only. Capacitance of the CFE was measured by using the equation

$$C_{obs} = I / 2 < A$$

Where I is the background current at 0.75 V in (A); < is the scan rate used for measuring the background current in (Vs^{-1}) and A is the area of the CFE in (cm^2). The area of CFE using the radius determined from the limiting current of ferricyanide at 50 mVs^{-1} at the CFE after the ECP as it was described above normalized the observed capacitance.

3. Results and Discussion

Effect of the electrochemical pretreatment on the carbon fiber sensor surface

The radius of the carbon fiber sensor was determined before the ECP from the limiting current of ferricyanide in 0.5 M KCl at a potential of -0.200 V vs SCE as shown by Fig.(1) and by using the diffusion coefficient of ferricyanide, 7.7 X 10^{-6} cm^2 s^{-1} [25]. The CFE radius was found to be 3.47 ± 0.05 μm. Also the kinetics of ferricyanide at the CFE was determined from the plots of potentials vs log i_l - i / i of ferricyanide [20] from the data obtained in ferricyanide. A slope of 89 ± 10 mV was obtained before ECP which shown an irreversible electrode reaction of ferricyanide with one electron redox reaction. In addition the calculated value of the half wave potential of $E_{1/2}$, E^0 was found to be 135 ± 10 mV comparing to the value of E^0 of ferricyanide (212mV) at 0.5 M KCl [27].

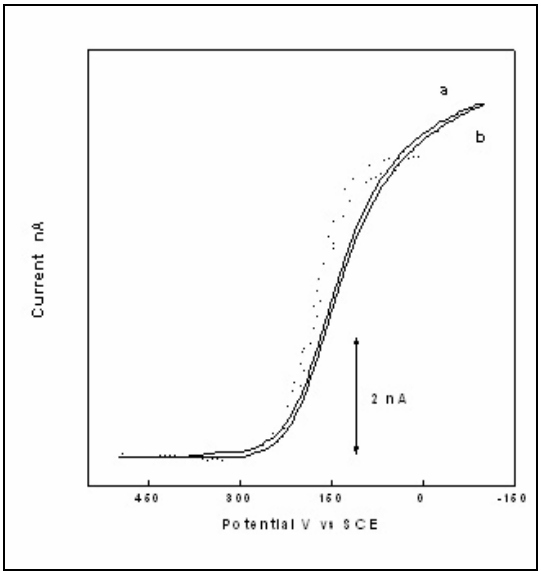

Figure 1 Cyclic voltammograms of ferricyanide at carbon fiber ultramicroelectrodes before (a) and after (b) the electrochemical pretreatment; 5.0 mmol l^{-1} $Fe(CN)_6^{3-}$, 0.5 M KCl, 50 mVs^{-1}, r = 3.47 ± 0.06 μm.

After ECP of the CFE in HBSS buffer pH 7.4 at a scan rate of 10 Vs^{-1} in the potential window from -1.0 to 1.5 V, by continuous cycling of the electrode potential, for 30 min, the slope of the plot of potential vs log i_l - i / i was changed to a value of 59 ± 0.1 mV which confirms a reversible reaction of ferricyanide after the ECP of the carbon fiber

sensor. Also the value of $E_{1/2}$ shifted after the ECP in HBSS buffer pH 7.4 to 175 ± 10 mV [28]. Figure 1 also shows that after the ECP the limiting current decreased by 30 ± 5 % and the separation between the forward and the reverse current traces of $Fe(CN)_6^{3-}$ increased as illustrated by (b) in fig. 1, comparing with the separation before the ECP as shown by (a) Fig.1,which indicates that the electrode capacitance increases.

The increasing in electrode capacitance determined by using the equation C_{obs} = I / 2 <A as discussed above was well noticeable from Fig. (2) which illustrates the background current before and after the ECP in HBSS buffer pH 7.4. By comparing the background current that measured at 0.75 V, before (a) in fig. 2 and after ECP (b), it is obvious that a large increase in the background current occurs, as a result of ECP, which is almost twice the value of the background current before ECP. This increment in the background current reflects the changes at the carbon fiber sensor surface due to the ECP by continuous cycling of the electrode potential, for 30 minutes, at 10 Vs^{-1} in the potential window from -1.0 to 1.5 V vs SCE.

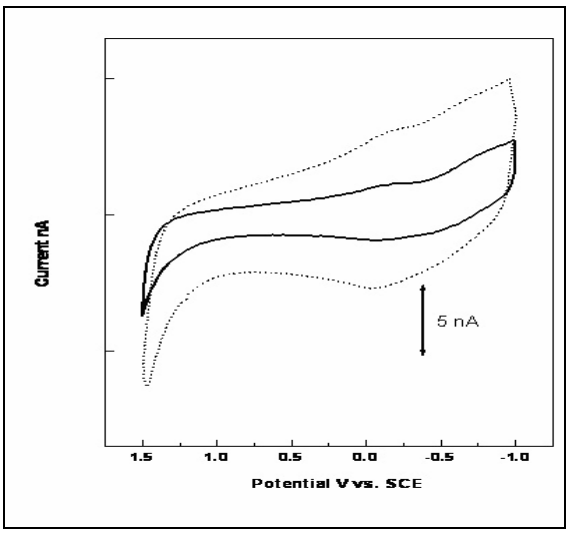

Figure2. Background current at carbon fiber ultramicroelectrode before (—) and after (----) the electrochemical pretreatment. For pretreatment conditions see Experimental. Average current shown in HBSS buffer, pH 7.4, after 30 min of continues cycling in the potential window shown. Scan rate 10 Vs^{-1} (3600 cycles), r = 3.47 ± 0.06 μm.

The value of the background current observed after the electrochemical pretreatment in HBSS buffer pH 7.4 was found to be higher than that observed in the electrochemical pretreatment in 7×10^{-2} M phosphate buffer pH 7.4 as illustrated previously [28] due to the difference in the compositions between the two buffers. HBSS buffer contains electro active materials that could be responsible for the higher value of the background current than in the case of using 7×10^{-2} M phosphate buffer for treatment.

As a result of the ECP a nonstructural CF surface was formed [20] and also a stable background current was achieved [16]. A stable background current in FSV which is needed to be used in background subtraction where a more efficient background subtraction.

Measurements of Adenosine Sensitivity at Carbon Fiber Sensor

The low concentrations of adenosine could be successfully measured with good sensitivity, at 1.0 V vs SCE by FSV (500 Vs^{-1}), at CFE after the activation of the CFE surface by the electrochemical pretreatment of the CFE surface. The formation of the nonstructural carbon fiber surface was found to be independent on the buffer used for treatment [29].

Figure (3) shows typical voltammogram of 20 μM adenosine that was obtained by FSV at 500 Vs^{-1} with 250 cycles at CFE after the ECP of the electrode surface in

HBSS buffer, pH 7.4, and after the background current subtraction. Adenosine showed a well-developed oxidation peak at a potential of ca 1.0 V vs SCE with a sensitivity of 0.18 ± 0.007 nA μM^{-1}. Adenosine sensitivity was measured from the calibration curve of adenosine with a linear dynamic range from 2-12 µM and a limit of detection of 3 µM (Figure 4). The high value of the background current in the case of using HBSS buffer, which composed of electro active materials, in treatment and measurements leads to lower value of the measured sensitivity compared to the sensitivity measured in a simple physiological buffer such as phosphate buffer [28]. The high background current value results in poor background current subtraction in fast scan measurements of adenosine sensitivity [28].

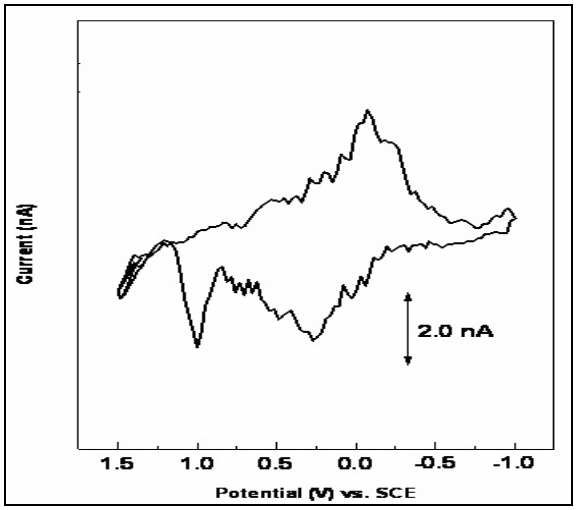

Figure 3 Cyclic voltammograms of 20 µ M adenosine in HBSS buffer pH 7.4 at 500 Vs^{-1}, with 250 cycles average, results after background subtraction, r = 3.47 ± 0.05

According to the accessions about the electyrooxidation of adenosine at CFE [30], it was explained that the electrochemical oxidation of adenine, which is the purine moiety of adenosine, involves oxidation with oxygen transfer. The formed oxidation product endures further oxidation to give a product, which yields the reversible peak at 1.0 V, which was used for the determination of adenosine, and the reduction of this product results in the formation of the reduction peak at ca. 0.0 V. Also the oxidation peak, which appear at 0.25, is due to the oxidation of HBSS buffer and the reduction products showed a reduction peak at 0.0 V, which may accumulate with the reduction response of adenosine to give a well-developed reduction peak at 0.0 V.

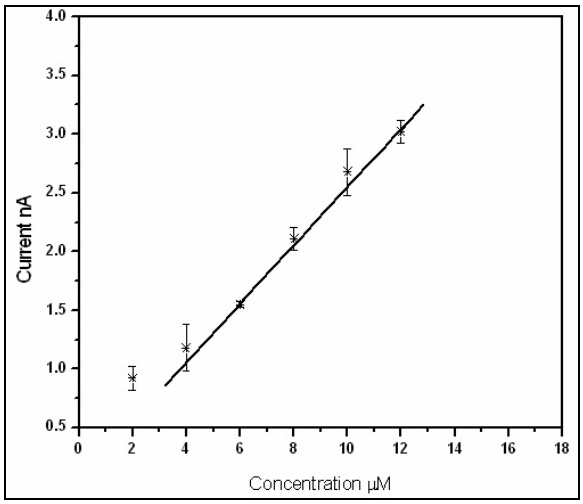

Figure 4. Adenosine calibration curve in 70 mM phosphate buffer pH 7.4 at 500 V/s with 250 Cycles, with a correlation factor of 0.9976.

Using Uncouplers of Oxidative Phosphorylation in the Biological Cell Measurements

A solution of (DNP) was added to the cultured cells. The purpose of using DNP will be explained briefly. The oxidation (electron transport) by O_2 of nicotineamide adenine dinucleotide (NAD) and flavin adenine dinucleotide (FAD), which are coenzymes involved in large number of biological oxidations and reductions, and the synthesis of ATP (oxidative phosphorylation) are normally tightly coupled [31]. In the resting state, when oxidative phosphorylation is minimal, the electrochemical gradient across the inner mitochondrial membrane builds up to the extent that it prevents further proton pumping and

therefore inhibits electron transport.

However, many compounds including DNP have been found to "uncouple" these processes. The mechanism by which these uncouplers act is : the presence in the inner mitochondrial membrane of an agent that increases its permeability to H^+ uncouples oxidative phosphorylation from electron transport by providing a route for the dissipation of the proton electrochemical gradient that does not require ATP synthesis. Uncoupling therefore allows electron transport to proceed unchecked even when ATP synthesis is inhibited [31]. DNP is lipophilic weak acid that, therefore, readily passes through membranes. In a pH gradient, it binds protons on the acidic side of the membrane, diffuses through, and release them on the alkaline side, thereby dissipating the gradient. Thus, such uncoupler is proton-transporting ionophore and the metabolic rate increases by such compounds.

Measurements of 10 µM and 100 µM 2,4 - dinitrophenol at activated Carbon Fiber Sensor

A solution of 10 µM DNP in HBSS buffer was measured at electrochemically pretreated CFE in a freshly prepared HBSS buffer, pH 7.4, at 500 Vs^{-1} with 250 cycles in the potential window from –1.0 to 1.5 V vs SCE which is the same potential window used for ECP and for the measurements of adenosine sensitivity at treated CFE.

Fig 5-a shows the resulted cyclic voltammogram of 10 µM DNP solution, which gave an oxidation current of 7.7 nA at 0.25 V and a reduction current of 6.7 nA at -0.25 V. In addition a solution of 100 µM DNP, was measured at treated CFE at 500 Vs^{-1} with 250 cycles, in the same potential window mentioned above. The pH of this solution was adjusted at 7.4 before the measurements. The resulted cyclic voltammogram shown in fig. 5-b shows an oxidation peak at 0.5 V with a peak current of 10.0 nA and a reduction peak at -0.5 V with a current of 12.0 nA .

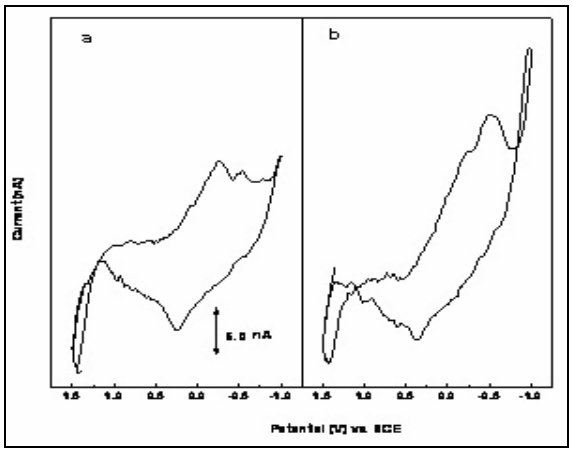

Figure 5.Cyclic voltammograms of 10 µ M 2,4 - dinitrophenol (DNP) (a) and 100 µ M DNP (b) in HBSS buffer pH 7.4 at 500 Vs^{-1} with 250 cycles average, results after background subtraction

Measurements of Control at 4 °C and 37 °C

Controls, which contain cells in HBSS buffer only without DNP prepared at 4 °C and at 37 °C, respectively, were measured at the electrochemically pretreated carbon fiber sensor at 500 Vs^{-1} in the potential window from –1.0 to 1.5 V vs SCE. The pH of the frozen control solutions was adjusted to 7.4. The results show an oxidation peak at 0.25 V with a peak current of 3.0 nA in the case of the control at 4 °C and of 5.0 nA in the case of the control at 37°C. Also a reduction peak at -0.25 V was observed with a peak current of 7.0 nA in the case of both solutions of controls, at 4 °C and at 37 °C respectively.

The observed peaks were suggested to be referred to HBSS buffer, for this reason a solution of HBSS buffer was prepared in our Lab. and was possessed frozen, as a result of that its pH became 7.8 and then it was adjusted to 7.4. This HBSS buffer solution was measured at the activated CEF in a potential window from –1.0 to

1.5 V vs SCE at the same scan rate of 500 Vs^{-1}. The measurements show similar results as obtained in the case of controls at 4°C and 37 °C with lower oxidation and reduction current, which might be refers to the absence of the DDT_1 MF-2 cells in this solution. This result could explain the response, which was observed in measuring Controls solutions to be due to HBSS buffering itself.

Measurements of adenosine released from DDT_1 MF-2 cells with 10 µM and 100 µM DNP at CFE

The response of adenosine was measured in a sample of DDT_1 MF-2 cells with 10 µM DNP in HBSS buffer, pH 7.4, (sample1) at an activated CF sensor at a scan rate of 500 Vs^{-1}, in the potential window from –1.0 to 1.5 V vs SCE. The pH of sample 1 was measured and adjusted at 7.4 before measurements. As shown in fig. 6-a, a small peak was detected at 1.12 V, which may refer to adenosine as adenosine was measured previously at 1.0 V [29]. This peak was well defined after subtraction of the signals of 10 µM DNP (Fig. 5-a) from the signals of sample 1 (Fig. 6-a). The resulting peak after the subtraction showed a current of 8.7 nA at 1.14 V as shown by Fig. 6-b.

It was obvious from Fig. 6-b that, at 0.25 V, an oxidation peak of peak current of 20. 0 nA was observed as well as a reduction peak at -0.25 V with peak current of 12.0 nA. This high value of the current may arise from the presence of DDT_1 MF-2 cells with DNP and HBSS buffer.

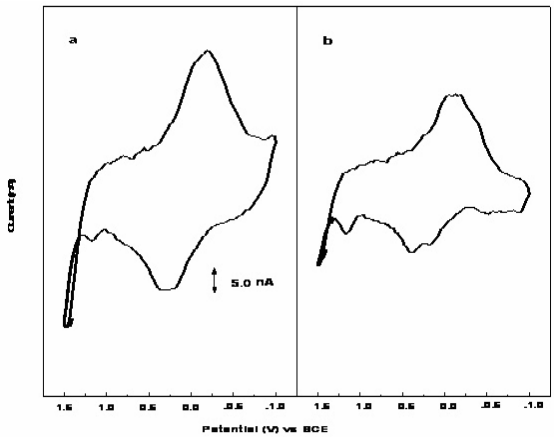

Figure 6. (a) Cyclic voltammogram of DDT_1 MF-2 cells with 10 µ M DNP in HBSS buffer pH 7.4 at 500 Vs^{-1} and (b) cyclic voltammogram resulted from subtraction of the response of 10 µM DNP from (a)

As it was discussed previously [29], low concentrations of adenosine (1-20 µM) were measured at an electrochemically activated CFE at 1.0 V, the recognized shift in the peak potential to higher positive value (1.14 V) after the subtraction of the response of 10 µM DNP from the response of sample 1 at CFE, measured at 500 Vs^{-1} , may be due to higher concentration of adenosine released from DDT_1 MF-2 cells in sample 1.

To verify this assumption, two solutions of 50 µM and 100 µM adenosine were prepared in HBSS buffer, pH 7.4, and were measured at CFE in the same potential window used for the measurements at 500 Vs^{-1}. The results of measuring 50 µM adenosine showed a peak current of 5.50 nA and a sensitivity of 0.11 nA μM^{-1} at 1.10 V, while 100 µM adenosine gave a peak current of 10.83 nA with a sensitivity of 0.11 nA μM^{-1} at 1.10 V as shown in Fig. (7). From these results it was assumed that the high concentration of adenosine is responsible for the shift in the potential to a higher positive value and it was assumed that the concentration of adenosine measured in sample 1 might be 60-70 µM.

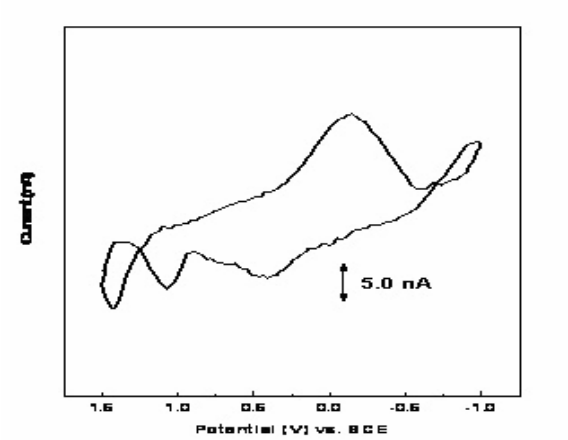

Figure 7 Cyclic voltammograms of 50 µM adenosine in HBSS buffer pH 7.4 at 500 Vs^{-1} , with 250 cycles average

Measurements of high concentration of adenosine in a mixture with 10 µM and 100 µM DNP

In these measurements a mixture of 50 µM adenosine with 10 µM DNP (mixture 1) in HBSS buffer, pH 7.4, was prepared in our Lab. and measured at 500 Vs^{-1} in the potential window from –1.0 to 1.5 V vs SCE. Similar measurements were done with 50 µM adenosine with 100 µM DNP (mixture 2) which was also prepared in our lab. In HBSS buffer, pH 7.4, the results showed a well-defined peak that appeared at 1.10 V, which gave a current of 4.55 nA in the case of mixture 1. The same result was obtained in mixture 2, which gave also a well-developed peak at 1.10 V with a current of 9.63 nA. Subtraction of the signals resulted from measuring a solution of 10 µM DNP at CEF in HBSS buffer, pH 7.4 (Fig 5-a) from the signals resulted from mixture 1 was done. The resulted cyclic voltammogram shown in Fig. 8, in which it is obvious that a well-defined peak at 1.12 V with a peak current of 6.0 nA and a sensitivity of 0.12 nA μM^{-1} was observed.

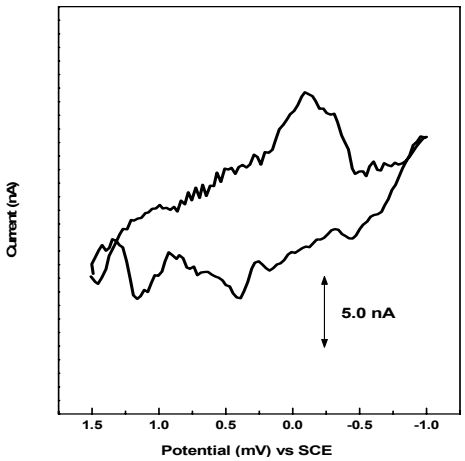

Figure 8. Cyclic voltammograms of 50 µM adenosine in HBSS buffer pH 7.4 at 500 Vs^{-1}, with 250 cycles average, results after subtraction of the response of 10 FM DNP in HBSS buffer from the response of a mixture of 50 µM adenosine with 10 µM DNP in HBSS buffer.

Also the cyclic voltammogram of the solution of 100 µM DNP in HBSS buffer, pH 7.4, was subtracted from the cyclic voltammogram of mixture 2, the results showed also a well-developed peak at 1.12 V with a peak current of 6.0 nA and a sensitivity of 0.12 nA μM^{-1}. The resulted peak that appeared at 1.12 V with a current of 6.0 nA was very close to the peak of adenosine itself that was measured at CFE in the absence of DNP (Fig.7). This indicates that the well-developed peak that was observed in Fig. 8 was due to the presence of adenosine with a concentration of ca. 60-70 µM. Also these results indicate that the high concentration of DNP may not affect the release of adenosine from the DDT_1 MF-2 cells but reduce the resolution of the response of adenosine due to the high value of current that could be measured from 100 µM DNP. It was obvious from these results that adenosine released from DDT_1 MF-2 cells could be measured with good sensitivity with 10 µM and 100 µM DNP at an electrochemically activated carbon fiber sensor.

4. Conclusion

Direct voltammetric detection of adenosine with a carbon fiber sensor (CFS) and fast scan voltammetry is a suitable method for biological measurments of adenosine. The method has the advantages of simplicity, speed, and ease of miniaturization. Before measurments of adenosine CFS was activated in a process which nanostructured the fiber surface and generated a stable surface for reproducible voltammetric detection of adenosine over time.

Adenosine with high sensitivity was measured by voltammetry at 1.0 V at 500 Vs^{-1} in HBSS buffer at pH 7.4. Also adenosine released from DDT1 MF-2 cells was measured in the presence of (DNP) at the CFS in HBSS buffer at pH 7.4 with good sensitivity 0.16 ± 0.008 μM nA^{-1} and selectivity at 1.0 V at 500 Vs^{-1} .

Acknowledgment

The financial support by the Deanship of Scientific Research at King Faisal University is gratefully acknowledged.

References

[1] B.B. Fredholm, Life Sci., **41**, 837 (1987).

[2] T.V. Dunwiddie , B.B. Fredholm, Naunyn-Schmie-Deberg's Arch. Parmacol., **326**, 294 (1984).

[3] T.K. Chen, T.G. Strein, T. Abe, A.G. Ewing, Electroanalysis, **6**, 746 (1994).

[4] P. Meghji, Drug Dev. Res., **28**, 214 (1993).

[5] P. Meghji, R. Rubio, R.M. Berne, Life Sci., **43**, 1851 (1988).

[6] M.M Borst, J. Schrader, Circ. Res., **68**, 797 (1991).

[7] J. A. Stamford, J. Neurosci. Meth., **17,** 1 (1986).

[8] C. A. Amatore, A. Jutland, F. Pfluger, J. Electroanal. Chem., **218,** 361 (1987).

[9] D. O. Wipf, E. W. Kristensen, M. R. Deakin, R. M. Wightman., Anal. Chem., **60,** 306 (1988).

[10] M. I. Montenegro, D. Pletcher, J. Electroanal. Chem., **200,** 371 (1986).

[11] C. C. Hsueh; A. Brajter-Toth, Anal.Chim. Acta, **321**, 209 (1996).

[12] C. A. Marsden, M. H. Joseph, L. Z. Kruk, N. T. Maidment, R. D. O'Neill, J. O. Schenk, J. A. Stamford, Neuroscience, **25**, 389 (1988).

[13] G. W. Kuhr, R. M. Wightman, Brain Res., **381**, 168 (1986).

[14] D. J. Wiedemann, T. K. Kawagoe, R. T. Kennedy, E. Ciolkowski, R. M.Wightman,

Anal. Chem., **63**, 2965 (1991).

[15] R. Bravo, C. C. Hsueh, A. Jamarillo, A. Brajter-Toth, Analyst **123**, 1625 (1998).

[16] C. C. Hsueh, R. Bravo, A. Jaramillo, A. Brajter-Toth, Anal. Chim. Acta, **349**, 67 (1997).

[17] J. E. Baur, E.W. Kristensen, L. J. May, D. J. Wiedemann,; R. M. Wightman, Anal. Chem., **60**, 268 (1988).

[18] J. Stamford, Trends in Neurosc., **12 (10)**, 407 (1989).

[19] R. Bravo, A. Brajter Toth, Chem. Anal. (Warsaw), **44**, 423(1999).

[20] A. Brajter-Toth, K. Abou El-Nour, E. T. Cavalheiro, R. Bravo, Anal. Chem., **72**, 1576 (2000).

[21] R. Dulbecco, G. Freeman, Virology, **8**, 396 (1959).

[22] J. D. Smith, G. Freeman, M. Vogt, R. Dulbecco, Virology, **12**, 185 (1960).

[23] C.C. Hsueh, A. Brajter-Toth, Anal. Chem., **65,** 1570 (1993).

[24] J. Kawaik, J. P. Kulesza, Z. Galus, J. Electroanal. Chem., **226,** 305 (1987).

[25] M. Stackelberg, M. Pilgram, V. Toome, Z. Electrochem., **57**, 342 (1953).

[26] R. Kelly, R. M. Wightman, Anal. Chim. Acta**, 187,** 79 (1986).

[27] A. J. Bard, "*The Encyclopedia of The Electrochemistry of The Elements"*, Marcel Dekker, New York, 233 (1973).

[28] K. Abou El-Nour, A. Brajter-Toth, The Analyst, **128 (8)**, 1056 (2003).

[29] K. Abou El-Nour, A. Brajter-Toth, Journal of Electroanalysis, **12 (11)**, 805 (1999).

[30] G. Dryhurst, *"Electrochemistry of Biological Molecules"*, Academic Press, New York, pp 137. (1997).

[31] Spurlock, L. D., Jaramillo, A., Prserthdam, A., Lewis, J., and Brajter-Toth, A., Anal. Chim. Acta, **336,** 37, (1996).

Arabian J. Chem. Vol. 1, No. 3,307-317(2008)

Determination of Selenium(IV) in Pharmaceutical Products by Differential Pulse Voltammetry and Inductively Coupled Plasma Optical Emission Spectroscopy

M. COULIBALY[a, b], M. E. GHANJAOUI[a,c], A. GONZÁLVEZ[c], M. de la GUARDIA[c], M. EL RHAZI[a*]

[a] Laboratoire d'Electrochimie et de Chimie Physique, Faculté des Sciences et Techniques - BP146, Mohammedia, Maroc

[b] Laboratoire des Sciences; Physiques Fondamentales et Appliqués de l'Ecole Normal Supérieure d'Abidjan 08BP 10 Abidjan 08 Abidjan Côte d'Ivoire

[c] Department of Analytical chemistry, jeroni Muñoz Bulding, University of Valencia, 50 Dr. Moliner St., 46100 Burjassot, Valencia, Spain.

***E-mail*: elrhazim@hotmail.com (Mama. El Rhazi)**

Abstract

In this work, the suitability of a carbon paste electrode coupled with differential pulse voltammetry (DPV) has been investigated for the determination of Se(IV) after complexation with 2, 3-Diaminonaphthalene(2,3-DAN). A decrease of oxidation current of 2, 3-DAN was observed due to the formation of a complex of 2, 3-Diaminonaphthalene with Se(IV). The different parameters affecting the reaction rate between Se(IV) and 2,3-DAN were studied; such as temperature, pH, time of reaction and concentration of 2, 3-DAN. The calibration plots were linear in the range from 1 to 10 µg/l with r = 0.998 and 10 to 100 µg/l with r = 0.998. The relative standard deviation for five replicate analyses of 10 µg/l of selenium was 2.5%. The limit of detection was 0.7 µg/l. The voltammetric method was used for the determination of Se(IV) in tap water and pharmaceutical preparation. The results obtained by DPV method were validated by Inductively Coupled Plasma optical emission spectroscopy (ICP-OES) .

Keywords: Selenium; Differential Pulse Voltammetry; 2, 3 –Diaminonaphthalene; piazselenol; ICP-OES.

1. Introduction

Selenium is an essential trace element for plants, animals and human (glutathione peroxidase). The biological function of selenium shows dual characteristics. It can cause disease by its deficiency, but is toxic at level relatively close to those required for health [1-3].The daily intake of selenium depends on its concentration level in food and on the amount of food consumed. The recommended intake is 80µg/day for men and 55µg/day for women [4]. The high selenium concentration can produce

chronic toxicity symptoms as liver carcinoma, cirrhosis, teeth, hair and losses, irritation of eyes and paralysis [5, 6]. The maximum concentration accepted in drinking water is 10 µg/L. Many studies have been reported from two human diseases associated with severe nutritional selenium deficiency, a juvenile cardiomyopathy called Keshan disease and chondrodistrophy called Kaschin-Beck disease [7, 8].

The beneficial role of micro-amount of selenium in biological system and its toxicity at high levels with a small relatively difference between these values has encouraged the development of analytical strategies for its determination at trace levels. Accurate, precise and sensitive methods have been developed for the determination of selenium in several matrices [9-11]. A number of methods have been used for the determination of selenium, such inductively coupled plasma mass spectrometry (ICP- MS)[12], atomic absorption spectrometry (AAS) [13], atomic fluorescence spectrometry [14] and chromatography [15]. The main disadvantages of these techniques are the complexity and cost of the instrument.

Spectrophotometric or fluorimetric methods have been also widely used for detection of Se(IV) in several samples based on piazselenol complex formation between the reagent and selenium. The common reagents are o-diamine-3, 3-diaminobenzidine [16], dithizone, o-phenylenediamine [17], 6-amino-1-naphthol-3-sulphonic acid [18], 2, 3-Diaminonaphthalene [19], and 2, 3-diamino-1, 4-dibromonaphthalene [20]. 2, 3-Diaminonaphthalene is a widely used reagent for standardization and pharmaceutical testing owing to its lack of toxicity and ready availability [14, 21]. Se(IV) reacts with 2, 3-DAN yielding the complex 4, 5-benzopiazselenol which allows the determination of the selenium in different matrix [22-25].

These techniques, commonly used for trace measurement of selenium in laboratory, are not suitable for the task of on- site testing and monitoring. The portable nature and excellent sensitivity of electrochemical techniques make them very attractive for field monitoring of trace metals [26]. Electrochemical methods such stripping voltammetric techniques have been shown to be useful for the determination of trace levels of Se(IV) ion at bare electrode or at chemically modified electrodes [27-31]. Sook et al used gold electrode modified with poly 1.8 Diaminonaphthalene for detection of selenium [32]. Determination of selenium has been performed at gold electrode modified with 3,3-diaminobenzidine based on piazselenol complex [33].

In the last few years, our group has reported several studies of minerals elements analysis based on the effect of the presence of analyte ions on the current due to the oxidation of the complexant agent or based on modified electrode by conducting polymers [34-37]. Among the chemically modified electrode, the carbon paste electrode (CPE) which can provide a suitable electrode substrate due to their interesting advantages such as their versatility and, low cost, ease of preparation and renewability of their surface.

In this work, the suitability of a carbon paste electrode has been investigated for the determination of Se(IV) after complexation with 2, 3 DAN in samples of water and pharmaceuticals products. Since it is well known that Se(IV) ions give a specific reaction with aromatics diamine to form piazeselenol, this reaction will be used for the selective determination of small amount of Se. For this, the oxidation current of 2, 3-DAN in acidic medium was measured in the presence and in the absence of Se(VI) ions. The decrease of the oxidation current of 2, 3-DAN caused by the formation of an electro-inactive complex was studied. The experimental conditions and analytical parameters were optimized, such as concentration of 2,3-DAN, temperature, pH and time of reaction. The method was applied to the determination of selenium(IV) in water sample and pharmaceutical preparation. Finely,

the results obtained by our method were compared to those obtained by the ICP-OES.

2. Experimental

2.1 Apparatus

Voltammetric measurements were carried out with an autolab PGSTAT 10 Potentiostat (Ecochimie, Utrecht Netherlands) controlled by GPES 4.8 Software. The three electrode system consists of a carbon paste or glassy carbon electrodes as working electrode, a saturated electrode calomel (SCE) as the reference electrode and a platinum wire as the counter electrode. The pH was adjusted using a Fisher Scientific Accumet AB15 BASIC pH meter.

ICP-OES Analysis were carried out using a Perkin Elmer Model Optima 5300 DV spectrometer (Norwalk, CT, USA) equipped with an autosampler AS 93-plus and a Meinhard nebulizer. Argon C-45 (purity higher than 99.995%) supplied by Carburos Metálicos (Barcelona, Spain) was employed as a plasmogen and carrier gas.

A microwave laboratory system Ethos SEL from Millestone (Sorisole, Italy) equipped with an optical fiber sensor for automatic temperature control, an automatic gas detector and 10 high pressure vessels of 100 ml inner volume, operating at a maximum exit power of 1000 W was employed for microwave-assisted digestion of samples.

2.2 Reagents and samples

All chemicals used were analytical reagent grade. Aqueous solutions were prepared with distilled water. Selenite solution was prepared by dissolving 0.1405 g of SeO_2 in 100 mL distilled water. Solutions of 2,3-diamino-naphthalene were prepared by appropriate dilution of 2,3-DAN (Sigma) using small quantity of acetonitrile and distilled water. Tap water samples were collected in the laboratory; tablets from pharmaceutical samples were weighted and dissolved in distilled water.

For ICP-OES measurements, A multi-elemental standard solution of 100 µg mL^{-1} containing 26 elements (Li, Al, As, Ba, Be, B, Cd, Ca, Cr, Co, Cu, Fe, Pb, Li, Mg, Mn, Mo, Ni, K, Se, Na, Sr, Tl, Ti, V, Zn) was dissolved in 5 % HNO_3, supplied from Scharlau (Barcelona, Spain) and a multi-elemental (100 µg mL^{-1}) solution containing 16 lanthanide elements dissolved in 5% HNO_3 purchased from Alfa Aesar (Karlsruhe, Germany) were used as stock solutions for calibration.

For sample digestion HNO_3 69% (w/v) from J.T. Baker (Deventer, The Netherlands) was employed, H_2O_2 35% reagent grade from Scharlau and nanopure water with a maximum resistivity of 18.2 MΩ cm^{-1}, obtained from a Milli-Q Millipore system (Bedford, MA, USA).All reagents used were of the highest purity and all solutions were prepared in ultra pure water (resistively of 18.2 MΩcm) obtained from a Milli-Q system (Millipore, Bedford, USA).The standard stock solutions (1000 mg/l) for the ICP-OES were supplied by Merck (Darmstadt, Germany).

2.3 Procedure

2.3.1- Preparation of carbon paste electrode

The carbon paste electrode (CPE) was prepared by thoroughly mixing 1 g of graphite powder and 0.3 mL of paraffin oil until a uniformly wetted paste was obtained. The paste was then inserted into the electrode cavity 2 mm deep and having a diameter of 3 mm. A stainless still wire provided the electrical contacts. The electrode surface could be renewed by simple extrusion of a small amount of paste from the tip of the electrode. Before each use of CPE, it was rubbed with a piece of paper until a smooth surface was observed.

2.3.2- Procedure for selenium(IV) determination by DPV method

Electrochemical determination of selenium requires three steps:

First step: The electrode was immersed in aqueous solution containing 2, 3-DAN in acidic medium. The anodic current due to the oxidation of 2, 3-DAN was measured by cyclic voltammetry between +0.4V to +1. 0 V at a sweep rate of 50 mV/s. Quantitative measurements are performed by differential pulse voltammetry (The parameters used were a potential step height of 10 mV, pulse amplitude of 50 mV, the potential was scanned between +0.4V to +1. 0 V). The current response of 2, 3-DAN was measured as I_1.

Second Step: A Standard solutions or water samples containing a selenite ion are added to the 2, 3-DAN solution and kept on boiling water between 5 to 30 min. When selenite ions are added to 2, 3-DAN solution, they form an electro-inactive complex with 2,3-DAN characterized by the colour development.

Third step: Unreacted 2, 3-DAN was then measured as described in the first step. A decrease of 2, 3-DAN signal was observed and the current I_2 was measured. The percentage of decrease in the 2, 3-DAN signal due to the addition of Se(IV) ions can be expressed as

$$I\% = \frac{(I_1 - I_2)}{I_1}.100$$

2.3.3- Procedure for selenium determination by ICP-OES method

The selected analytical emission lines (nm) were automatically determined by the instrument as described elsewhere [38]. The calibration standards were prepared by diluting a 100 mg L^{-1} multi-elemental standard solution and a lanthanide standard solution in 0.5% nitric acid. The calibration range for all the 41 elements was evaluated from 0.005 to 5 mg L^{-1}. Calibration ranges were modified according to the expected concentration ranges of the elements of interest.

2.3.4- Preparation of real sample

a- Tap water

The tap water was collected from our laboratory. For the determination of Se(IV), water was acidified with nitric acid and analysed without any pre-treatment.

b- Pharmaceutical preparation

For the determination of Se(IV) by the proposed method in pharmaceutical preparation samples, two methods were used for preparation of samples.

a- One tablet equivalent to 75µg of Se was placed in 100 ml volumetric flask and dissolved in distilled water. The solution was filtered with paper filters and it adjusted to pH 1. 8 (*procedure a*).

b- One tablet equivalent to 75µg of Se was placed in 50 ml volumetric flask, 5 ml of nitric acid 65% and 2 ml of hydrogen peroxide were added. The mixture subjected to microwave for approximately 5 min in order to digest the sample. After digestion, for reduction all Se to Se(IV) the samples are treated with 6 mol/l of HCl 37% by heating for 5 min**.** The resultant solution was transferred to volumetric flask and diluted with distilled water (*procedure b)*.

c- The same treatment of digestion was used for ICP-OES analysis, but with the following microwave program: step 1, 10 min to reach 200 °C; step 2, 10 min at 200 °C; step 3, cooling down. After cooling to ambient temperature, the reactors were opened. The resultant solution was transferred to volumetric flask and diluted with distilled water until 50 ml.

2.3.5- Real sample analysis

The procedure of determination as described in paragraph 2.3.2. Because of complexity of matrix, the selenium content was always determined by the multiple standard addition method, each data point used was the average of at least five distinct measurements.

3. Results and discussion

The oxidation potential of aromatic diamine is important parameter for their oxidative polymerisation and this potential can easily be determined on the basis of the first cycle voltammetry scan. Fig 1a shows the first cycle detected during the oxidation of 16 mg/l 2, 3-DAN in acidic aqueous solution at carbon paste electrode. The 2, 3-DAN showed a well defined anodic peak at 0.7 V in agreement with the literature data [34]. The irreversible anodic peak was attributed to oxidation of the amino group to corresponding cation radical.

The electropolymerisation of diaminonaphtalene in acidic media yields non-conducting polymers as reported by different authors [36, 37]. This aspect will not be discussed in this work, because we will focuse our study on the first cycle of 2, 3-DAN. The effect of scan rate on the current of the monomer oxidation peak was studied. A plot of the logarithm of faradic current vs logarithm of rate was found to be linear with slope value equal to 0.5 over a wide range of scan rates, indicating that the process is under diffusion control.

Figure 1b shows a cyclic voltammogram obtained in acidic media containing 8 $mg.L^{-1}$ Se(IV). As shown in figure 1b no redox peak was observed, indicating that selenite ions cannot be detected directly at carbon paste electrode. In order to exploit the electro-oxidation of 2, 3-DAN for analytical purposes, and since our aim is to study the influence of selenite ions on the signal of 2,3-DAN, the differential pulse voltammetry techniques was chosen for further studies.

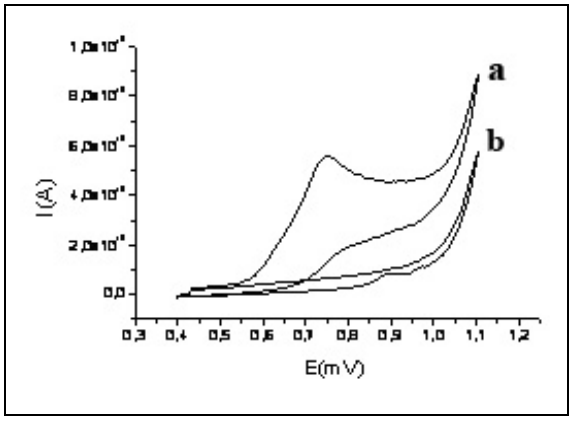

Figure 1: Cyclic voltammetry of 16 mg/L of 2, 3-DAN (a), 8 mg/L of Selenium (b); Scan rate 50mV/s

Figure 2a shows the differential pulse voltammogram for 16 mg/l 2,3-DAN recorded in acidic media. A well defined anodic peak (I_1) was observed at 0.66 V for 2,3-DAN. When selenite ions are added to the solution (using the procedure described in paragraph 2), they form an electro-inactive complex with 2, 3-DAN and a decrease of 2,3-DAN current (I_2) and a small shift in the potential about 15 mV was observed as shown in Fig 2b.

Incorporation of Se(IV) ions into the solution containing 2, 3-DAN was examined by recording a series of differential pulse anodic voltammogram obtained at a carbon paste electrode. Fig 2 shows the effect of different Se(IV) concentrations on peak current of 2,3-DAN. Increasing the selenite concentration resulted in a decrease of the 2,3-DAN current. The percentage decrease in 2, 3-DAN signal due to the addition of 5 mg/l of Se(IV) ions reached 65%. This result is in agreement with the results of several works which have been devoted to the study of the Se(IV) and 2, 3-DAN by fluorometry [15, 24]. Se(IV) ions react with 2, 3-DAN yielding the complex 4,5–benzopiazselenol which allows the determination of selenium by spectrophotometry.

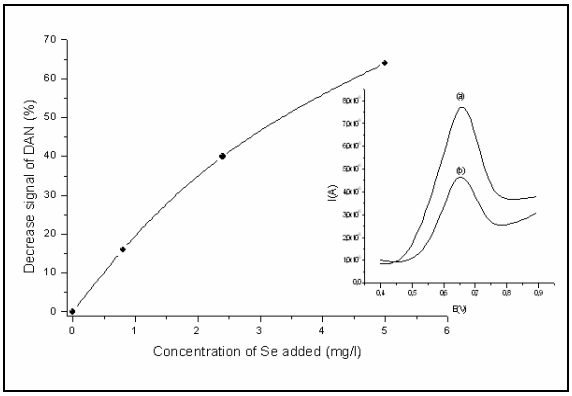

Figure 2: The percentage decrease in 2, 3-DAN signal as a function of the selenium concentration added using DPV method. Figure 2 show also response of Differential pulse voltammetry in absence (a) and in presence of 2.4 mg/L selenite ion (b), electrolyte 0.1 mol.L^{-1} sulfuric acid, DPV conditions : step=10 mV, amplitude pulsation= 50 mV.

The complex formation was used for analytical purposes; the parameters which most influence the measurements were optimised: these were the temperature of reaction, concentration of 2, 3-DAN, time of reaction and pH of solution.

The effect of the temperature on the formation of Se-2, 3-DAN complex was studied. It is reported that Se(IV) ions slowly reacts with 2,3-DAN at room temperature and heating stage is needed to complete reaction in a short time. Figure 3 shows that the rate of reaction increases with increasing the temperature. The percentage of decrease recorded at 20°C was 15%. This percentage reached a maximum value at 80°C (55%). A great influence of temperature on rate of formation of piazselenol was observed. Similar results were obtained by other authors. As described in literature, heating can accelerate the reaction between Se(IV) ions and 2, 3-DAN [24].

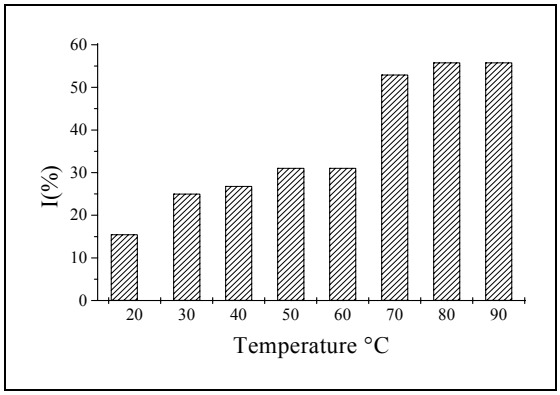

Figure 3: Effect of the temperature of the reaction on the formation of Se-2, 3-DAN complex, 2, 3-DAN 16 mg/L; Se 0.8 mg/L; 0.1mol.L^{-1} sulfuric acid, DPV conditions : step=10 mV, amplitude pulsation= 50 mV pH =1. 4; time of reaction 30 min

The influence of 2, 3-DAN concentration on the percentage of inhibition was also investigated at fixed concentration of Se(IV) ions (100 µg/l). The concentration of 2,3-DAN was varied between 3 to 250 µmol l^{-1}. Increasing the 2, 3-DAN concentration resulted in an increase in the 2, 3-DAN signal (I_1) showing a good correlation between concentrations and peak current. The linear regression equation is: I_P (µA) = 0.273 µA + 2.89 C (µmol/l), (r=0.997). The presence of Se(IV) ions at 100 µg/l greatly influences the percentage decrease of 2, 3-DAN due to the formation of the Se-2, 3-DAN complex. The results are shown in Table 1. A maximum degree of conversion of Se(IV) to Se-2, 3-DAN complex is reached from 50-fold 2, 3-DAN to Se molar ratio. The same results have been reported by other authors [24].

Table 1: Effect of the 2, 3-DAN concentrations of the formation of Se-2, 3-DAN complex

[2, 3-DAN] (µM)	3	7	12	60	120	250
Molar ratio	2	5	10	47	94	196
I (%)	23	30.34	41.61	52.82	56.28	50.34

Since our aim is to improve the limit of detection of Selenium, for a small concentration of Selenium, the same investigation was performed. Therefore, for the rest of the work, the concentration of 2, 3-DAN used was18 mg/L for the determination of Selenium between 10 to 100 µg/l and a concentration of 9 mg/L 2, 3-DAN was chosen for concentration of Se between 1 to 10 µg/l.

To determine the time required for the reaction to be completed, a 100 µg/l selenium(IV) was incubated with 18 mg/L 2, 3-DAN in an acidic medium for varying periods of time (2 -60 min). The results are reported in figure 4. The experimental results show that a maximum degree of conversion of Se(IV) to Se-2, 3-DAN complex is attained between 5 to 10 min. After 30 min the percentage decrease of 2, 3-DAN signal was unstable. This can be explained by the two consecutive reaction, the formation and the decomposition of the Se-2, 3-DAN complex as reported in the literature by several authors [40, 41], both favoured by temperature. Since the best results were obtained at 90°C for 5 min, therefore 5 min was chosen as the time of reaction.

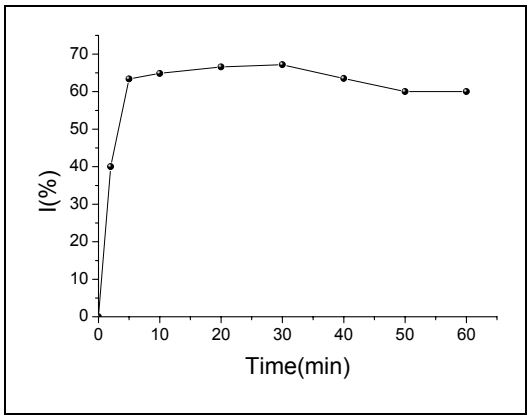

Figure 4: Effect of the time of reaction on the formation of Se-2, 3-DAN complex; 2, 3-DAN 18 mg/L; Se100 µg/l, electrolyte 0.1mol. L^{-1} sulphuric acid, DPV conditions: step=10 mV, amplitude pulsation= 50 mV pH =1.4 ; Temperature 90 °C

The effect of the solution pH on the Se-2, 3-DAN complex formation was investigated by measuring the decrease of peak current of 2, 3-DAN after addition of Se(IV) at different pH values varied between 0 to 2.8. Measurements were carried out at 90°C , time of reaction was 5 min. Maximum decrease of peak current was obtained at pH 1.8. These results are consistent with those reported previously for the determination of Se(IV) by fluorometry or micellar liquid chromatography [21-24].

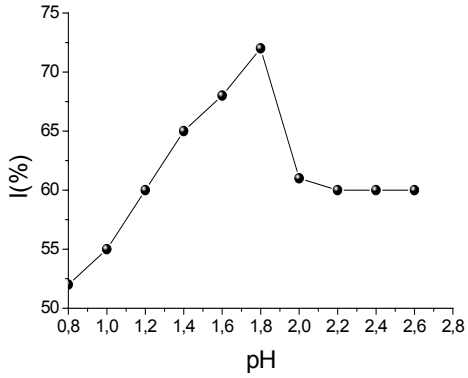

Figure 5: Effect of pH of reaction on the formation of Se-2, 3-DAN complex, 2, 3-DAN 18 mg/L; Se 100 µg/l, DPV conditions:, step=10 mV, amplitude pulsation = 50mV, incubation time 5 min ; Temperature 90 °C

Under the chosen optimised condition (temperature =90°C, pH=1.8, time for reaction =5 min), the variation of the percentage decrease in the 2, 3-DAN signal as a function of concentration of selenite ions added to the solution was studied. Two calibration curves were run using standard solutions of Se(IV), changing the concentration of 2, 3-DAN in order to cover a wide range of concentrations, from 10 to 100 µg/l (calibration 1: Concentration of 2, 3-DAN =18 mg/L) and from 1 to 10µg/l (calibration 2: Concentration of 2, 3-DAN = 9 mg/L).

We have chosen two ranges for calibration plot, because the molar ratio of 2, 3-DAN/Se influence the degree of conversion to the complex Se -2, 3-DAN. Table 2 shows the characteristics of both calibration graphs. The limit of detection (LOD) was calculated by the equation LOD =k. SD/b where SD and b are the estimated standard deviation and the slope of the analytical calibration function, respectively (k = 5).

Table 2: Calibration curve parameters

	Calibration 1	Calibration 2
Calibation range(µg/l)	10 – 100	1 – 10
Equation*	Y = -0.52 + 0.439 C	Y =0.914 + 3.48 C
r^2	0.998	0.998
RSD (n=5)	2.5% (at 10 µg/l of Se)	2.5%
Detection limit (µg/l)		0.7

*Y is the percentage decrease in 2, 3-DAN signal and C the concentration of selenite ions

3.4. Interférences

To assess the selectivity of this method, the same experiment was carried out in the presence of different metal ions: Zn^{2+}, Cu^{2+}, Cr^{2+}, Fe^{2+}, Mg^{2+} under the optimised conditions given above. According to the data of the manufacturer of pharmaceutical preparation, 200-fold quantities of Zn(II) and 100-fold quantities for other ions relative to the selenium content were studied (Table 3). It was found that theses ions have no significant effect on the selectivity and sensitivity of the analysis. From these results it can be concluded that it is not necessary to use the masking agent. Regarding the metal ion of iron(II), EDTA solution can be used as a masking agent.

Table 3: Interference of other metallic ions with the determination of 100 µg/l of selenium

Ion	Cu^{2+}	Fe^{2+}	Mg^{2+}	Zn^{2+}	Cr^{3+}
% of variation	-8.6	+18.2	-5.7	-12.9	-7.1

3.5 Analysis of real samples

The analytical performance of the proposed method was first assessed by determination of Se(IV) in tap water samples. Water was collected in the laboratory and analysed without any pre-treatment. The multiple standard addition method was employed and the measurements were done in triplicate. Average recovery values above 96% were obtained and show that the procedure can be applied for the determination of Se(IV) as shown in Table 4.

Table 4: Determination of Se(IV) in tap water

Sample N°	Se added (µg/l)	Se found (µg/l)	recovery (%)
1	10	9.15	92
2	20	19.3	96
3	30	30.75	102

The method was also applied to the determination of selenium in pharmaceutical products that are characterized by a complex matrix. For this study, electrochemical measurements were performed using the standard addition method. Digestion and reduction steps as well as adjustment of pH were carried out according to the procedure described in section 2.3. Table 5 summarises the results obtained according to the method used (DPV or ICP) and sample preparation.

The spiked samples without sample digestion gave low recovery (76%). This suggests that all the selenium ions are not labile and thus unavailable to form complex with 2, 3-DAN. Therefore, the samples were digested. Sample digestion and Se reduction were made in MW oven as described in experimental section. An acceptable recovery of 91% and good precision was obtained when the measurements were carried out using electrochemical method.

Table 5: Results for the determination of Se(IV) in a multivitamin tablets 17µg of selenium /g of pharmaceutical preparation.

	Se concentration in multivitamin tablet	Se (IV) found µg/g	Recovery% µg/g
procedure a (DPV)	17µg/g	13	76
procedure b (DPV)	17µg/g	15.5	91
procedure c ICP-OES	17µg/g	19.7	116

The pharmaceutical product were also analysed by ICP-OES after microwave digestion. The results obtained suited well with those obtained by the voltammetric method. The data in Table 5 shows that the results of Se(IV) determination in pharmaceutical products are in good agreement with the data declared by the manufacturer.

4. Conclusion

The above results demonstrate the suitability of a voltammetric procedure for the determination of trace Se(IV). The procedure has been optimised in depth by examining the influence of the 2, 3-DAN concentration, pH, temperature and time of incubation. It has been showed that under optimised conditions, the voltammetric determination of Se(IV) with 2, 3-DAN is very simple, rapid and easy for determination of low level of selenite in real sample. The digestion and incubation time are quite short compared with other techniques. This method could be applied to different kind of matrix. The results obtained by voltammetric techniques were validated by ICP-OES.

References

[1] A. D. Lemly, Ecotoxicology and Environmental Safety, 1997, 36, 275.

[2] EPA (U.S Environmental Protection Agency) Aquatic Life Water Quality Criteria for Selenium**,** EPA, 2004.

[3] J. E. Spallholz, L.M.Boylan, M.M.Rhaman, Sci. Total Environment, 2004, 323,21.

[4] S. B. Goldhaber, Regulatory toxicology and pharmacology, 2003, 38, 185.

[5] D. L. Watts, Journal of Orthomolecular Medicine, 1994, 9, 111.

[6] R.F. Burk, Selenium in Biology and Human Health. Springer- Verlag ,1994, 221

[7] J. Tan, W. Zhu, W.Wang, R.Li, S.Hou, D.Wang , L. Yang. Sci. Total Environment, 2002, 284,227.

[8] P. Reinhard, F. Schweinsberg , D. Wernet , I. Kötter, .Toxicology Lett., 1998**,** 96, 177.

[9] L. Coo , I. S.Martinez , Talanta, 2004, 64, 1317.

[10] V. Sladkov , A. Bolyos , F. David, Electroanalysis, 2002**,** 14, 128.

[11] L. Rahman , W. T. Corns , D. W. Bryce , P. B.Stockwell , Talanta, 2000, 52 ,833.

[12] N. Lewen , S. Mathew , M. Schenkenberger , T. Raglione , J. Pharm. Biomed. Anal., 2004**,** 35, 739.

[13] M. A. Akl , D. S. Ismael , A. A. El –Asmy , Microchem. J., 2006**,**83**,** 61.

[14] L. G. Gracia , M. D. Luque de Castro , Talanta, 1999, 50, 875.

[15] J. L.G. Ariza , J. A. Pozas , I. Giràldez , E. Morales , Talanta, 1999**,** 49, 285.

[16] D. B. Porcella , G. L. Bowie , J. G. Sanders , G. A. Cutter , J. Water Air Soil Pollution. 1991**,** 3, 57.

[17] A. D. Campbell , A. H. Yahaya , Anal. Chim. Acta,1980**,** 171, 119.

[18] K. N. Ramachandran , R. Kaveeswar , V. K.Gupta, Talanta,1993**,** 40,781.

[19] Y. Tamari , S. Ohmori , K. Hiraki , Clin. Chem. 1986**,** 32/8 , 1464.

[20] K. Johansson, X. Luo, A. Olin, Talanta, 1995**,** 42, 1979.

[21] A. U. Kulikov, J. Pharmaceutical and Biomedical Analysis. 2007, 43, 1283.

[22] K. N. Ramachandran , G. S. Kumar , Talanta.1996**,** 43, 1711.

[23] E. M. R. Rodrigues , M. S. Alaejos , C. D. Romero, , Anal.Chim. Acta., 1996, 334, 161.

[24] J. Pedro , F. Andrade , D. Magni , M. Tudino , A. Bonivardi , Anal.Chim. Acta. 2004**,** 516**,** 229.

[25] H. Shichi, J.C.Demar, Exp. Eye Res., 1990**,** 50, 513.

[26] C. M. A. Brett, Electroanal.,1999**,** 11,1013**.**

[27] F. A. Bertolino , A. A. J. Torriero , E. Salinas , R. Olsina , L. D. Martinez , J. Raba , Anal. Chim. Acta. 2006**,** 572, 32.

[28] T. Ferri , G. Favero , M. Frasconi , Microchem. J. 2007, 85, 22.

[29] C. F. Pereira , F. B. Gonzaga , A. M. G. Santos , J. R. Souzade , Talanta., 2006**,** 69, 877.

[30] A. I. Stoica, G. R. Babaua, E. E. Iorgulescu, D. Marinescu, G. E. Baiulescu, J. Pharma. Biomed. Anal. 2002**,** 30, 1425.

[31] C. Locatelli, Electroanalysis. 2004, 16, 1478.

[32] M. S. Won , J.H. Yoon , Y. B. Shim , Electroanal., 2005, 17, 1952.

[33] M. R. Nateghi, M. H. Mosslemin, H. Hadji mohammadi, Reactive., Functional Polymers. 2005**,**64, 103.

[34] L. Idrissi, A. Amine, M. El Rhazi, F. E. Cherkaoui , Anal. Lett., 2005, 38, 1943.

[35] S. Majid, M. El Rhazi, A. Amine, C. M. A. Brett, Anal Chim. Acta. 2002, 464, 123

[36] S. Majid, M. El Rhazi, A. Amine, A. Curulli, G. Palleschi, Microchim. Acta, 2003, 143, 195.

[37] I. Adraoui, M. El Rhazi, A. Amine, L. Idrissi, A. Curulli, G. Palleschi, Electroanalysis, 2005, 17, 685.

[38] P. C. Montesionos, A. de la guardia, C. Teutsch, M. L. Cervera, M. de la guardia, JAAS, 2004, 19, 696.

[39] P. F. Lott, P. Kukor, G. Moriber, J. Solga, Anal. Chem., 1963**,** 35, 1159.

[40] X. Huang, N.Jie, W. Zhang, Y. Sun, H. Shao, Fresenius J. Anal Chem.1996, 354, 195.

[41] E. M. Rodriguez, M. T. Sang, C. Diaz Romero, Talanta.,1994, 41, 2025.

Arabian J. Chem. Vol. 1, No. 3, 319-331(2008)

Modelization and Optimization by Experimental Designs Method of Production of Activated Carbon+

ELMERZOUKI, K.[1]; KHALIDI, A.*[1] and CHAAIR, H.[2], BEN EMBAREK, M.[3]

[1] Physical Chemistry and Electrochemistry laboratory, Mohammedia Faculty of Sciences and Technical, B.P 146 - Avenue Hassan II-20650 Mohammedia, Morocco.

elmer_khad@yahoo.fr; *khalidiabderrahim1@yahoo.fr

[2] Laboratory of Engineering of Process, Faculty of Sciences and Technical. Morocco.

[3] Central Laboratory of Analyses and Analytical Recherche

73/87, Bd Moulay Ismaïl – B.P.: 3103 – Roches Noires – 20300 – Casablanca (Morocco)

Abstract

The valorisation of waste from sawmills by the production of the activated carbon used for the treatment of the liquid discharges, was studied by applying a central composite design with the isovariance by rotation and the uniform precision. This study has allowed us to develop a mathematical model which describes the influence of the variables: the temperature of carbonization, acid concentration, acid quantity and the time of carbonization, as well as their interactions on the responses: the yield of mass of the activated carbon, the iodine index and the methylene blue index. The exploitation of this model in the space of variable has allowed us to define the optimum conditions (T = 380 °C, $[H_3PO_4]$ = 65 %, q = 2 ml/g and t = 1.25 h) to obtain an activated carbon with a yield of mass , methylene blue index and an iodine index as %R = 58%, I_{BM} = 486 mg/g, and I_d = 850 mg/g, respectively, which is approaching the standard imposed by AWWA (i.e, I_{BM} = 500 mg/g, I_d = 900 mg/g).

Keywords: activated carbon, modelization, optimization, experimental design.

1. Introduction

The activated carbon is a substance obtained after several operations such as pyrolysis and activation to make it more porous. Its vast porosity gives it a specific surface area ranging from 500 to 2000 m^2/g [1,2], which contributes to its great power as an adsorbent. The activated carbon is generally used as a powder or granulated.

This work concerns with the valorisation to the waste from sawrnills, which is considered very abundant, in order to prepare from this waste activated carbon which is used largely in liquid discharges treatment. We have used several techniques for the characterization of activated carbon prepared from Sawdust. Its porous texture and the chemical nature of its surface were analyzed by means of adsorption of methylene blue and iodine. Because of its great capacity of adsorption, it will be applied in the field of water treatment to reduce the concentration of various existing pollutants in wastewater [3], as well as an agent of treatment for the air pollutants .

2. Materials and methods

The chemical activation of the whitewood is made by phosphoric acid. To a 1 g of the sawdust of the whitewood, whose particles with an average size of 1mm, we added the desired volume (2-4ml) phosphoric acid having a purity of (65-85%). This mixture is treated thermally with the required temperature (300-700°C) in a muffle furnace for about (0.5-2.5h).

To eliminate the excess of phosphoric acid, the carbon obtained is washed with large amount of distilled water using Buchner then soxhlet. After this, it's dried for about 24 hours in a steam room at 120°C. The method used for the determination of the iodine index and the methylene blue index, is same as the one used by the National Office of Potable Water (ONEP), based on the standard AWWA [4].

Description of the methodology

Experimental design is frequently performed in agriculture, biology and chemistry [5] to study the empirical relationships between one or more measured responses and a number of variables. In this part we discuss the principles governing the construction and the analysis of a central composite design in which responses (ŷ) are the iodine index (I_d), methylene blue index (I_{BM}), and yield of the mass of activated carbon (% R) and the variables x_j are: the temperature, acid concentration, acid quantity and duration of carbonization, hereafter called x_1, x_2, x_3 and x_4, respectively . This study was carried out using JMP software [6].

Table 1 shows the central composite design with the isovariance by rotation and the uniform precision presented according to the standard order; the values of the coded variables X_j are dimensional. The values of the natural variables are summarized in Table 2. The graphical representation of the distribution of these experimental points is given in Figure 1. The 31 experiments are run according to the orthogonal design which means that the coefficients do not change when any model parameter changes and are also run according to the following .

(i) The first 16 experiments belong to a 2^4 factorial experiments carried out at the corners of the cube; the ± 1 coded values X_j were obtained using the equation:

$$X_j = \frac{x_j - x_{jo}}{\Delta x_j} \qquad (1)$$

Where, X_j: the dimension value of an independent variable,

x_j: the real value of an independent variable,

x_{j0}: the value of x_j at the centre point,

Δx_j: the step of variation.

(ii) The next 2 x 4 experiments are the points on the axes, at a distance ± α from the centre. This distance α was calculated to have vectors of square variables X_j^2 that are rota table and in the present design, α equals to:

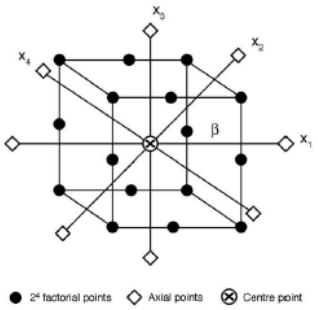

Figure 1: A central composite rotatable design for four factors x_1, x_2, x_3 and x_4.

Table 1. The central composite design presented according to the standard order.

Logical order	Random order	Coded variables values			
		X_1	X_2	X_3	X_4
1	30	-1	-1	-1	-1
2	22	-1	-1	-1	1
3	21	-1	-1	1	-1
4	26	-1	-1	1	1
5	1	-1	1	-1	-1
6	5	-1	1	-1	1
7	29	-1	1	1	-1
8	4	-1	1	1	1
9	27	1	-1	-1	-1
10	25	1	-1	-1	1
11	20	1	-1	1	-1
12	13	1	-1	1	1
13	10	1	1	-1	-1
14	8	1	1	-1	1
15	18	1	1	1	-1
16	23	1	1	1	1
17	24	-2	0	0	0
18	31	2	0	0	0
19	12	0	-2	0	0
20	3	0	2	0	0
21	6	0	0	-2	0
22	28	0	0	2	0
23	15	0	0	0	-2
24	19	0	0	0	2
25	7	0	0	0	0
26	11	0	0	0	0
27	16	0	0	0	0
28	17	0	0	0	0
29	9	0	0	0	0
30	14	0	0	0	0
31	2	0	0	0	0

Table 2. Natural and coded variables.

Natural variables (x_j)	*Coded variables X_1, X_2, X_3, X_4*				
	-2	-1	0	+1	+2
x_1 = T(°C)	*300*	*400*	*500*	*600*	*700*
x_2 = [H_3PO_4] (%)	*65*	*70*	*75*	*80*	*85*
x_3 = q (ml/g)	*2*	*2.5*	*3*	*3.5*	*4*
x_4 = t (h)	*0.5*	*1*	*1.5*	*2*	*2.5*

$$\alpha = \pm\left(\frac{x_{j\max} - x_{j0}}{\Delta x_j}\right) = \pm 2 \qquad (2)$$

(iii) In this center the seven last experiments were realized to estimate reproduct ibility of the obtainedresults [7,8, 9].

3. Results

The analyses results are regrouped in Table 3. Starting from these 31 experiments, we established the relationship between the experimental responses and the four variables [10,11]. This relationship is represented in the equation as the following:

$$\hat{y} = b_0 + \sum_{j=1}^{4} b_j X_j + \sum_{j=1}^{4} \sum_{j'=1}^{4} b_{jj'} X_j X_{j'} + \sum_{j=1}^{4} b_{jj} X_j^2 \qquad (3)$$

The 31 values of X_j^2 have a sum value different from zero, and a mean of 0.77; therefore the variable X_j^2 was replaced by the centred variable $U_j^2 = X_j^2 - 0.77$. Consequently, the estimated model was:

$$\hat{y} = b_0 + \sum_{j=1}^{4} b_j X_j + \sum_{j=1}^{4} \sum_{j'=1}^{4} b_{jj'} X_j X_{j'} + \sum_{j=1}^{4} b_{jj} U_j^2 \qquad (4)$$

where, $\hat{y}$: theoretical response function;

X_j: coded variables of the system;

b_0, b_j, $b_{jj'}$ and, b_{jj} : real model coefficients.

Let $b_u X_u$ be the general term of $\hat{y}$; the 15 generally terms used for the construction of the model must be mutually

orthogonal 2 by 2. And the normal equation gives the b_u coefficients using the least squares method:

$$b_u = \frac{Y_u}{\sum_{i=1}^{n} X_{iu}^2} \quad (5) \text{ where } \quad Y_u = \sum X_{iu}\ y_i$$

X_{iu} and y_i being the X_u and y values for the i^{th} experiment; Y_u is named contrast.

The 15 terms are easily calculated by substituting data values in the expressions for the least squares estimates of the coefficients (Table 4, 5, 6). The models adapted to the responses are written as follows:

- Yield of the mass (% R):

$\hat{y}_{\%R} = 45.407143 - 8.748333\ X_1 ..... - 1.9875\ X_4$ (6)

$- 2.79375\ X_2 X_1 ..... - 0.26875 X_4 X_3$

$-3.97472\ X_1^2 ..... - 0.283452\ X_4^2$

"Table 3. The experimental data for iodine index, methylene bleu index and yield of activated carbon mass remaining in solution according to centred composite plan".

Logical order	Response Id	Response I_{BM}	Response %R
1	539,6	483,5	49,5
2	558,4	480,97	42,4
3	271,5	484,19	44,6
4	257	480,97	49,6
5	381	499,14	65
6	387,8	494,62	56,8
7	265,8	489,5	49
8	436	492,91	41,6
9	539,6	499,65	41
10	431,2	493,34	38
11	460,1	480,54	39
12	454,25	490,78	31,6
13	385,6	491,63	36,8
14	321,99	489,93	34,8
15	431,21	481,82	37,2
16	429,58	480,97	23,4
17	417,23	489,5	51,6
18	430,87	500,06	4,47
19	433,52	486,51	45
20	408,45	490,35	44
21	443,52	479,26	51,5
22	330,44	474,57	39,8
23	270,68	494,05	44
24	327,33	491,63	41,6
25	377,2	486,93	45,77
26	382,1	487,37	45,62
27	380,2	487,79	45,46
28	383,99	488,5	45,2
29	382,1	488,22	45,1
30	377,9	487,5	45,3
31	382,1	488,65	45,4

- Iodine Index I_d (mg/g):

$\hat{y}_{Id}$ = 380. 79857 + 15. 987917 X_1 … + 4. 79625 X_4 (7)
-10. 05437 X_2X_1…. + 18.414375 X_4X_3
+ 15. 256086 X_1^2 ..... - 16. 00516 X_4^2

– Methylene blue index I_{BM} (mg/g):

$\hat{y}_{IBM}$ = 487. 85143 + 0. 9991667 X_1 … - 0.43X_4 (8)
– 4. 15625 $X_2 X_1$…+ 1. 54 $X_4 X_3$
+ 1. 7592262 X_1^2. + 1. 2742262 X_4^2

Table 4. Estimation of the coefficients associated with the model for I_d.

Coefficient (b_u)	Estimation	Least of Squares	F_{exp}	*P*
b_0	*380.79857*	-	-	*<.0001*
b_1	*15.987917*	*6134.724*	*4.6170*	*0.0473*
b_2	*-21.78375*	*11388.762*	*8.5713*	*0.0099*
b_3	*-31.91292*	*24442.422*	*18.3955*	*0.0006*
b_4	*4.79625*	*552.096*	*0.4155*	*0.5283*
b_{21}	*-10.05437*	*1617.447*	*1.2173*	*0.2862*
b_{31}	*45.828125*	*33603.473*	*25.2902*	*0.0001*
b_{32}	*44.50937*	*31697.351*	*23.8557*	*0.0002*
b_{41}	*-22.54937*	*8135.589*	*6.1229*	*0.0249*
b_{42}	*13.856875*	*3072.208*	*2.3122*	*0.1479*
b_{43}	*18.414375*	*5425.427*	*4.0832*	*0.0604*
b_{11}	*15.256086*	*6655.607*	*5.0091*	*0.5283*
b_{22}	*14.489836*	*6003.830*	*4.5185*	*0.0494*
b_{33}	*5.9885863*	*1025.534*	*0.7718*	*0.3927*
b_{44}	*-16.00516*	*7325.237*	*5.5130*	*0.0321*

Table 5. Estimation of the coefficients associated with the model for I_{BM}".

Coefficient (b_u)	Estimation	sum of Squares	F_{exp}	*P*
b_0	*487.85143*	-	-	*<.0001*
b_1	*0.9991667*	*23.96002*	*2.9983*	*0.1026*
b_2	*1.4275*	*48.90615*	*6.1200*	*0.0250*
b_3	*-2.52*	*152.40960*	*19.0721*	*0.0005*
b_4	*-0.43*	*4.43760*	*0.5553*	*0.4670*
b_{21}	*-4,15625*	*276.39062*	*34.5867*	*<.0001*
b_{31}	*-1.86125*	*55.42803*	*6.9361*	*0.0181*
b_{32}	*-0.57125*	*5.22123*	*0.6534*	*0.4308*
b_{41}	*0.515*	*4.24360*	*0.5310*	*0.4767*
b_{42}	*-0.115*	*0.21160*	*0.0265*	*0.8728*
b_{43}	*1.54*	*37.94560*	*4.7484*	*0.0446*
b_{11}	*1.7592262*	*88.50031*	*11.0747*	*0.0043*
b_{22}	*0.1717262*	*0.84329*	*0.1055*	*0.7495*
b_{33}	*-2.707024*	*209.54899*	*26.2223*	*0.0001*
b_{44}	*1.2742262*	*46.42955*	*5.8101*	*0.0283*

Table 6. Estimation of the coefficients associated with the model for %R.

Coefficient (b_u)	Estimation	sum of Squares	F_{exp}	*P*
b_0	*45.407143*	-	-	*<.0001*
b_1	*-8.79*	*1836.8001*	*97.2442*	*<.0001*
b_2	*0.2875*	*2.6004*	*0.1377*	*0.7503*
b_3	*-2.9875*	*208.2704*	*11.0263*	*0.0039*
b_4	*-2.029167*	*94.8037*	*5.0191*	*0.0363*
b_{21}	*-2 .73125*	*124.8806*	*6.6115*	*0.0232*
b_{31}	*0.59375*	*4.5156*	*0.2391*	*0.5927*
b_{32}	*-2.25625*	*86.0256*	*4.5544*	*0.0545*
b_{41}	*-0.53125*	*5.6406*	*0.2988*	*0.6319*
b_{42}	*-1.18125*	*24.7506*	*1.3104*	*0.2936*
b_{43}	*-0.20625*	*1.1556*	*0.0612*	*0.8520*
b_{11}	*-3.964286*	*451.7630*	*23.9173*	*0.0002*
b_{22}	*0.1519643*	*0.5729*	*0.0303*	*0.8542*
b_{33}	*0.4394643*	*5.2640*	*0.2787*	*0.5965*
b_{44}	*-0.273036*	*2.2975*	*0.1216*	*0.7415*

4. Discussion

Variance analysis

Analysis of variance allows us to see whether the variables for modelling have as a whole, a significant effect on the response. The results of the analysis of variance (Table 7,8,9) shows that the experimental values of Scnedecor is largely higher than the critical value, [$F_{0.001}$ (14. 16) = 5.41], of the F distribution [12], at a 99.9 % level of confidence with 14 and 16 degrees of freedom. The regression is thus very significant.

Modelization

The significance of effects may be estimated by comparing the values of the ratio b_u^2/s_{bu}^2 to a critical value [$F_{0.01}(1,16)$ = 8,41] of the F distribution [12] at a 99 % level of confidence with 1 and 16 degrees of freedom. For the three responses, it appears that all the coefficients as their interactions have a significant effect on the response except for the interactions X_4, X_2X_1, X_3X_4, X_4X_2 and X_3X_3 which is not significant for the response (I_d), the interactions X_1, X_4, X_3X_2, X_4X_1, X_4X_2 and X_2X_2 which are not significant for the response (I_{BM}) and the interactions X_2, X_1X_3, X_4X_1 , X_4X_2, X_4X_3, X_2X_2, X_3X_3, X_4X_4 which is not significant for the response (%R). Consequently the models associated with all the responses are written as the following:

a) For iodine index I_d (mg/g):

$$\hat{y}_{Id} = 380.79857 + 15.987917\,X_1 - 21.78375\,X_2 - 31.91292\,X_3 \quad (9)$$

$$+ 45.828125\,X_3X_1 + 44.509375\,X_3X_2 - 22.54937\,X_4X_1$$

$$+15.256086X_4^2 + 14.489836\,X_2^2 - 16.00516\,X_4^2$$

b) For methylene blue index I_{BM} (mg/g):

$\hat{y}_{IBM} = 487.85143 + 1.4275\ X_2 - 2.52\ X_3 - 4.15625\ X_2\ X_1$ (10)

$- 1.86125\ X_3\ X_1 + 1.54\ X_4\ X_3 + 1.7592262\ X_1^2 - 2.707024\ X_3^2$

(± 0.7) (± 0.7) (± 0.53) (0.53)

$+ 1.2742262\ X_4^2$

(± 0.53)

c) For yield of the mass (% R):

$\hat{y}_{\%R} = 45.407143 - 8.79\ X_1 - 2.9875\ X_3 - 2.029167\ X_4$ (11)

(± 1.64) (± 0.89) (± 0.89) (± 0.89)

$- 2.73125\ X_2\ X_1 - 2.25625\ X_3\ X_2 - 3.964286\ X_1^2$

(± 1.08) (±1.08) (0.81)

Table 7. Regression analysis for I_d.

Source	Model	Residual	Total
Degree of freedom	14	16	30
Sum of squares	148576.41	21259.42	169835.84
Average square	10612.6	1328.7	
F_{exp}	*7.9871*	-	-
P	*<.0001*	-	-

Table 8. Regression analysis for I_{BM}.

Source	Model	Residual	Total
Degree of freedom	14	16	30
Sum of squares	994.9455	127.8599	1122.8054
Average square	71.0675	7.9912	
F_{exp}	8.8932	-	-
P	<.0001	-	-

Table 9. Regression analysis for %R.

Source	Model	Residual	Total
Degree of freedom	14	16	30
Sum of squares	2881.2144	302.8640	3184.0784
Average square	205.801	18.929	
F_{exp}	10.8723	-	-
P	<.0001	-	-

The values between brackets and below each coefficient of the models represent the standard deviation. S_{bu} determined starting from the estimated variance of the S_{bu}^2 coefficients obtained by applying the following formula:

$$S_{bu}^2 = s_r^2/\sum X_{iu}^2 \qquad (12)$$

Where s_r^2 is the estimated variance of the experimental errors obtained by dividing the residual sum of squares $\sum e_i^2$ by ν (number of degrees of freedom = number of experiments minus number in the model, i.e. 30 - 14 = 16) (Table 4,5,6) :

sr^2_{Id} = 147079.7/16 = 9192. 48 (Table 4)

sr^2IB_M = 954. 47/16 = 59. 65 (Table 5)

$sr^2_{\%R}$ = 2842. 11/16 = 177. 63 (Table 6)

Validity of the models

The experimenters usually need to have a reliable tool to make decisions, the statistics is required, particularly, statistical tests to formulate a probability. In other words a degree of confidence with regard to a formulated hypothesis. We report the value of residues according to estimated responses as illustrated in Figure 2. It can be seen from the obtained results that there is an increase of residues according to y. This results confirms that the model of regression explaining well the experimental result. Therefore, this model can be used for optimization [10, 13].

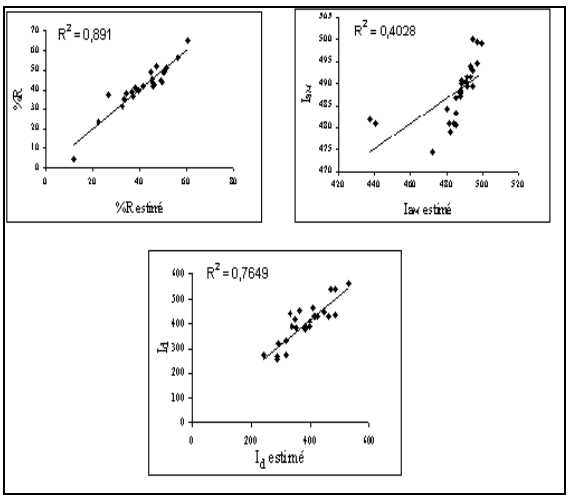

Figure 2: Graphs of adequacy of applied model for %R, I_{BM} and I_d

Optimization

The determination of optimal conditions for the production of activated carbon, in accordance with the standa rds of AWWA [4] imposed for the activated carbon to be used for water treatment with the following values, the iodine index is higher than 900 mg/g, the methylene blue index is also higher than 180 mg/g and the specific surface area of more than 1000 m^2/g.

These conditions can be determined easily by graphical analysis. The surfaces of responses are graphic in three dimensions (Figure 3). The horizontal design of the figure represents the domain of variation of the two factors; the vertical axis represents the variation of the response. Beyond the two factors, it is necessary to maintain to a constant levels factors for which variations are not described in the horizontal design.

The geometric representation of the response % R (Figure 4) in the graph of T and t, for the values of $[H_3PO_4]$ = 65% (X2 = -2) and q = 2 ml/g (X3 = -2), shows that when the T increases and the t remains unchanged or converse the yield increases but for the first case the yield rises to the level of 45% where it starts to decreases, and when the t and T simultaneously increase the yield increases to an optimum after which it remains unchangeable in the experimental domain, this optimum equals to a 45%.

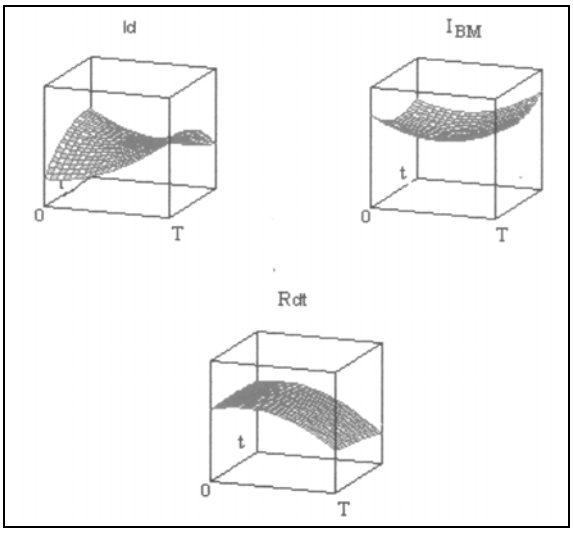

Figure 3: surfaces of responses of iodine index, methylene blue index and a yield ($[H_3PO_4]$ of 65% and quantity of acid = 2 ml/g).

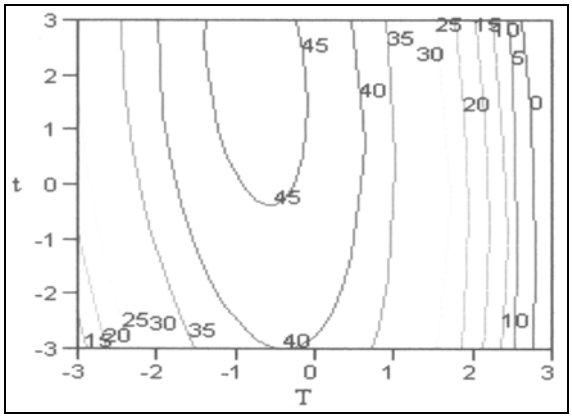

Figure 4: curve of iso-responses of yield ([H_3PO_4] =65% and quantity of acid = 2ml/g).

The geometric representation of the response I_{BM} (Figure 5), in the same graph, shows that when the T and t increase simultaneously, or when T increases and t remains unchanged, the I_{BM} increases. From the geometric representation of the response I_d (Figure 6), always in the same graph, we see that when the t increases and T remains unchanged or when T and t increase simultaneously the I_d decreases. But when the T increases and t remains unchanged simultaneously, the I_d decreases to a level from which it increases.

Subtraction of the after two representation (Figure 4 and 6) shows limits of the set of values operating parameters for the preparation of activated carbon in which the value of iodine index approaching the standard AWWA [4] and with the maximum yield. The results are reported in Table 10.

Table 10. Optimal domain of parameters for the activated carbon preparation

Variables	Experimental domain (%R)	***Experimental domain (I_d)***
T (°C)	*[340, 480]*	*[300, 380]*
[H_3PO_4](%)	*65*	*65*
q (ml/g)	*2*	*2*
t (h)	*[1.25 , 2.5]*	*[0.875 , 1.5]*

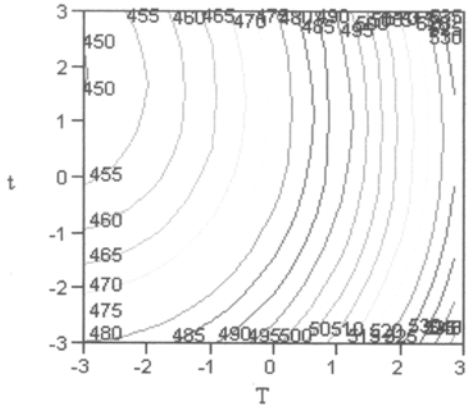

Figure 5: Curve of iso-responses of methylene blue index ([H_3PO_4] =65% and quantity of acid = 2 ml/g).

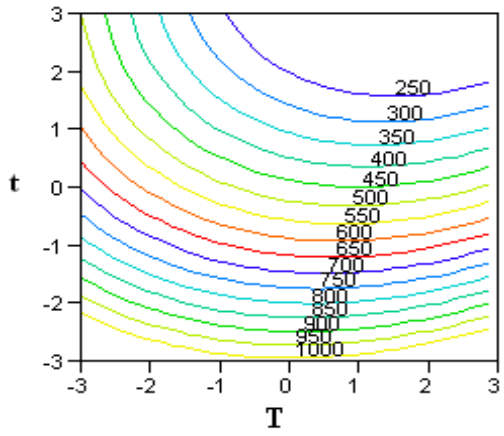

Figure 6: Curve iso- responses of iodine index ([H_3PO_4] =65% and quantity of acid = 2ml/g).

These results show that for the T and t factors, a range of experimental values can be defined. However, we can not afford such factors any value even if they are inside the range defined. In order to limit the domain of intersection of T and t factors corresponding to the two best responses % R and I_d, we have superimposed the two curves iso-responses of these two responses. The results are compiled in Table 11.

However, according to Figure 5, there was interest to working with a high temperature and a short time to obtain a high value of methylene blue index I_{BM}. Indeed, we see in Figure 4. I_{BM} increases when T increases and the t decreases. Therefore, the T will be set at 380 ° C (X1 = -1.2) and t will be set at 1h 15min (X4 = -0.5). In these conditions, the values of the responses (%R, I_{BM}, I_d) estimated for the preparation of activated carbon from the sawdust is collected in Table 13.

Table 11. Optimal domain of parameters of activated carbon preparation

Variables	***domain***
T (°C)	*[340; 380]*
[H_3PO_4](%)	*65*
q (ml/g)	*2*
t (h)	*[1,25 ; 1,5]*

Table 13. Estimated responses of activated carbon preparation at optimal conditions

Estimated responses	*Results*
%R	*45*
I_{BM} *(mg/g)*	*486*
I_d *(mg/g)*	*850*

5. Conclusion

By application of the methodology of experiences plan for modelization and optimization the fabrication of activated carbon, prepared from the wood saw, it was possible to construct a centred composite plan with a minimum number of experiments (31 instead of 625). The realization of this design of experiments has led to develop mathematical models that describe the variation in responses studied (I_d, I_{BM}, %R), depending on various factors of production (T, $[H_3PO_4]$, q, t) taking in account their interactions.

Graphic representations of these models in the space of variables led us to obtain iso-responses curves. Exploitation such have curves allowed us to define the optimal conditions for production of activated carbon with a value iodine index close to 900 mg/g and a value of methylene blue index above 180 mg/g. These operating conditions are: T = 380 ° C, $[H_3PO_4]$ = 65%, q = 2 ml / g and t = 1h15 min.

This study has enabled us to prepare activated carbon iodine index equal to 850 mg / g, methylene blue index equal to 486mg/g and yield equal to 58%.

References

[1] Diaz-Teran, J.; Nevskaia, D.M.; Lopez-Peinado, A.J.; Jerez, A., Eng. Asp., 2001, 187 (188), 167-175.

[2] Diaz-Teran, J.; Nevskaia, D.M.; Fierro, J.L.G.; Lopez-Peinado, A.J.; Jerez, A., Microporous and Mesoporous Materials, 2003, 60, 173-181.

[3] Yang, X.Y. ; Al-Duri, B., The Chem. Eng. J., 2001, 83(1), 15-23.

[4] AWWA standard of powder activated carbon (AWWA B600-90) 1991.

[5] Bchitou, R.; Hamad, M.; Heughbaert, J. C.; Foutlane, R., Vecteur Environ., 2003, 36 (1), 79-82.

[6] JMP Version 3.2 Introduction guide. User's guide and Statistic and Graphics Guide, SAS Institut, USA.1995

[7] Bassiname, A. ; Porte, C. ; Delacroix, A., Analysis ; 1997 ; 25, 168.

[8] Goupy, J. ; Murray, M., Rev. Info. 1991, 37 (1), 5-22.

[9] Myers, R.H.; Khuri, A.I.; Carter, W.H., Techn-ometrics 1988, 31 (2), 137-157.

[10] Box, G.E.P.; Hunter, J.S., Ann. Math. Statist. 1957, 28, 157-241.

[11] Box, G.E.P.; Draper, N.R., Empirical model-building and response surfaces; Wiley: New York, 1987, pp 521-565.

[12] Statistics for experimenters: An introduction to design, data analysis, and model building; Box, G.E.P.; Hunter, J.S., Ed.; John Wiley and sons: New York, 1978.

[13] Goupy, J., Plans d'expériences pour surfaces de réponse ; Dunod : Paris, 1999.

Arabian J. Chem. Vol. 1, No. 3,333-336 (2008)

Biological Activity of Alcoholic Extract of Jordanian Propolis

Nawal Hassan Al Bahtiti

Chemistry Department, Faculty of Science, Applied Science Private University,

Amman 1193, Jordan

Abstract

A bee glue which is called a propolis has been used in folk medicine since ancient times, due to its many biological properties. In this work, Alcoholic extracts of Jordanian propolis were tested for bactericidal activity against five different microorganisms. Alcoholic extracts enhanced the bactericidal activity against *Staphylococcus aurous ATCC 2592, Bacillus. Lichenformis NCIB1097* and *Streptococcus subtitles NCTC3610* while a limited activity against *Peseudom aeruginosa ATCC27853 and Staphylococcus. Epidermidis ATCC 1228* was observed.. Alcoholic extracts seem to be efficient due to their different chemical compositions. It was shown that Jordanian propolis had the same effect as Turkish propolis that collected from Anatolia.

Keywords: Propolis; biological activity, bactericidal, Alcoholic extract.

1. Introduction

Propolis or bee glue is a resinous hive product collected by honey bees from leaf and cracks in the bark of various plant sources [1]. Propels displays strong antimicrobial activity and has been used as chemotherapeutic agent since ancient times [2]. It was also used recently as antibacterial, antiviral, fungicidal, local anesthetic and anti-inflammatory [3]. It has shown that the chemical composition of propolis seems to vary with its vegetal source. The alcoholic extract of the resin is called propolis wax, while the aqueous extract is called propolis balsam.

Alcoholic extracts of propolis indicate anti-inflammatory and antibiotic activities both *in vitro* and *in vivo* [4]. Aqueous extract has a protective effect on hepatocytes [5], the exact mechanism for this effect is not clear. This activity may be partially due to the presence of flavonoids in propels [6]. For all these reasons, we decided to study the Jordanian propels extracts obtained by ethanol extraction, try to identify the composition by high performance liquid chromatography (HPLC) and test their biological activity [7].

2. Experimental

Materials and Methods

The propolis sample was from the neighboring honeybees nest in Nauor region. One hundred milligrams of propolis were cut to small pieces and extracted with 5 ml of ethanol at room temperature. After 24 hours, the extracts were filtered with a 0.45 µm filter prior to injection of a 10 µl solution into the HPLC system (GRD-10-0062) with a UV-visible photodiode array (PDA) detector.

For the analysis of the sample, a Cap cell Pak UG 120 C 18 column was used. The mobile phase consisted of water with 2% acetic acid (A) and acetonitrile with 2% acetic acid (B). The gradient was 20-80% B in 60 min at a flow rate of 0.20 ml/min. UV spectra were recorded at 280 nm at a rate of 0.8 S^{-1} spectrum and a resolution of 4.0 nm .The microorganisms used in this study for the

determination of antimicrobial activity were: *S. aurous* ATCC25923, *B. licheniformis* NCIB1097, *S. subtilis* NCTC3610, *P. aeruginosa* ATCC27853 and *S. epidermidis* ATCC 1228.

The samples were tested for their antimicrobial testing *in vitro* by the agar dilution technique. All compounds were dissolved in dimethy sulphoxide solvent (DMSO) for the antibacterial test and the solutions were sterilized by membrane filtration. Aliquots of compounds were diluted with melted typtic Soya agar, tryptone, soytone, sodium chloride and agar to give concentrations of 2000, 1500, 1000, 500, 250, 125, 62.5 and 31.3 µg/ml. The minimum inhibitory concentration (MIC) values were noted after 24 h. at 37ºC. as shown in Table 1.

3. Results and Discussion

Composition analysis was performed using HPLC with UV-VIS detection, whereby compounds in the propolis samples were identified by comparing their retention times and UV spectra with those of standard compounds. Figure (1) presents the structures of the investigated compounds, while Table 2 lists the compound contents in the alcoholic extract of propolis sample, and the retention times.

Results of analysis showed the contents vary from 0.79 to 19.07 mg/g. All products showed antimicrobial activity against the three Gram-positive bacterial species tested,. Our results indicate that the quality of commercially available propels products requires verification. The main compounds of propolis samples were, (A) 2,2-Dimethyl-8-prenylchromene; (B) 4-hydroxy-3,5-diprenyl cinnamic acid (artepillin C); (C) 3-prenyl cinnamic acid allyl ester; (D) kaempferide; (E) propolis benzofuran A, (F) Farnesol a sesquiterpenoid., Figure (1). Although propolis samples were collected at Jordan but they are similar to samples collected from different regions of Anatolia (Turkey) all showed significant antimicrobial activity against the Gram positive bacteria and yeasts.

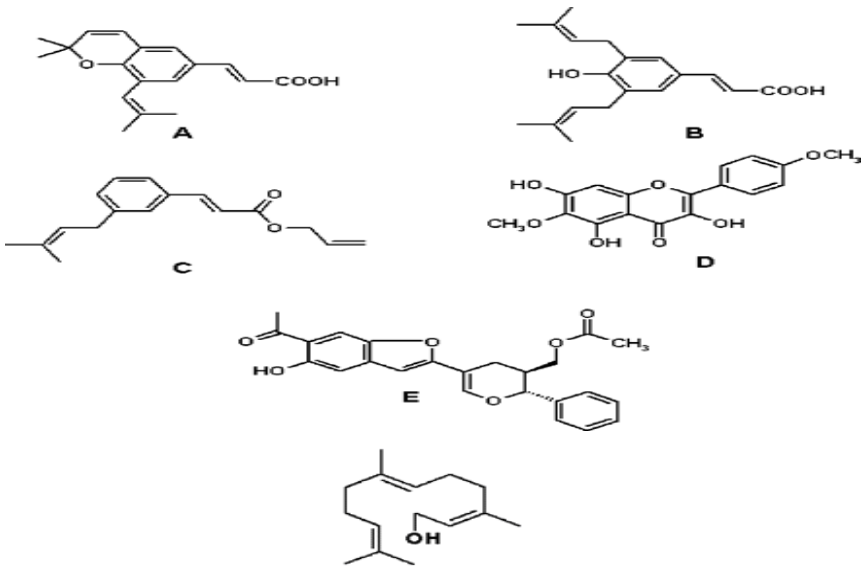

Fig. 1. Structures of compounds isolated from green propolis. (A) 2,2-Dimethyl-8-prenylchromene; (B) 4-hydroxy-3,5-diprenyl cinnamic acid (artepillin C); (C) 3-prenyl cinnamic acid allyl ester; (D) kaempferide; (E) propolis benzofuran A, (F) Farnesol a sesquiterpenoid.

Table1. Minimum inhibitory concentration (MIC) of alcoholic extract of propolis (µg/ml)

Microorganism	µg/ml
Gram positive bacteria	
S. aureus ATCC25923	12.5
B. licheniformic NCIB1097	62.5
S. subtilis NCTC3610.	12.5
Gram negative bacteria	
P. aeruginosa ATCC27853	250
S. epidermidis ATCC 1228	500

Table 2. composition of the alcoholic extract of propels samples (mg g^{-1} of dried extract).

Compounds	concentration mg/g	Retention time (min)
(A) 2,2-dimethyl-8-prenylchromene	1.23	12.5
(B) 4-hydroxy-3,5-diprenyl cinnamic acid (artepillin C)	2.34	7.0
(C) 3-prenyl cinnamic acid allyl ester	0.79	6.0
(D) kaempferide;	19.07	19.0
(E) propolis benzofuran	2.39	7.5
(F) A sesquiterpenoid	12.60	17.0

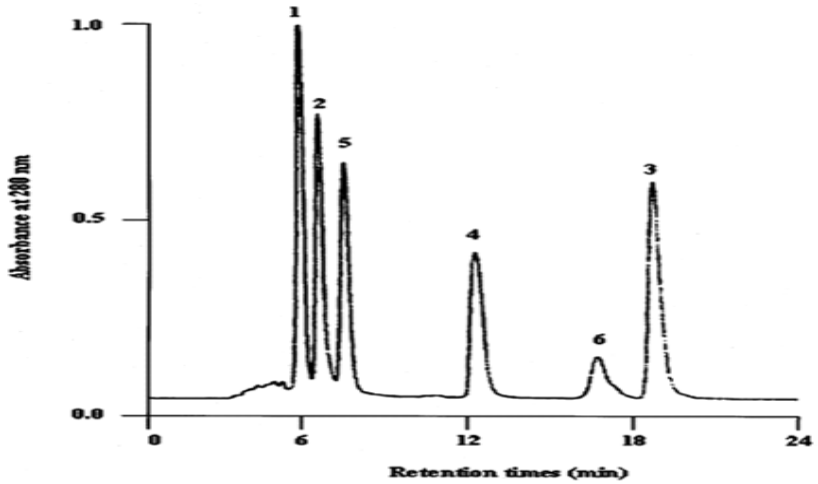

Figure 2. HPLC chromatogram of separation alcoholic extract compounds. The peaks are: 1=C, 2=B, 3= D, 4=A, 5= E, 6 =F. The conditions were:, A cap Cell Pak UG 120C 18 column. Solvent was water with2%acetic acid (A) and acetonitrile with 2% acetic acid (B), a flow rate of 0.20 ml/min.UV spectra 280 nm.

4. Conclusion

Six main compounds were isolated in propolis samples. Jordanian propolis samples showed significant antimicrobial activity against the Gram positive bacteria . Therefore, propolis can prevent dental caries since it demonstrated significant antimicrobial activity against the microorganisms such as *Streptococcus aureus*, and *Streptococcus subtilis* which involves in oral diseases. A further analysis is required to study aqueous and alcoholic extracts.

Acknowledgement:

The author acknowledges Mr Mazin Gannam at pharma International company for HPLC analysis.

References

[1]Hgashi ,KO., International J. Pharma., 1994, 43(2):1.

[2] Kilena, V., Journal of Insect Science, 2001, 1(1)57.

[3] Shigenori, K.,. Chemi pharma Bull.2003, 51(16):740.

[4] Erica W. and Ginseppina N., Evid. Based Complement Alternative Med.,1998, 2 (1):85.

[5] Maria G., J. Separation. Sci 2007, 30:595-603

[6] Nagatani Y. and Warashina T. Chem..pharma.Bull., 2001, 49:1388.

[7] Orsi Ro, and Sforcin J., Int.J. Pharma., 2005 , 5(2) : 359.

المجلة العربية للكيمياء

المجلة العربية للكيمياء:

ﻣﺠﻠة للبحوث علمية مُحكمة أسسها اتحاد الكيميائيين العرب

المملكة العربية السعودية – جامعة الملك سعود بالرياض – كلية العلوم – قسم الكيمياء – بالتعاون مع الجمعية الكيميائية السعودية

رئيس التحرير :

أ.د. عبدالرحمن بن عبدالله الورثان

قسم الكيمياء – كلية العلوم – جامعة الملك سعود – الرياض ČČďĐČ û î . ā : čďĐĐ

المملكة العربية السعودية

E-mail: awarthan@ksu.edu.sa , aalwarthan@yahoo.com

هيئة التحرير :

أ.د. سلطان توفيق أبوعرابي

رئيس جامعة الطفيلة التقنية û الطفيلة û الأردن

E-mail: abouorabi@yahoo.com

أ.د. يسري عيسى

قسم الكيمياء – جامعة القاهرة – القاهرة – جمهورية مصر العربية

E-mail : yousrymi@yahoo.com

سكرتير المجلة :

أ. عبد الرحمن بن سعد الطليحي

قسم الكيمياء – كلية العلوم – جامعة الملك سعود – الرياض ČČďĐČ – î . ā čďĐĐ

E-mail : aaltulihe@ksu.edu.sa